

A SMART MOTOR DRIVE SYSTEM FOR DOMESTIC AND INDUSTRIAL APPLICATIONS

Hossien Mahdavian

B.E. Electronic Eng., Shiraz University, Iran,
M. Eng., Victoria University Of Technology, Australia

A Thesis Submitted For The Research
Degree of Doctor Of Philosophy

February 2001



23504781

FTS THESIS

621.46 MAH

30001007181920

Mahdavian, Hossien

A smart motor drive system
for domestic and industrial
applications

CONTENTS

CONTENTS.....	i
TABLE OF FIGURES.....	vii
LIST OF TABLES.....	x
ABBREVIATIONS AND SYMBOLS.....	xi
STATEMENT OF ORIGINALITY.....	xiv
PUBLICATIONS.....	xv
ACKNOWLEDGEMENTS	xvii
ABSTRACT.....	1
CHAPTER 1	4
THESIS OVERVIEW	4
1.1 INTRODUCTION.....	4
1.2 HISTORY	4
1.3 EVOLUTION OF STANDARDS.....	5
1.4 IMPORTANT DEVELOPMENTS IN PRESENT DRIVE SYSTEMS	6
1.4.1 Energy Efficient Motors	7
1.4.2 Constant Power Operation (CPO).....	8
1.4.3 ASD For Domestic And Industrial Applications	9
1.4.4 Sensorless Detection Of Position And Speed	13
1.5 THE PROBLEM WITH EXISTING TECHNOLOGIES	14
1.6 THE AIM OF THIS RESEARCH.....	15
1.7 METHODOLOGY AND TECHNIQUE.....	17
1.8 ORIGINALITY OF THIS WORK.....	19
1.9 ORGANISATION OF THE THESIS.....	20
CHAPTER 2	23
LITERATURE REVIEW	23
2.1 GENERAL REQUIREMENTS ABOUT MOTORS	23
2.1.1 Common Enclosure Classification	23

2.1.2	Altitude	23
2.1.3	Insulation Classification	24
2.1.4	Effect Of Cable Length.....	25
2.1.5	Bearing Classification.....	26
2.1.6	Safety Classification	27
2.1.7	Coupling.....	28
2.2	MORE ON THE SUBJECT OF BEARING LIFE IN ASD	29
2.3	EVALUATION FOR HARMONIC, EMI AND SUSCEPTIBILITY	30
2.4	THE CASE OF CONTROLLER.....	31
2.5	COMMON MOTOR DRIVE SYSTEMS	32
2.6	VECTOR CONTROL INDUCTION MOTOR DRIVE.....	33
2.6.1	IM Sensorless Speed/Position Detection.....	36
2.7	SWITCHED RELUCTANCE MOTOR DRIVE (SRM).....	37
2.7.1	SRM Sensorless Speed/Position Detection.....	40
2.8	PERMANENT MAGNET BRUSHLESS MOTOR DRIVE (PMBM)....	41
2.8.1	PMBM Sensorless Speed/Position Detection	45
2.9	COMPARISON OF COMMON MOTOR DRIVE SYSTEMS	48
2.10	ELECTRIC VEHICLE (EV)	49
2.11	SUMMARY	52
CHAPTER 3	54
WOUND ROTOR BRUSHLESS MOTOR.....		54
3.1	THE WOUND ROTOR BRUSHLESS MOTOR CONSTRUCTION.....	54
3.2	INTRODUCTION.....	54
3.3	CONSTRUCTION OF THE WRBM.....	55
3.4	WRBM DRIVE SYSTEM.....	56
3.5	SENSORLESS DETECTION OF SPEED AND POSITION	58
3.6	HIGH FREQUENCY (HF) TRANSFORMER.....	64
3.7	SUMMARY	66
CHAPTER 4	68
HIGH FREQUENCY POWER CONVERSION		68
4.1	INTRODUCTION	68

4.2	TRANSFORMER MODEL OPERATING AT HIGH FREQUENCIES	68
4.2.1	Magnetisation Inductance	71
4.2.2	Leakage Inductance	71
4.3	DESIGN CRITERIA REVISITED	72
4.4	CHARACTERISTICS OF A TRANSFORMER WITH HIGH LEAKAGE INDUCTANCE	73
4.4.1	HF Transformer Model.....	74
4.4.2	Non_Resonant Circuit Analysis.....	75
4.4.3	Resonant Circuit Analysis.....	76
4.5	BASIC CIRCUIT SIMULATION	81
4.5.1	Half-Bridge Circuit Simulation And Experimental Results	84
4.6	SUMMARY	90
CHAPTER 5		92
SENSORLESS SPEED/POSITION DETECTION		92
5.1	INTRODUCTION	92
5.2	PEAK DETECTOR CIRCUIT	92
5.3	METHOD.....	94
5.4	SOLUTION.....	97
5.5	COMMUTATION PULSE GENERATION	101
5.6	VARIABLE TORQUE ADJUSTMENT PROBLEM.....	102
5.7	SPEED CALCULATION.....	103
5.8	RESONANT CIRCUIT	104
5.9	SUMMARY	108
CHAPTER 6		110
MOTOR DESIGN METHODS		110
6.1	INTRODUCTION.....	110
6.2	COMMON DESIGN OBJECTIVE.....	110
6.3	CLASSICAL DESIGN METHOD.....	112
6.3.1	Motor Specification	113
6.3.2	Permanent Magnet Materials	115
6.4	SIZING	117

6.4.1	Electric Loading	118
6.4.2	Magnetic Loading.....	119
6.4.3	Current Density	122
6.5	FINITE ELEMENT ANALYSIS (FEA)	123
6.5.1	Preprocessing	124
6.5.2	Solution.....	127
6.5.3	Post-Processing	127
6.5.4	FEA Software.....	129
6.6	SUMMARY	130
CHAPTER 7		132
MOTOR DESIGN WITH LOW AIRGAP FLUX DENSITY		132
7.1	INTRODUCTION.....	132
7.2	PERMANENT MAGNET (PM) MOTOR DESIGN.....	133
7.2.1	Sizing.....	133
7.2.2	Phase Numbers.....	134
7.2.3	Pole Numbers.....	134
7.2.4	Winding Configuration.....	136
7.2.5	Magnet Material And Rotor Dimension.....	137
7.2.6	Calculation Of Flux.....	138
7.2.7	Number Of Turns Per Coil.....	138
7.2.8	Wire Size.....	140
7.2.9	Coil Total Length	141
7.2.10	Torque Calculation.....	142
7.2.11	Current Density Calculation	143
7.2.12	Losses Calculation.....	144
7.2.13	Efficiency.....	145
7.2.14	Motor Parameter Summary.....	146
7.3	PERFORMANCE TEST	148
7.3.1	Low Speed Power Calculation	148
7.3.2	High Speed Power Calculation	148
7.4	FEA OF THE MOTOR.....	150

7.5 CONCLUSION	152
CHAPTER 8	154
HIGH AIRGAP FLUX PERMANENT MAGNET AND	154
WOUND ROTOR BRUSHLESS MOTOR DESIGN	154
8.1 INTRODUCTION	154
8.2 DESIGN PROCEDURE	154
8.3 MOTOR DESIGN WITH HIGH REMANENCE FLUX MAGNET	156
8.3.1 Constant Power Operation	158
8.3.2 Comparison Of Motors With High And Low B_r	160
8.3.3 FEA Of Motor With High B_r	164
8.4 WOUND ROTOR BRUSHLESS MOTOR (WRBM) DESIGN	164
8.4.1 Static Magnetic Field Generation	165
8.4.2 Calculation Of The Rotor Winding Area	166
8.4.3 Wire Diameter	168
8.4.4 Low Speed Operation	169
8.4.5 High Speed Operation	170
8.4.6 Current Density	171
8.4.7 Efficiency	171
8.4.8 FEA	172
8.4.9 Other Losses	175
8.5 SUMMARY	176
CHAPTER 9	178
CONCLUSION	178
9.1 INTRODUCTION	178
9.2 THE QUEST FOR A VERSATILE DRIVE SYSTEM	178
9.2.1 The Question Of Efficiency	180
9.2.2 Further Improvement In Efficiency	181
9.2.3 Improvements In Power Conversion Section	182
9.3 SENSORLESS DETECTION OF POSITION AND SPEED	184
9.4 MOTOR OPERATION	185
9.5 DESIGN REVIEW	189

9.5.1 Low Cost.....	190
9.5.2 Braking.....	190
9.5.3 Bearing Current.....	191
9.5.4 Small Size	191
9.5.5 Simple In Manufacturing	192
9.5.6 Disadvantages	192
9.6 SCOPE FOR FUTURE WORK.....	193
9.7 OTHER APPLICATIONS.....	194
BIBLIOGRAPHY.....	195
READING BIBLIOGRAPHY.....	206
INTERNET WEB SITES.....	211
APPENDIX A.....	A1
APPENDIX B.....	B1
APPENDIX C.....	C1
APPENDIX D.....	D1
APPENDIX E.....	E1

TABLE OF FIGURES

Figure 1. 1 Torque-speed characteristics of a domestic washing machine [16].	11
Figure 1. 2 Constant power operation torque-speed characteristics for wash- spin cycle in a domestic washing machine [16].	12
Figure 2. 1 Cross section of an induction motor	33
Figure 2. 2 Equivalent circuit of an induction motor	34
Figure 2. 3 Operation of induction motor at field weakening region.....	35
Figure 2. 4 Cross section of a SRM.....	37
Figure 2.5 Torque-Speed characteristics of a SRM.	39
Figure 2. 6 Cross section of a PMBM motor.	41
Figure 2. 7 PMBM torque-speed characteristics.....	44
Figure 3.1 Construction of the WRBM.	55
Figure 3.2 Simplified WRBM drive system.	57
Figure 3.3 Primary and secondary of the HF transformer.	58
Figure 3.4 Current transformer circuit.....	59
Figure 3.5 A typical voltage across R_2 in Figure 3.4.	61
Figure 3.6 Block diagram of the WRBM controller.....	63
Figure 3.7 HF model and the power conversion simplified circuit.....	64
Figure 4. 1 Model of a high frequency transformer.	69
Figure 4.2 The model of high frequency transformer.	74
Figure 4.3 Simplified schematic of the high frequency transformer with the resonant capacitor.	77
Figure 4.4. V_o/V_i ratio for different Q	79
Figure 4.5 Maximum output power vs load resistance for different Q	80
Figure 4.6 Simplified schematic of the prototype transformer.	81
Figure 4.7 Ac analysis of the circuit of Figure 4.6 for $Q=1-5$	82
Figure 4.8 Transient response of the Figure 4.6 for $Q=0.1$ and $f_L=25$, 40 and 55 kHz.	83

Figure 4.9 Transient response of the Figure 4.6 for $Q=1$ and $f_L=25$, 40 and 55 kHz.	83
Figure 4.10 Transient response of the Figure 4.6 for $Q=3$ and $f_L=25$, 40 and 55 kHz.	83
Figure 4.11 Transient response of the Figure 4.6 for $Q=5$ and $f_L=25$, 40 and 55 kHz.....	84
Figure 4. 12. Half-bridge circuit used in simulation.	85
Figure 4. 13. Primary winding current of the transformer a), and the load voltage b), non-resonant circuit, simulation result.	86
Figure 4.14 Primary winding current of the transformer a), and the load voltage b), non-resonant circuit, experimental result.	87
Figure 4. 15 Primary winding current of the transformer a), and the load voltage b), resonant circuit, simulation result.	88
Figure 4.16 Primary winding current of the transformer a), and the load voltage b), resonant circuit, experimental result.	89
Figure 5. 1 Primary winding current vs magnetisation inductance L_m for various effective resistance from 40-100 (highest to lowest) ohms with increments of 10 ohms.	98
Figure 5. 2 Variation of the transformer current vs L_m for $R=10$ ohms.	99
Figure 5. 3 Variation of the transformer current vs L_m for $R=100$ ohms.	100
Figure 5. 4 Variation of the transformer current vs L_m for $R=1000$ ohms.	101
Figure 5. 5 Primary winding current vs magnetisation inductance L_m for various effective resistance from 40-80 (highest to lowest) ohms with increments of 10 ohms, resonant mode.	105
Figure 5. 6 Variation of the transformer current vs L_m for $R=10$ ohms, resonant mode.....	106
Figure 5. 7 Variation of the transformer current vs L_m for $R=100$ ohms, resonant mode.	106
Figure 5. 8 Variation of the transformer current vs L_m for $R=1000$ ohms, resonant mode.....	107

Figure 5. 9 Variation of the transformer current vs L_m for $R=1000$ ohms, resonant mode, operating frequency of 26kHz.	108
Figure 6. 1 Stator dimensions (in centimeter) for design of PMBM.....	112
Figure 6. 2 Assignment of material property in model generation	125
Figure 6. 3 Mesh generation for Figure 6.2 example.	126
Figure 6. 4 Post-processing contour plot of Figure 6.2 example.	128
Figure 6. 5 Magnetic field intensity plot of Figure 6.2 example.....	129
Figure 7. 1 FEA of the motor with Ferrite permanent magnet.	150
Figure 7. 2 Magnetic field intensity of the motor with Ferrite magnet.	151
Figure 8. 1 Cross section of a WRBM.....	167
Figure 8. 2 Contour of the magnetic flux density of WRBM.	173
Figure 8. 3 Magnetic field intensity of the WRBM.....	174
Figure 8. 4 Modified rotor for increased winding area.....	175
Figure 9. 1 High frequency transformer.....	183
Figure 9. 2 High frequency transformer with the test bulb.....	184
Figure 9. 3 Resonant converter for power induction to the rotor.....	186
Figure 9. 4 Stator winding driver circuit.	187
Figure 9. 5 Operation of the prototype motor with the test bulb connected to rotor.....	188

LIST OF TABLES

Table 1. 1 Wash-spin cycle in a domestic washing machine [16].	11
Table 2.1 Comparison of different motor drive systems.	48
Table 6. 1 Preliminary specification of the variable speed drive system for domestic applications.....	114
Table 6. 2 TRV value for different motors [63].....	121
Table 6. 3 Typical current densities.	122
Table 7. 1 Stator winding parameters.....	137
Table 7. 2 Rotor dimensions.	137
Table 7. 3 Summary of the designed motor parameters.	147
Table 7. 4 Comparison of the motor parameter vs the target specification.	149
Table 8. 1 Motor parameter with a high remanence flux magnet.	157
Table 8. 2 Comparison of the motor performance vs the target specification for the motor with high B_r	159
Table 8. 3 Motor design parameter comparison.....	161
Table 8. 4 Efficiency comparison between the rare earth and ferrite magnet motors for constant power operation.....	163
Table 8.5 Comparison of the efficiency of the WRBM with permanent magnet motor.	171

ABBREVIATIONS AND SYMBOLS

θ	<i>Angular Position Of Rotor</i>
ω	<i>Angular Velocity Of Rotor</i>
ϕ	<i>Magnetic Flux</i>
ρ	<i>Pole Numbers</i>
α_f	<i>Fill Factor</i>
ω_L	<i>Natural Resonant Frequency Of L_L And C_1</i>
ω_{nl}	<i>Rotor No-Load Speed</i>
μ_0	<i>Vacuum Permeability, $4\pi \times 10^{-7} \text{ Hm}^{-1}$</i>
ω_t	<i>Natural Resonant Frequency Of $(L_L + L_m)$ And C_1</i>
a	<i>Number Of Parallel Paths</i>
A_p	<i>Rotor Pole Area</i>
ASD	<i>Adjustable Speed Drive</i>
A_{slot}	<i>Stator Slot Area</i>
B_m	<i>Airgap Flux Density</i>
B_r	<i>Permanent Magnet Remanence Flux Density</i>
C_1	<i>Resonant Capacitance</i>
CPO	<i>Constant Power Operation</i>
D_r	<i>Rotor Diameter</i>
DS	<i>Depth Of A Stator Slot Opening</i>
DSP	<i>Digital Signal Processor</i>
D_w	<i>Wire Diameter</i>
D_y	<i>Rotor Yoke Diameter</i>
E	<i>EMF Voltage</i>

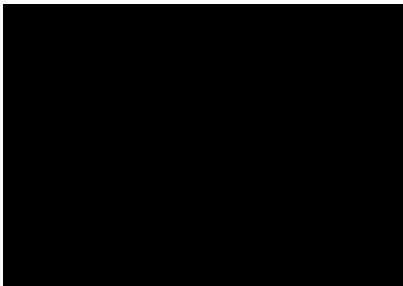
EEM	<i>Energy Efficient Motor</i>
E_L	<i>Electric Loading</i>
EMF	<i>Electro-Motive Force</i>
EMI	<i>Electromagnetic Interference</i>
FEA	<i>Finite Element Analysis</i>
f_o	<i>Operating Frequency</i>
g	<i>Airgap length</i>
ID	<i>Stator Inward Diameter</i>
IM	<i>Induction Motor</i>
I_r	<i>Rotor Current</i>
I_s	<i>Stator Current</i>
I_{sc}	<i>Short Circuit Current</i>
I_{tm}	<i>Maximum Transformer Primary Winding Current</i>
J_s	<i>Current Density</i>
K_E	<i>EMF Constant</i>
K_T	<i>Torque Constant</i>
L_L	<i>Leakage Inductance</i>
L_m	<i>Magnetisation Inductance</i>
l_m	<i>Length Of Magnetic Path</i>
L_{mag}	<i>Permanent Magnet Width</i>
L_{max}	<i>Maximum Magnetisation Inductance</i>
L_{min}	<i>Minimum Magnetisation Inductance</i>
L_{stk}	<i>Stator Stack Length</i>
M_L	<i>Magnetic Loading</i>
N	<i>Total Number Of Slot Conductors</i>
$n1$	<i>Transformer Primary turns</i>
$n2$	<i>Transformer Secondary turns</i>

<i>NEMA</i>	<i>National Electrical Manufacturers Association</i>
N_p	<i>Primary turns</i>
N_t	<i>Current Transformer Turns</i>
<i>OD</i>	<i>Stator Outward Diameter</i>
P_{co}	<i>Core Loss</i>
P_{cu}	<i>Copper Loss</i>
P_m	<i>Mechanical Power</i>
<i>PMBM</i>	<i>Permanent Magnet Brushless Motor</i>
<i>PWM</i>	<i>Pulse Width Modulation</i>
Q	<i>Quality Factor</i>
<i>RFI</i>	<i>Radio-Frequency Interference</i>
R_L	<i>Load Resistance</i>
R_p	<i>Stator Phase Resistance</i>
<i>rpm</i>	<i>Round Per Minute</i>
R_s	<i>Source Resistance</i>
<i>SEM</i>	<i>Standard Motor</i>
<i>SN</i>	<i>Stator Slot Numbers</i>
<i>SRM</i>	<i>Switched Reluctance Motor</i>
T	<i>Torque</i>
TS	<i>Teeth Space</i>
V_d	<i>Diode Forward Voltage Drop</i>
<i>VSD</i>	<i>Variable Speed Drive</i>
<i>WRBM</i>	<i>Wound Rotor Brushless Motor</i>
<i>WS</i>	<i>Width Of Stator Slot</i>
Z	<i>Total Number Of Conductors</i>

STATEMENT OF ORIGINALITY

I hereby certify that the work embodied in this thesis is the result of original research and has not been submitted for a higher degree to any other University or Institution.

This thesis may be made available for consultation within the University Library and may be photocopied or lent to libraries for the purpose of consultation if accepted for the award of the degree.



Hossien Mahdavian

PUBLICATION

1. H. MAHDAVIAN, A. ZAYEGH, A. KALAM ; 2001, "Sizing of a Motor for Domestic Application", Proceedings of IEE/JIEEEEC'98 International Conference in Electrical and Electronic Engineering, Amman, Jordan, 16-18 April, (submitted).
2. H. MAHDAVIAN, A. ZAYEGH, A. KALAM, 2000; " Model of High Frequency Transformer for Contact-less Power Conversion for Motor Applications ", Proceeding of the IASTED International Conference on Power and Energy Systems, September 19-22, Marabella Spain, pp. 313-316.
3. H. MAHDAVIAN, A. ZAYEGH, A. KALAM; 2000, " Novel Brushless Motor with Wound Rotor for Constant Power Applications", IEEE Transaction on Industry Application, (submitted).
4. H. MAHDAVIAN, A. ZAYEGH, A. KALAM; 1998, " Model of an Intelligent Speed and Position Detector for Induction Motor ", AMSE Journal MODELLING, MEASUREMENT & CONTROL, France, Vol. 82, No 3, pp. 47-51.
5. H. MAHDAVIAN, A. ZAYEGH, A. KALAM; 1998, " A Sensorless Position and Speed Detector for Brushless Motor with Wound Rotor "; AMSE Journal MODELLING, MEASUREMENT & CONTROL, France, Vol. 72, No 3, pp. 64-69.
6. H. MAHDAVIAN, A. ZAYEGH, 1999; " Analysis and Applications of Transferring Power by High Frequency Transformer with High Leakage Inductance", Proceedings of the International Conference on Electrical and Electronic Engineering IEEE/ELECO'99, 1-5 December 1999, Bursa-Turkey, Vol. 1, Invited paper, pp. 64-71.

7. H. MAHDAVIAN, A. ZAYEGH, A. KALAM ; 1999, “ Brushless Motor with Sensorless and Intelligent Speed and Position Detector for Robotic Applications ” , Proceeding of the IASTED International Conference on Robotic and Applications, October 28-30, Santa Barbara, California, USA, pp. 240-243.
8. H. MAHDAVIAN, A. ZAYEGH, A. KALAM ; 1998, “ Requirements of Power Transfer to Rotor in a Brushless Motor with Wound Rotor ” , IEEE/IEE International Conference on Communication, Computer and Power ICCCP'98, Muscat- Sultanate of Oman, Dec. 7-10, 1998, pp. 147-150.
9. H. MAHDAVIAN, A. ZAYEGH, A. KALAM ; 1998, “ Model of an Intelligent Speed and Position Detector for Induction Motor ” , Proceedings of AMSE / SIGEF International Conference on Contribution of Cognition to Modelling CCM'98, Lyon, France, 6-8 July, Vol. 1, pp. 13-36-13.39.
10. H. MAHDAVIAN, A. ZAYEGH, A. KALAM ; 1998, “A Novel Motor For Constant Power Domestic and Industrial Application”, Proceedings of IEE/JIEEEEC'98 International Conference in Electrical and Electronic Engineering, Amman, Jordan, 27-29 April, pp.96-100.
11. S. H. MAHDAVIAN, A. ZAYEGH, A. KALAM; 1997, “A Novel Model of Brushless Motor for Domestic and Industrial Applications”, Proceedings of the Third International Conference on Modelling and Simulation MS'97, Melbourne Australia, October 29-31, pp. 311-316.

ACKNOWLEDGEMENT

I wish to thank Associate Professor Zayegh and Professor Kalam my supervisors whom I have had privilege to know and work with for the past 11 years. Getting a postgraduate degree is difficult and getting a degree on part-time basis is very difficult. I am sure that I could not have got this far without the help and understanding of my supervisors particularly Associate Professor Zayegh who kindly spent time with me on this work during many of our after hour meetings.

ABSTRACT

In many industrial and domestic applications an electric motor is required to operate in the so-called constant power region. Constant power, when referred to an electrical motor, is characterised by a constant mechanical output power of the motor at any rated torque and speed.

The mechanical output power of a motor is the product of its torque and speed. For constant power operation, this means that at low speed, a high torque is generated and at high speed a low torque is produced. Electrical Vehicles (EV), washing machines and most domestic appliances, milling machines and many of industrial applications operate in constant power operation region.

In selecting a low cost and low maintenance variable speed direct drive system for constant power applications, three drive systems can be considered. These drive systems are Induction Motor (IM) drive, Switched Reluctance Motor (SRM) drive and Permanent Magnet Brushless Motor (PMBM) drive.

Induction Motor drive systems have lower torque per volume and usually are oversized to generate sufficient torque at low speed. Switched Reluctance Motor drive systems have torque speed characteristics similar to pumps and fans and hence as the speed is increased the power is increased. Permanent Magnet motors have the higher torque per volume and the highest efficiency among other drive systems but are inefficient at high speed due to the constant airgap flux.

Literature review reveals that induction motor at high speed operates better than other motors in constant power region while the PMBM is the best available drive

for low speed torque, torque per unit volume and efficiency but there are two major problems associated with it:

- The high cost of the motor due to the high cost of the permanent magnets.
- High-speed inefficiency due to the constant magnetic field of the permanent magnets.

To rectify these deficiencies and reduce the cost of the PMBM, a new design of brushless motor is discussed for constant power applications. This motor is called Wound Rotor Brushless Motor (WRBM) which has a wound rotor with no brushes for electrical connection to the rotor winding. Instead, the power to the rotor is supplied by high frequency magnetic induction of power from the stator to the rotor. The ac voltage of the secondary winding is rectified with rectifiers that are attached to the rotor and which rotate with it. The converted dc voltage is used to supply the rotor winding to generate a static magnetic field that acts as magnetic field generated by permanent magnets in the PMBM.

Despite the losses in the rotor winding, this motor is expected to have a higher efficiency at high speeds compared to PMBMs. It is anticipated that the material cost of this motor will be 40-50% less than the material cost of a PMBM, in the power ranges 500-2000 Watts. Also, because of a variable static magnetic field it can offer many operational advantages over PMBM.

The primary work described in this thesis is in regard to the fundamentals of inducing power from a stationary object to a rotary object with a transformer with separated cores by a small air gap. The motor design and the ramifications and limitations of the power induction to generate the static magnetic field is also discussed. A basic motor design procedure for permanent magnet motors are described and power calculations for the PMBM and WRBM will be shown.

Increasing the power level (that can be induced from a stationary to a rotary device in a brushless motor) and sensorless detection of speed and position, are part of this work that have been patented by the author and supervisors.

Discussion in this thesis is original and for this reason not many references were cited with similar technology except during the patent search and application. The major part of the literature review is related to the motor drive systems in order to consider all aspects of the motor design in the design of the WRBM. For example, it was necessary to find out that induction of the power from the stator to rotor can affect the performance of the motor in any way. Hence, because the technology discussed in this work is specific to motor drive systems, all aspects of the present motor drive systems will be considered.

CHAPTER 1

THESIS OVERVIEW

1.1 INTRODUCTION

Nowadays, electrical motors play an important role in all aspects of human life. With the advent of the energy crisis and greenhouse effect, the need for energy efficient systems is being emphasised by international conventions and standards. Motors are no exceptions and for many years a widespread move has been initiated to design more efficient motors and drive systems. Use of motors in Electric Vehicles (EV) that have benefits in reducing greenhouse effect and energy consumption, has resulted in more advances in the field of energy efficient motor design and drive systems. Further advancements have been achieved in the field of household appliances and industrial drive systems with the aid of cheap semiconductors and powerful microprocessors. Variable speed drive systems in many applications is an example of these advancements that use the full potential of the availability of the cheap semiconductors and microprocessors. In this chapter, after a short history about the motors and their related standards, some of the advances in the field of the motor drive systems and their application in household appliances are discussed. Then the problems associated with the drive systems that withhold further use of variable speed drive systems in domestic and industrial applications are discussed. Finally the summary of the contribution of this work and the organisation of this thesis is discussed.

1.2 HISTORY

Electrical motors have been developed for the past 165 years. From 1820-1887, Faraday, Pixli, Richie, and Henry experimented with the basic electromagnetic law and pioneered the electrical motor science. However, Davenport, a blacksmith is

credited with obtaining a US patent for building an electrical motor. Independent work of Ferraris and Tesla were the most important contribution to the motor technology. Westinghouse acquired Tesla's patent and in 1892 he had a practical induction motor. In 1893 Chicago's world fair, Westinghouse exhibited a 300hp-two phase 220V induction motor powered by a pair of 60-500hp alternators. The first 3-phase induction motor (3kW, 1500 rpm 110V, 50Hz) was sold by General Electric in 1893 [1]. In 1891, Esson published the famous scaling relationship relating the airgap dimensions to the power rating.

$$W=kD^2 \times L \times n$$

Where D is the diameter of airgap in inches, L is the length of airgap in inches, n is the speed in rpm, and W is the power rating of the motor and k is a constant.

Since the invention of induction motor by Tesla in 1880, the cost and the size of the motors have dropped for the same output power. For example in 1890, a 5-hp motor weighed 1000 pounds and cost \$900.00. In 1957 the same 5-hp motor weighed 110 pounds and cost \$110.00 and nowadays a 5-hp motor weighs 50 pounds and costs \$50.00 [1].

Continuous improvement has been achieved over the years in the performance of motors and one factor has been the evolution of standards for electrical motors in as early as 1898.

1.3 EVOLUTION OF STANDARDS

In 1898, thermal classification of motors and in 1911 standards for limits of temperature rises were published. In 1929 the first motors based on NEMA (NATIONAL ELECTRICAL MANUFACTURERS ASSOCIATION) standards were introduced with standard dimensions and operation characteristics [1].

Nowadays NEMA standards are the major standards for application of electrical motors in industry and will be referred to in the following sections.

In recent decades, there has been a tendency towards the energy efficient systems and motors due to effects of energy crisis and global warming.

Energy ACT (USA) in 1992 requires that the transition toward energy efficient motors had to begin by October 1997. Although there have been exceptions to many types of motors in this ACT [2], the trend in industry is towards energy efficient motors for all types. In this subject, Campbell [2] states that the ACT does not include vertical motors, motors slower than 900 rpm and other types which add up to a total of 30% of the motors. There have been many discussions about viability of energy efficient motors in industry in terms of cost vs efficiency that will be discussed in the next section.

1.4 IMPORTANT DEVELOPMENTS IN PRESENT DRIVE SYSTEMS

Recent important developments in motor drive systems are:

- Energy Efficient Motor
- Constant Power Operation
- Adjustable Speed Drive Systems For Domestic And Industrial Applications
- Sensorless Speed/Position Detection

The summary of these developments are discussed in the following sections and their details in regards to all of the three important motor drive systems, Induction Motor (IM), Switched Reluctance Motor (SRM) and Permanent Magnet Brushless Motor (PMBM) drive systems will be discussed in Chapter 2. The performance of the Wound Rotor Brushless Motor in regard to these topics will be discussed in Chapters 4, 5 and 8.

1.4.1 Energy Efficient Motors

The term energy efficient motors apply to motors that operate at a higher efficiency at the specified operating condition. This operating condition is usually for full-load but the specification for these motors is specified at 75% load. Bennett [3] defends energy efficient motors by arguing with the general perception that energy efficient motors are not reliable and states that the opposite is true based on the following design criteria:

1. Efficiency
2. Power factor
3. Winding life
4. Speed-Torque characteristics
5. Starting and load current
6. Bearing life
7. Mechanical endurance
8. Audible noise
9. Electromagnetic property
10. Vibration
11. Service factor
12. Temperature rise

The power factor in energy efficient motors is lower as trade off to efficiency. The winding life of the insulation, doubles for every 10° C reduction in operating temperature. With these details, design based comparison and a set of field data, Bennett [3] concludes that the energy efficient motors (EEM) are more reliable than standard motors (SEM).

The factors discussed above in addition to other requirements are used later to predict and evaluate our Wound Rotor Brushless Motor design and performance.

Pillay [4] discusses the use of EEM instead of downsizing SEM. Based on his calculation of cost electricity and SEMs and EEMs, he concludes that the pay off period of upgrading motors to EEM in the petrochemical industry is more than 2-3 years.

In industry, traditionally gas turbines were used that nowadays are being replaced by energy efficient motors. The mechanical workhorse in petrochemical and irrigation are some examples. Rama et al [5] in a review compares the use of Adjustable Speed Drive (ASD) systems as a replacement to gas turbines in the petrochemical industry. The ASD offer 4-5% better efficiency, less maintenance and considerable less cost to drive due to lower cost of maintenance (\$7.00-\$10.00/hp/year as compared with \$65.00-100.00/hp/year). Ease of control and better performance are extra advantages of ASD compared with gas turbines.

1.4.2 Constant Power Operation (CPO)

In many systems that use a motor, constant power operation applies. Constant power operation in simple terms is related to an application that usually requires a high torque at low speed and a low torque at high speed. The governing CPO torque-speed characteristics have been illustrated in Equation 1.1 and Figure 1.2. Applications like Electric Vehicle (EV) machine tools are examples of constant power operation.

Vector Controlled Induction Motor Drive systems (VCIMD) operate well in constant power region. However, the operation of Permanent Magnet Brushless Motor (PMBM) systems at constant power region has power deficiencies at high speed [21-23]. Switched Reluctance motors characteristics also suit the

applications that require higher order torque-speed relation. These applications are like fans, pumps and jet engine starters [24-25] although specific applications for low speed operation has been reported [26].

Constant power operation is also desirable in most of the household appliances, although for the case of washing machine torque-speed profile a higher peak/average torque is required. Hence, a motor drive system that could generate higher peak torque/average torque can be applied to a larger variety of appliances. The Wound Rotor Brushless Motor has the capacity to generate a peak torque that is normally more than the torque of a permanent magnet motor, because the problem of de-magnetization of permanent magnets does not exist. This is a distinct advantage for the WRBM over other motor drive systems. Manz et al [27] have discussed the issue of starting torque which has similar requirements to the applications with high peak to average torque ratio in terms of maximum torque capacity. This reference discusses the NEMA MG 1,12.54 standard in terms of methods of increasing starting torque or boost. One method is to increase the stator voltage while lowering frequency at start up to increase the torque. The ability of each motor drive systems in regard to their suitability to operate in constant power region will be discussed in the next sections.

1.4.3 ASD For Domestic And Industrial Applications

Adjustable Speed Drive systems (ASD) have been used in industry for the past few decades. However their use in domestic applications is a relatively new development in industry. The major problem with the use of ASD in domestic applications has been the tougher regulatory status for domestic appliances and the reliability of electronic drives which in a sense affects the major factor that is the cost of the appliance with ASD. As new technologies evolve and electronic components become cheaper and energy saving ACTs are introduced,

manufacturers of domestic appliances are designing more electronic control in their products.

These days the use of modern control systems like fuzzy logic is widespread in refrigeration and washing machines and other white goods. However, the use of motor speed control has been limited to SCR systems which generate considerable amount of line harmonics with very poor low speed performance. Only a few reputable manufacturers of white goods have come up with their own motor design (permanent magnet brushless motor in cases that author has knowledge) to suit their specific product like a smart washing machine.

What many appliances need is a direct drive system that replaces the pulley and the belt or the gearbox, to deliver sufficient torque at low speed and a specific high speed efficiently.

At first glance in operation of the appliances that use a motor, it seems that the majority of these applications require a constant power system in which high-torque is required at low speed and low torque at high-speed. But detailed analysis reveals that a more versatile system is needed which calls for a drive system similar to an externally excited commutator type dc motor. For example, almost in every case a high peak to average torque is required. As it will be illustrated in the following sections, this characteristic mainly suits a permanent magnet drive system. But there have been other proposals like using an ASD with an induction motor with a pulley to achieve the low speed torque for domestic applications.

Rajamani et al [16] has discussed the torque requirement of a domestic washing machine and used an induction motor drive system with pulley to generate a washing machine with ASD control systems. The references in his work clearly identifies the need for a motor drive system that is able to deliver a high to average torque ratio while being able to operate in constant power region. Table 1.1 is an

extract from this reference which illustrates the wash-spin speed requirements. Figure 1.1 is also an extract from a cross-reference in reference [16] and illustrates the torque-speed requirement of a washing machine with a belt driven drum and pulley ratio of 14.5:1.

Table 1. 1 Wash-spin cycle in a domestic washing machine [16].

	Drum speed (rpm)	Motor speed (rpm)	Motor torque (N.M.)
<i>Wash</i>	55	825	0.85
<i>Spin</i>	800	12000	0.15-0.2

Rajamani et al [16] state that with a 14.5:1 pulley ratio the requirement of the torque-speed characteristics of Figure 1.1 can be met. In the commercial type of the washing machine, a universal motor was used and in the replacement an induction motor with ASD operating at 12000 rpm (field weakening region) for the spin cycle was used. The profile of the constant power region operation for the wash-spin cycle has been illustrated in Figure 1.2 [16].

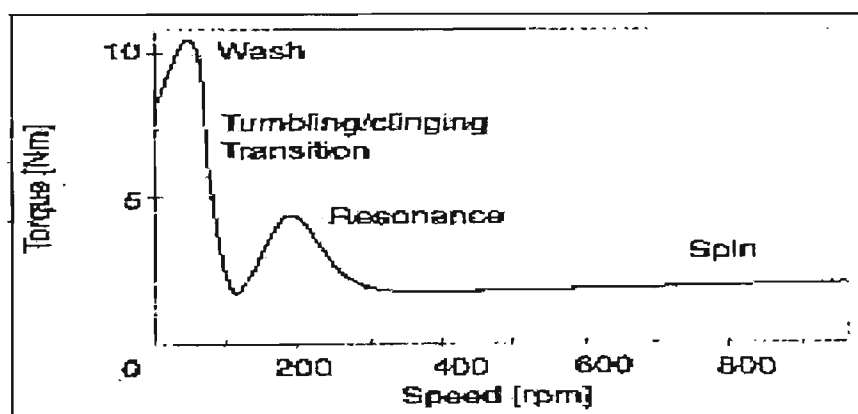


Figure 1. 1 Torque-speed characteristics of a domestic washing machine [16].

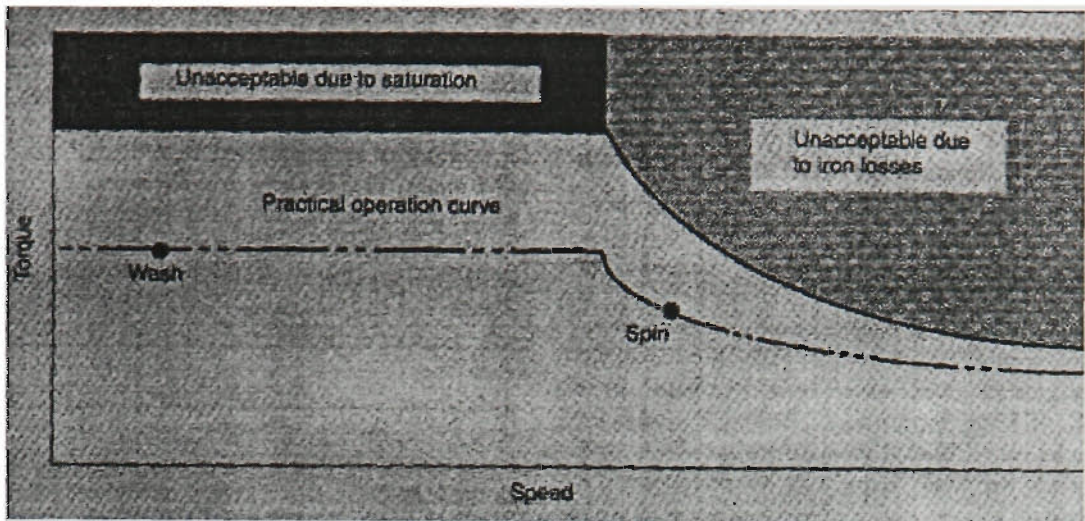


Figure 1. 2 Constant power operation torque-speed characteristics for wash-spin cycle in a domestic washing machine [16].

The relation between the torque and speed in constant power region and the field-weakening region is given by Equation 1.1 [16].

$$T_y = \frac{T_x \omega_x^2}{\omega_y^2} \quad \text{Equation 1. 1}$$

where T_x is the torque at speed ω_x and T_y is the torque at speed ω_y in the constant power region.

In the field-weakening region the flux is reduced. One way to achieve field weakening is to keep the driving voltage constant while increasing the driving frequency. In constant flux region, the torque cannot be increased even if the voltage is increased. This is due to the saturation of the iron. At high frequencies, the torque can be increased by increasing the voltage but the losses become unacceptable.

Kokalj [17] has addressed the problem that the commercial laundry machines are expensive and an ASD can reduce the cost of the system. The motor used in these

machines is a 2-18 pole motor that their speed can change from 340-3600 rpm with the aid of solid state switches that configure the windings.

Harmer et al [19] describes the design of a permanent magnet motor for the washing machine for a direct drive system. In this work it is stated that the Neodymium-Iron-Boron (N_dFeB) permanent magnets used in the design of this motor accounts for 72% of the total material cost for small quantities of supplies. This is a very good indication that the cost of the permanent magnets has been the major setback in the widespread use of high performance permanent magnet motors, in domestic applications.

As an interesting development in the use of smart controllers in domestic appliances, it is worthwhile to note the work of Errikson [18] in turbidity sensing which determines the amount of detergents in the water. Also, the work of Maudie et al [20] in their investigation in types of smart pressure sensors in domestic appliances. To the knowledge of the author, there is at least one manufacturer that uses all of the above methods or similar, besides their intelligent permanent magnet drive system in a washing machine which has been in the market for the past 5 years.

1.4.4 Sensorless Detection Of Position And Speed

Traditionally in motor drive systems and control applications, the position and speed of the motor are detected by optical encoders, tachometers and observers. The most common type has been the optical encoder that enables a very good accuracy for position detection. Almost since the evolution of these position detectors, there have been attempts to detect the position and speed of the motor with no sensors because of the extra cost, space and maintenance that the sensors bring to a drive system design. Almost any work and publication in any type of motor and drive systems is accompanied by many times research publications in

detection of the speed and position without a sensor. Examples are the speed and position detection in induction motors from third harmonic of the airgap flux [35], in permanent magnet motors from the back EMF [36] and in switched reluctance motor from the variable reluctance [37]. The availability of a sensorless detection is a distinct advantage in a drive system due to maintenance and cost factors and nowadays, there are many commercial products that have sensorless speed / position detection incorporated in their design. The issue of sensorless detection will be discussed in detail for each particular type of motor in the following sections.

1.5 THE PROBLEM WITH EXISTING TECHNOLOGIES

Usually the motive behind advancement in one field in a commercial environment is to reduce cost and improve performance. Application of variable speed drive systems in domestic and industrial environments follows the same rule. For example, use of a Vector Control Induction Motor drive system with oversized motor can be technically feasible for a washing machine but it is not cost effective. This is the major problem with application of variable speed drive systems for industrial and domestic applications. The details of the following discussion is given in Chapter 2 but the problems with present drive systems can be summarised as following:

- High cost
- Unbalance performance at high and low speed in terms of efficiency
- Size
- Reliability

Almost all of the problems associated with present motor drive systems are related to these four items and every research in this field is basically focused to improve these items. For example, an induction motor has an excellent high speed

performance but its low speed torque is low. As a result the cost of the induction motor drive system is high and the size of the motor is excessive. In contrast, a Permanent Magnet Drive system has excellent low speed torque but it is inefficient at high speed.

A brushed dc motor is the best available motor that satisfies the performance needed for domestic and industrial applications. But the cost of the maintenance and generated RFI is unacceptable in many if not all applications. In modern industrial plants these motors, despite their excellent performance, are obsolete due to maintenance costs. Unfortunately, a cost-effective replacement has not been found that provides the same performance at the same cost as a brushed dc motors.

As it is discussed in Chapter 2, neither of three major drive systems, IM, SRM and PMBM match the cost and the performance of a brushed dc motor and this is the main problem with existing technologies. In Chapter 2, it will also be discussed that the closest drive system to a dc motor is a PMBM with two major disadvantages, the high cost of the permanent magnet and the inefficiency of the motor at high speed. A PMBM has the desirable low speed performance and the IM drive system has the best high speed performance. The main design objective of the Wound Rotor Brushless Motor (WRBM) is to integrate the advantages of these drive systems into a single drive system similar to a brushed dc motor but without the maintenance problems.

1.6 THE AIM OF THIS RESEARCH

The general aim of this research program is to design, implement and evaluate a novel type of brushless motor drive system in the 500W-2000W power range. This motor drive system is principally similar to a PMBM but with two major differences:

- Reduced cost due to the replacement of the permanent magnets with a wound rotor.
- More control over the air gap flux density by electrically controlling the field flux.

A 40-50% reduction in material cost is expected from the preliminary costing due to the fact that 70-80% of the material cost in a PMBM is because of the cost of the permanent magnets [19].

The control over the air gap flux will result in a motor that is suitable for constant power applications. Despite the losses in the rotor winding and the high frequency converter, a higher efficiency at high speed results.

The summarized specific objectives of the research are:

1. To investigate the requirements of power induction from a stationary object to rotary object.
2. To increase the power levels that can be induced to suit a motor with 500-2000W.
3. To clarify the motor drive specifications in terms of torque-speed, cost, and efficiency.
4. To design a motor and investigate the operation of the motor at different conditions.
5. To design a sensorless speed, position and commutation control with their models for a complete motor drive system.
6. To built a prototype of the motor and the drive for experimental data collection in regard to the power induction section.
7. To evaluate the operational performance of the prototype.
8. To generalise the design equations of the power induction and motor design.

1.7 METHODOLOGY AND TECHNIQUE

The methodology in performing this research work is in the following sequence:

- Literature Review
- Preliminary Design Of The Motor Construction
- Detailed Analysis Of Power Conversion To Rotor
- Modeling and Simulation Of Power Conversion To Rotor
- Experimental Analysis Of Power Conversion To Rotor
- Prototyping and Testing Of Power Conversion Section
- Preliminary Design Of PMBM
- Detailed Design Of PMBM
- Transformation Of PMBM Design To WRBM Design
- Prototyping And Operational Testing Of The Motor
- Design Based Comparison Between PMBM And WRBM

An extensive literature review has been conducted to evaluate the operation of the WRBM-in every aspect of the design. Many important factors in the design of the motor is uncovered during the literature review, and state of the technology in regard to this field is investigated. An extensive literature review will make it possible for prediction of WRBM characteristics.

In preliminary design of the motor construction, the problems associated with the motor construction are identified and examined in regard to the cost implications. It will be investigated that the added hardware does not render the performance and the performance-vs-cost criteria compared with other drive system in particular the PMBM.

The detailed design of the power conversion is one of the most important parts of this work. Hence, the validity of the design is investigated by extensive calculations and simulations. The details of the design are investigated by two different and independent methods like MATLAB and circuit simulation. In this way, only when similar results are obtained from two independent methods, the design is accepted thus increasing the confidence in the design procedure.

After modeling of the power conversion to the rotor, further improvement and enhancements are possible with the aid of experimental results and fine tuning of the power conversion section of the drive system.

When the experimental part of the power conversion is satisfactory and complies with the theoretical and simulation results, the prototype of the power conversion of the WRBM are constructed and tested and experimental results are obtained.

Further hardware simulations are performed to evaluate the sensorless position method by manually rotating the rotor and simulating motor operation.

The preliminary design of the PMBM is investigated and the basic sizing of the motor is given. This process is a familiarisation process with the motor design concept. The same two independent design methods are followed to increase the reliability of the design. This preliminary design is followed by a detailed design of the PMBM that will be transferred to a WRBM design with similar parameters. This methodology has the advantage that a design based comparison can be made with PMBM.

After the above process is completed, a WRBM can be built and tested for operational performance. The detailed test of the motor is not the objective of this research work as it requires facilities that are not available, however an operation

evaluation is possible that will be supported by cost, efficiency and performance, in comparison with the PMBM motor in the conclusion to this work.

1.8 ORIGINALITY OF THIS WORK

At present the field of motor drive systems lacks a versatile drive system that is similar to a brushed dc motor with excellent performance and ease of control without its maintenance problem. Although nowadays the domestic drive systems seem to operate reliably based on universal motors, industrial drives have had problems with brushed motors for many years because motors usually operate for long hours. On the other hand, lower weight and cost, increased performance, and low maintenance requires a new drive system in the domestic appliances area that has excellent low speed torque and wide speed range. The closest that the technology has come up to this goal is the PMBM drive system that has high speed inefficiencies.

The contribution of this work to the motor drive system industry is to present a drive system that is cheaper than a PMBM drive system, but is more efficient at high speed. Although there has been some attempts to design a similar motor in the past, the fundamentals of the power conversion system and sensorless operation has not been presented before and there has not been any detailed design of the motor to what is called as WRBM (Appendix E, item 56).

By designing the WRBM, a new drive system is presented that fills the technological gap that exists today in this area in terms of a versatile motor that can operate at any torque speed and at a reasonable cost similar to the existing technologies if not cheaper.

The contribution of this work in the science of motor drive systems is divided in two sections:

1. Power conversion for generation of static magnetic field of the motor by means of the high frequency transformer.
2. WRBM design based on PMBM design with a remanence flux density similar to the generated field in section 1.

Section 1 includes Chapters 3-5 that are a major part of this work. Increasing the power levels that can be transferred from a stationary object to a rotary object with resonant method and sensorless detection of speed and position are original work and are protected by the Australian Patent described at introductory pages of this thesis.

Section 2 includes Chapters 6-8 and describes the detailed design of the Wound Rotor Brushless Motor (WRBM). Except for the generation of the airgap flux density, the design of the WRBM is similar to the design of a Permanent Magnet Brushless Motor (PMBM). Use of the high frequency power conversion and the design methodology for the WRBM is also original work and is protected by the same Patent.

1.9 ORGANISATION OF THE THESIS

Chapter 1 includes the thesis overview. After a short history about the motors and evolution of motor standards, recent developments in this field are discussed. The problems associated in variable speed drive systems, improvements resulted from this work and the research methodology are also explained in this chapter. General issues regarding the motor drive systems are discussed with preliminary literature review in this area.

Chapter 2 discusses general and specific issues of the common motor drive systems in more details. The performance of Adjustable Speed Drive systems are

examined in regard to existing standards like NEMA and basic issues in ASD are discussed. Induction Motor drive systems, Switched Reluctance drive systems and Permanent Magnet drive systems are discussed in this chapter. Methods for sensorless detection of the speed/position in each of the drive systems are discussed. Development of important technologies like smart domestic appliances and Electric Vehicle (EV) are discussed in details. Operation of each drive system in constant power region are discussed and compared. At the end of this chapter, a summary of the findings of the literature review is presented in a table and a target specification for the motor drive system is prepared as a design guide for the following chapters where the hardware design is discussed.

In Chapter 3, the requirements and advantages of the new WRBM are discussed. The construction of the motor is illustrated in details and basic parameters of the prototype motor selected for this task is explained. The prototype was built from an existing single-phase induction motor that is common in industry.

In Chapter 4, the fundamentals of the induction of power from a stationary object to a rotary object with a transformer are illustrated. The power limits that can be induced within a design set of parameters will be explored and methods to increase the power levels are introduced and examined. This section is the most important part of the project and is supported by simulations and experimental results.

In Chapter 5, sensorless detection of the position and speed is discussed in details. Different resonant modes that are described in Chapter 4 are re-examined in terms of their effect on sensorless speed/position detection.

In Chapter 6 the basic design of a permanent magnet motor is described. Design objectives are explained and a chassis is selected for design of the permanent magnet motor. Later on this chassis is used in every design in this work including WRBM to compare them in terms of torque, speed and efficiency. Summary of

classical design methods and Finite Element Analysis methods are described in this chapter.

In Chapter 7, the design of a permanent magnet motor with a magnet of low remanence flux density is described. Two different designs are explained based on the size of the magnets and the results are compared.

In Chapter 8, because of the similarities between the PMBM with high remanence flux density magnets and WRBM design procedures, the design of these motors are described. Then the operation of each motor in constant power region is examined and the results are illustrated in tables. In this chapter it is demonstrated that the WRBM performance is better than what had been expected especially at high speed.

In Chapter 9, the conclusion of this work is described and pictures of various part of the prototype motor is shown. Associated problems with the design of the power induction section and the design of the WRBM are described and recommendations are made for future work.

CHAPTER 2

LITERATURE REVIEW

2.1 GENERAL REQUIREMENTS ABOUT MOTORS

The general factors in purchasing a motor other than torque-speed characteristics are discussed in this section. Particular emphasis is on the subjects that might affect the design of the WRBM.

2.1.1 Common Enclosure Classification

Motors are classified for the enclosures based on the following definitions [6]:

1. Open Drip Proof (ODP)
2. Weather Protected Type 1 (WPI)
3. Weather Protected Type 2 (WPII)
4. Totally Enclosed Air to Air Cooled (TEAAC)
5. Totally Enclosed Fan Cooled (TEFC)
6. Totally Enclosed Weather to Air Cooled (TEWAC)

2.1.2 Altitude

At high altitudes the temperature rise is higher than low altitude. The governing Equation is [6]:

Temperature rise at Altitude = Temperature rise at sea level $\{1 + (\text{Alt} - 3300)/33000\}$.

2.1.3 Insulation Classification

2.1.3.1 Temperature

Usually a Class F insulation System with 80° C temperature rise is specified [2]. Higher temperature classes are not normally used because at higher temperatures the bearing fail. The maximum operating temperature is 155° C with shut down at 170° C. The relevant standards are NEMA MG1 (5) and ANSI CR50.41.

2.1.3.2 Break-down Voltage

NEMA requires a test voltage of 1600V with 0.1 microsecond duration for testing the insulation of the wires in a motor [7]. This test voltage is for motors that need to operate with Adjustable Speed Drive systems. For standard motors the amplitude of the test voltage is 1000 Volts for 2 microsecond.

The method of stator winding affects the robustness of a motor to withstand higher breakdown voltage [8]. There are two major types of winding, Random winding (RW) and Distributed winding (DW). In random winding the winding is spread in a random way and there is a possibility that the two parts of the coil attach to each other while belong to start part of the coil and end part of the coil. In distributed winding the windings are distributed in a regular way and the possibility that the start of the coil contacts the end of the coil is less. Hence, generally, a RW has lower breakdown voltages compared with DW. Bennett [8] describes the standards associated with insulation systems in a motor. The part 30 & 31 of MG1 standard and IEEE117 are discussed. IEEE117 specifies standards for test procedures of the random winding motors at 100% relative humidity at 40° C for 168 hours.

The length of the cable from the VSD to the motor also affects the breakdown voltage of the motor coil winding. High voltages as large as twice the supply voltage can be generated at the motor stator winding due to a phenomenon similar to the resonance in coaxial lines. This high voltage problem has been investigated by many [8][9][10][11] and will be discussed in the following section.

2.1.4 Effect Of Cable Length

Due to high frequency operation of a motor with ASD, single or multiple resonances can occur in the cable connecting the ASD to the motor, if the length of the cable and the frequency of operation are high. In many cases a few meters cable can generate a voltage peak as high as twice the supply voltage. The case of the a 670kW ASD for a subsea ASD [10] is discussed by Raad et al [10] for a very severe case of the long cable for ASD. The application is for a subsea pumping station for Vector Controlled Induction drive at 670kW and the distance of the motor from the supply is about 30km. The important findings in this paper are that a closed loop control mechanism was not possible because of the phase delays in the control loop. A voltage source inverter was better than current source inverters in generation high voltages. The start up required a boost voltage in order to compensate for the resistive drop across the cable.

Output filters have been proposed by Finlayson [9] to reduce the effect of the cable length in an ASD. As the driving pulse of the ASD decreases (faster switching) beyond 0.05-0.1 microsecond, the motor winding acts as a distributed capacitor. In random winding, 40-70% of the terminal voltage falls across the first coil of a phase. This results in additional stress on winding insulation. Adding a filter at the output of the PWM inverter of the ASD results in an averaged drive voltage to be applied to the motor winding. Hence, the life of the insulation in motor winding is deteriorated by the high voltage impulses. The relation between the generated high voltage due to the cable length is:

$$V_2 = \frac{V_1(R-Z)}{R+Z}$$

where V_2 is the additional voltage on top of the supply voltage V_1 , R is the load resistance and Z is the characteristics of the supply voltage cable to the motor.

$$Z = \sqrt{\frac{L}{C}}$$

Motors above 100Hp have higher winding capacitance resulting in 1.7-1.8 times the supply voltage overshoot. Adding an output inductor adds 40-100% to the volume, and 50-70% addition to cost and 1-1.5% reduction in efficiency. The supply voltage to the motor is also reduced to 90%. Filters are added after the ASD. Additional filters can be added at the motor that reduces the efficiency by further 1%. Shielded cables or cables in conduits are used for EMI reduction. Inverters from 5Hp will normally require a 3% Inductor for cable length between 30-150 meters. Inverters rated at 7.5-15Hp require a 3% inductor for distances 100-200 meters and 20Hp and above inverters require 3% inductor for distances from 150-200 meters.

Bennett [8] describes the calculation for cable length and its relation to the insulation tests.

2.1.5 Bearing Classification

The bearings are specified based on their life expectancy and operation temperature [2]. One common type specified in NEMA is L10 life expectancy in excess of 100,000 hours with 100° C operating temperature.

Bearing failure is the most common cause of a motor failure [12][13]. Perrin [12] has specified an equation for estimation of the bearing life based on the motor speed and dynamic performance of the motor. As expected the bearing life is inversely proportional to the motor speed. Later on, the effect of leakage current from the chassis to the ground through the bearing on the life of bearings will be discussed. The leakage current is particularly a serious problem in ASD systems where the high dv/dt of the switching drive voltage generates a current to the earth due to leakage capacitance between motor winding and the chassis through the bearing. This current generates electric discharges that cause the bearing to fail prematurely. Although there have been many solutions to this problem it is necessary to check the effect of this leakage current in any ASD design.

2.1.6 Safety Classification

Motors are classified for safety. The set of standards in USA are from, National Fire Protection Association (NFPA), National Electrical Code (NEC), and American Petroleum Institute (API). Occupational Safety & Health Administration (OSHA) specifies a quantity similar to normalised 8 hour average sound level which is called Time-Weighted Average Sound Level (TWA). This average is calculated as $TWA = 90 + 16.6 \log_{10}(D/10)$ where D is the total noise dose in %. Current law requires corrective action above 85dBA sound pressure and penalties above 90dBA sound pressure. IEEE standard 85 describes the measurement method. NEMA MG3 standard publication is also referred.

IEEE RP-519-1992 addresses the effect of harmonics on the line by the motors. This standard limits the line distortion to 5%.

2.1.7 Coupling

Different types of load coupling to the motor have been discussed by Hodowanec [14]. The value for axial force F_a has been specified in this reference as:

$$F_a = \frac{2Tu}{P_d}$$

Where

T = The torque transferred through the coupling

u = Coefficient of friction between sliding parts which is in 0.05-0.35 range

P_d = Pitch displacement of coupling.

It is stated that the bearing life is reduced if the axial force is high [14]. In the design of the WRBM, the tolerance of the axial movement of the rotor is important in the design of the transformer airgap and its effect on the resonant frequency of the drive circuit. The reason is that the rotary part of the transformer is attached to the rotor and its movement with respect to the stationary part (primary side) must be within a specified range for a practical design.

Donner et al [15] have specified the general specifications of a motor, which can be referred to for further details.

2.2 MORE ON THE SUBJECT OF BEARING LIFE IN ASD

In previous sections it was stated that bearing life is reduced by flow of stray electrical currents from the stator windings, through the chassis and bearing to earth. Due to high dv/dt of PWM inverters of the ASD, the problem is more severe in ASD systems but it can occur in standard motors which operate at mains voltage and frequency.

There have been many research activities investigating in the effect of stray currents on bearing life [28][29] and work has been reported to quantify the amount of leakage current from the chassis to the earth [30].

Busse et al [28] based on data from bearing manufacturers has reported that 8% of the bearing failures in ASD are due to so called bearing electrical current. In this reference it is also claimed that the soft switching is not reducing the failure rates contrary to the expectation that lowering dv/dt should reduce the leakage currents. NEMA specifies that the shaft voltage must be less than 1v rms at 60Hz.

The mechanism of the bearing failure has been described in this reference [28] and is summarized. At low speeds, the electrical resistance between the shaft and the chassis is low. Above 100RPM due to the oil lubricant film of 0.2-2um the impedance between the shaft and the chassis becomes capacitive while resistance increases. Hence, the voltage between the shaft and the chassis is increased until a voltage is reached when partial discharge occurs. This discharge passes a current that results in burned dots on the bearing and results in premature failure. Generally if the current density levels are less than 0.4A RMS/mm², the bearing life is limited by mechanical failure. For current densities above this level three methods can be used to bypass or to block the bearing current:

1. Use of conductive lubricant has shown reduction in the mechanical life of the bearing.
2. Use of a brush to short the shaft current to the ground.
3. Increase insulation between the shaft and the chassis (i.e. using rubber enclosure for bearings).
4. Use of a conductive shield at the airgap. This is particularly suitable for ASD drives and has been reported to be effective, while not degrading the motor performance [28].

Chan et al [29] has recommended method 2 and 3 to prevent bearing failure from electrically induced currents. Ogasawara [30] has proposed a method by using a small transformer to reduce and dampen the leakage currents in PWM inverters and can be used in bearing current minimisation.

2.3 EVALUATION FOR HARMONIC, EMI AND SUSCEPTIBILITY

Similar to switched mode power supply in lighting industry, new standards are evolving in the area of ASD in terms of passing harmonics to the mains, generating EMI and susceptibility to external changes in mains like interference, sags and surges. IEEE519/1992 (only harmonics) and IEC77A/1993 specify harmonics and EMI limitations for ASD systems. Strangas et al has proposed line inductors between 0.8-3mH or using synchronous rectifiers for better performance in harmonic generation and withstanding sags. It is stated that synchronous rectification can reduce the total harmonic distortion to less than 1% for 20hp system. Other standard methods used in inverters like 6-12 pulse rectifiers and dc link inductors have been suggested to reduce line harmonics. Multistage switching methods have also been proposed [31][32] to reduce harmonics, but they require complex electronics and are expensive. In these methods a number of dc voltage sources must be present and by switching on and off, each voltage source at

different stages, a close to sinusoidal input current is synthesized and hence the harmonics are reduced.

The harmonic issue will be discussed later when the design of the WRBM is explained. Because a power supply is required for inducing power to the rotor, a synchronous rectifier can be used to generate two separate voltage sources besides inducing the power to the rotor. The advantages are that the drive of the stator winding becomes simpler, the harmonics are reduced, and the power factor is increased to close to unity.

2.4 THE CASE OF CONTROLLER

Nowadays, implementation of a control system for closed loop torque/speed control has been made easy by availability of dedicated high level languages, compilers and simulators. Microcontroller chip manufacturers like SGS-Thompson and Texas Instruments (TI) market compilers that can implement control algorithms like fuzzy logic and traditional control methods on a compiler based system. From literature review however it seems that the majority of controllers are based on TI DSP chips which can perform significant amount of calculations per second. This enables the designer to design controllers with fast response time while performing many calculations like torque, speed and position by only detecting a few of motor parameters like stator phase voltage and current.

Despite the availability of the powerful microcontrollers and DSPs, the reliability and accuracy of the controller depends on the accuracy of transducers, reference voltages and currents and other sections used in the design. Chung et al [33] has discussed the performance of a VCIM in regard to the scaling error and offset error. It is stated that the offset error causes oscillation at stator voltage frequency and scaling error results in torque oscillations at twice the stator voltage frequency. The high frequency torque ripple is filtered by the rotor inertia and the

low frequency torque ripple is removed by the PI controller. Offset error is due to the deviation from the set point due to deviation of the references and the scaling error is the error in ADC scaling.

A fully digital controller has been proposed by Xiang et al for a SRM drive system [34]. There are two types of torque control systems based on average and instantaneous torque control. In vector control methods, using orthogonal two-axis model of ac motor, the instantaneous torque can be expressed in terms of instantaneous current. All vector control strategies and state-space based methods such as non-linear feedback control, variable structure control and adaptive control fall into the instantaneous control methods [34].

In the following sections, it is illustrated that the advantage of PMBM is that the output torque is proportional to stator current. This makes the control of a PMBM and similar motors like WRBM relatively simple for most domestic applications and many of industrial applications. However, when a high level of torque/speed/position accuracy is required, a proper control algorithm must be selected.

2.5 COMMON MOTOR DRIVE SYSTEMS

In this section the most common drive systems for domestic and industrial applications are discussed. The major benefits and shortfall of these drive systems are then explained and methods employed in the design of each system to enhance its performance are described. These methods are like sensorless speed and position detection and extraction of commutation pulses from inherent characteristics of the motor.

The performance of each drive system at constant power region will particularly be investigated and after tabulating the advantage and disadvantage of each

system, the best performing system for a common constant power application, traction or Electric Vehicle (EV) will be discussed. It will be illustrated that despite high speed deficiencies, a Permanent Magnet Brushless Motor (PMBM) drive system is the best choice for such applications considering the low speed performance and cost of the system. Supporting evidence that has been collected from Internet will be presented and finally in a separate section on EV, the current state of art technology and literature survey will be presented.

At present three types of drive systems are considered in high performance variable speed drives in industry; Vector Control Induction Motor Drive, Switched Reluctance Motor Drive, and Permanent Magnet Brushless Motor Drive. These drive systems are discussed in the following sections.

2.6 VECTOR CONTROL INDUCTION MOTOR DRIVE

Induction motors have been in the market for the past century and the fundamental theory of their operation is well known. Figure 2.1 illustrates the cross section of an induction motor with cage shape rotor and Figure 2.2 illustrates the equivalent circuit of an induction motor.

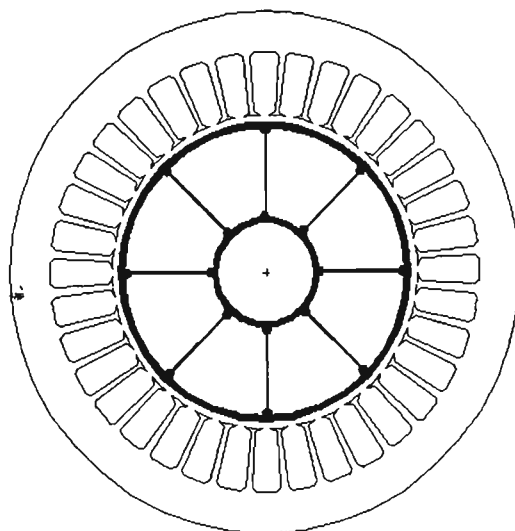


Figure 2. 1 Cross section of an induction motor

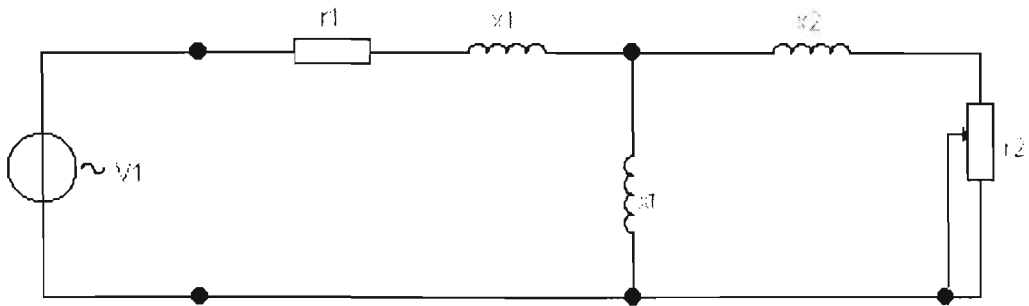


Figure 2. 2 Equivalent circuit of an induction motor

The governing equation relating to the operation of the induction motor is [38]:

$$T = \frac{1}{\omega_s} \frac{q_1 V_{1a}^2 \left(\frac{r_2}{s}\right)}{\left(R_1 + \frac{r_2}{s}\right)^2 + (X_1 + x_2)^2}$$

where

T = The motor torque

q_1 = Number of phases

S = Slip

$x_{11} = x_1 + x_f$

x_2 = Rotor's reactance

r_2 = Rotor's resistance

$Z = R_1 + jX_1 \approx r_1 + jx_1$ in parallel with jx_f

$V_{1a} = \frac{jx_f}{r_1 + jx_{11}} V_1$ Thevenin's equivalent of stator voltage

$$\omega_s = \frac{4\pi f}{poles} V_1$$

Vector Control Drives for Induction Motors have been in the market for a few years. But the control of the torque and speed require complex algorithms. In these drives, during the standstill the motor parameters are extracted from the motor by measuring the current and voltage of the motor [39]. This process is called parameterisation. From the motor parameters, torque can be controlled by controlling voltage, current and frequency. This control mechanism in conjunction with a Fast Fourier Transform of the stator current results in sensorless speed control [40].

The desired constant power operation in this drive system is usually achieved by flux weakening method [83]. In this method the operation of the motor above the synchronous speed is permitted with reduced torque. To achieve all of the above, a very powerful calculating machine is usually required for high performance Vector Control Induction Motor drives. The result is that the controller becomes expensive although the price of the motor is relatively low compared to permanent magnet motors. Figure 2.3 illustrates the operation of induction motor in field weakening region to achieve constant power operation and the underlying equation for operation at constant power is:

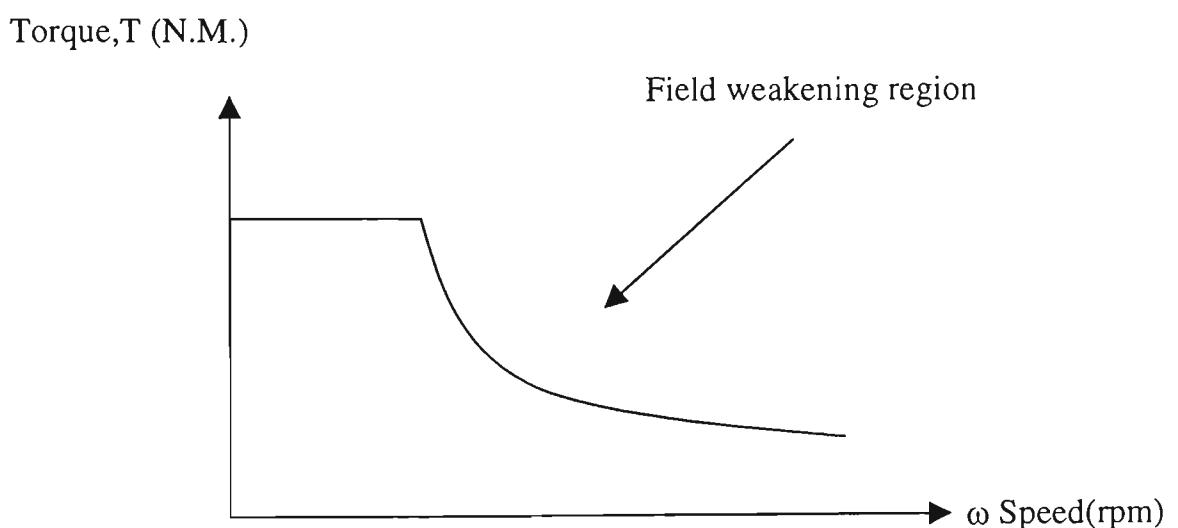


Figure 2. 3 Operation of induction motor at field weakening region.

The main characteristics of an Induction Motor Drive System are; low cost of motor, high cost of drive, excellent field weakening operation but low speed torque deficiency.

Low speed torque of Induction Motors are lower compared to Switched Reluctance Motors and Permanent Magnet Motors and usually inverter and motor oversizing is required for high torque-low speed application [41].

Another type of induction motor is doubly-fed and is also being investigated for a variable speed drive system [88]. In this motor, two separate phase windings exist where only one of them is fed by an inverter and the other winding is continuously supplied from the mains. This results in a motor drive system that is cheaper at the expense of lower speed range and difficulty in closed loop operation because one source of supplied energy is not controlled [88].

2.6.1 IM Sensorless Speed/Position Detection

The main method in induction motor drive system for sensorless speed detection is by spectral estimation of the current harmonics [40].

Speed-related harmonics arise from rotor mechanical and magnetic saliencies such as rotor slotting and rotor eccentricity. They are independent of time-varying motor parameters and exist at any non-zero speed. Digital signal processing (DSP) and spectral estimation techniques can extract these harmonics and by processing them the speed of the rotor can be detected [40].

In an induction motor with large airgap that is used in X-ray machines, a method has been reported to detect the speed of the motor with no sensor [42]. The speed of the motor with large airgap is proportional to the phase voltage. The phase

voltage is interrupted for 5 cycles and the voltage is measured at 180 Hz. Also the rotor temperature that can reach 500 degrees in these motors can be measured from the increase in the resistivity of the rotor which results in phase difference between the voltage and the current [42].

2.7 SWITCHED RELUCTANCE MOTOR DRIVE (SRM)

Switched Reluctance Motors have been investigated by industries and universities with great optimism and excitement despite that SRM power/volume is similar to induction motors. Similar to an induction motor, the rotor of a SRM has no winding and the operation of the motor is totally based on reluctance torque. This makes the cost of SRM comparable with induction motors. Figure 2.4 illustrates a typical SRM.

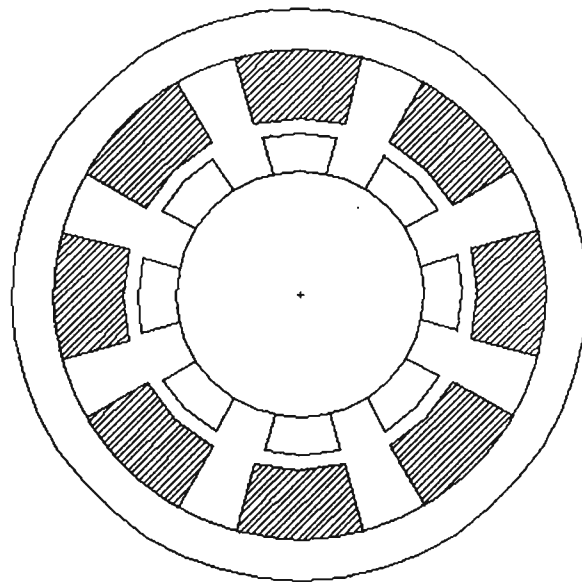


Figure 2. 4 Cross section of a SRM.

The governing equation relating the operation of a SRM is [84]:

$$T = \frac{1}{2} \frac{k_L I^2 L_{\max}}{\Delta\theta_r}$$

where

θ_r = Rotor rotation angle between the position resulting in minimum and maximum inductances.

L_{\min} = Minimum stator inductance

L_{\max} = Maximum stator inductance

$$k_L = 1 - \frac{L_{\min}}{L_{\max}}$$

The features of SRM that have recently attracted attention are, unipolar drive [43], simple construction [44], and its fault tolerant nature [45]. SRM seems to be an evolution of IM and PMBM. The simplicity of the motor is similar to an IM and its drive and control is similar to a PMBM.

SRM requires a position detector for the control of its commutation signals. Sensorless position detection algorithms have been reported for commutation control [46][47][48].

SRM have some known disadvantages. The vibration and audible noise are relatively higher in SRM than IM and PMBM [49][50][51] and more importantly its operation in constant power region is questionable. Figure 2.5 illustrates a typical torque-speed characteristic of a SRM and clearly indicates the inefficiency of the motor at high speeds for constant power operations because as the speed increases the torque also increases (unnecessary for constant power operation) and as a result the input power increases.

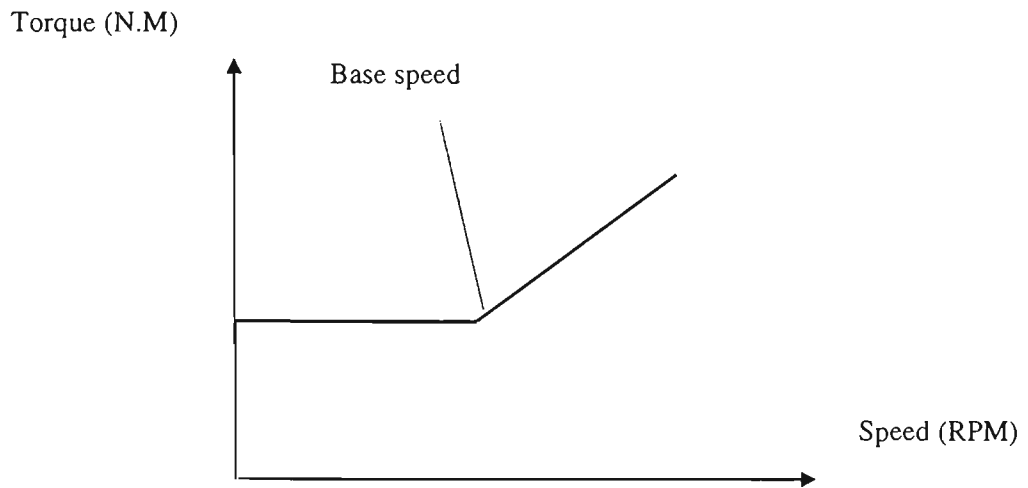


Figure 2.5 Torque-Speed characteristics of a SRM.

It is important to note that the unipolar drive circuit proposed by many sources for SRM, requires high voltage transistors compared with standard half-bridge or full-bridge converters used in commercial drives. The price of these transistors are high and one can conclude that there is no cost saving in SRM compared with a PMBM in terms of the drive circuit.

In terms of the torque-speed characteristics, it seems that SRM can be an excellent drive system for fans, pumps and aerospace technologies [47][52][53]. In these applications a higher torque is required at high speed which is similar to the SRM characteristics. However, for the operation of SRM in constant power region, further research in this field is required. In any case, the information from web sites indicates that reasonable commercialisation of SRM will not take place before the turn of the century.

Many variety of SRM have been investigated. A multiphase motor has been reported to reduce the cogging torque, reduce the harmonic losses, reduce the current per phase without increasing the voltage per phase, reducing current harmonics, increase reliability and torque/amp of the motor [54]. Increasing the phase numbers results in contribution of the higher harmonics in the generated

torque, i.e. in a 3 phase motor only the fundamental generates torque, in a 5 phase motor, the third harmonic contribute to the torque besides the fundamental.

2.7.1 SRM Sensorless Speed/Position Detection

Due to the saliency of the rotor in a SRM, sensorless detection of speed and position is less difficult compared to induction motor drive. Speed and position can be detected by the third harmonic component of the stator voltage when the machine is in saturation [55]. A resonant method has been proposed to detect the position of the rotor by the series resonance of the phase inductance, that is a function of angular position of the rotor [56]. The advantage of this method is its simplicity, robustness and inherent amplification in the detected signal because of its resonant nature.

The present technology problems in the case of SRM are:

- The modest position estimation accuracy.
- Low estimate update rate and hence poor control performance.
- Special switching in diagnostic mode and injecting high frequency signal for position detection which has been stated to be the common method [57].

A high accuracy, low and high speed sensorless speed detection algorithm has been described with a 2 degree resolution for a wide speed range. The method requires a relatively complex start up procedure to detect the initial position of the rotor [57].

A sensorless position and speed SRM for a turbine starter has been described where the position of the rotor is extracted from the phase voltage and current and a look-up table with flux linkage information [58].

Accurate position detection has been reported for the SRM for control applications [47]. The method is based on current measurement. The self and mutual inductances of the motor depends on the rotor position and hence the rate of change of current that is associated with the inverter switching depends on the rotor position. This method has been particularly proposed for low speed operation [47].

2.8 PERMANENT MAGNET BRUSHLESS MOTOR DRIVE (PMBM)

Permanent Magnet Brushless Motors have been well established in industry in terms of the knowledge of their fundamentals of operation. A major influence in its development has been advances in the permanent magnet materials. Higher remanence flux densities, better operational temperature and higher demagnetisation flux densities have resulted in high performance PMBMs, however at higher prices. In fact, the cost of permanent magnets in a PMBM can account for 70-80% of the material cost of the motor [19]. There are different types of mounting permanent magnets on the rotor [85]. Figure 2.6 illustrates a typical permanent magnet motor cross section.

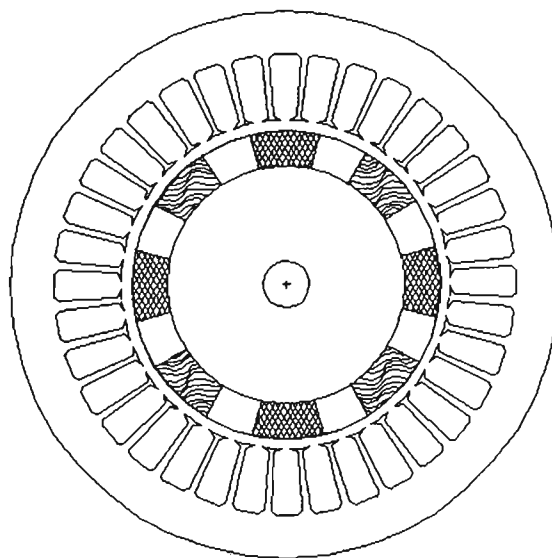


Figure 2. 6 Cross section of a PMBM motor.

A position detection mechanism is generally required for commutation control in a PMBM drive. Traditionally, rotor position has been detected by Hall effect sensors but many different sensorless detection methods have been developed for PMBM. The most widely used sensorless detection of speed is from the detection of the back EMF generated by the permanent magnets. This method is used in low cost commercially available motors (like small fans) but it has detection errors at low speeds [60]. Other methods have been reported for particular type of application based on current and inductance calculation [60][61][62]. Torque control in PMBM is also easier to achieve compared to Vector Control IM drive and SRM drive. The generated torque T in a PMBM is directly proportional to the input current I from the following relation:

$$T = K_E \cdot I$$

where K_E is the torque constant. This equation is for an ideal case where the magnetic heating, armature reaction and the effect of the stator inductance are ignored. With high performance Neodymium-Iron-Boron N_d-F_e-B material and a well designed PMBM, the relationship between the torque and the input current can be assumed to be linear [63].

The high efficiency, ease of control and excellent low speed torque capability of PMBM makes them very attractive in many medium power applications. At high power, the cost of the motor becomes very high due to the cost of the permanent magnets. PMBM above 1MW has also been reported [64].

In practice there are many problems associated with a particular application that has made the dc brushless motors less general purpose than induction motors. These problems have led some manufacturers of goods that use motors to develop

or to collaborate with the motor manufacturers in the development of application specific PMBM [59][65][66].

One major problem with PMBM which is similar to SRM but to a lesser extent, has been its lack of high efficiency operation at high speeds. This problem has been indicated by many sources for applications operating in constant power region [66][67][68].

Figure 2.7 shows a typical torque-speed relationship of a PMBM. Compared with a desirable constant power operation, the torque-speed slope is steeper. This sharp slope is due to the fact that the flux generated by permanent magnets is constant. Hence, the torque generated by the motor at high speed can be higher than what is needed by the load. The result is higher power consumption at high speeds. Many solutions have been proposed to reduce the airgap flux at high speed. Patterson et al [66] reported a mechanical mechanism to reduce the airgap flux in an axial type motor. Of course this method only works for axial motors where a physical separation of the rotor and stator is possible.

At high speed Chan et al [68] reported a method to decrease the rotational EMF in phase decoupling PMBM to achieve constant power operation. Phase decoupling PMBM are made with physical separation of the magnetic flux of each phase and by reduction of mutual inductances between different phase windings. This method results in higher operational efficiencies and better controllability due to a separate flux path in each phase [68].

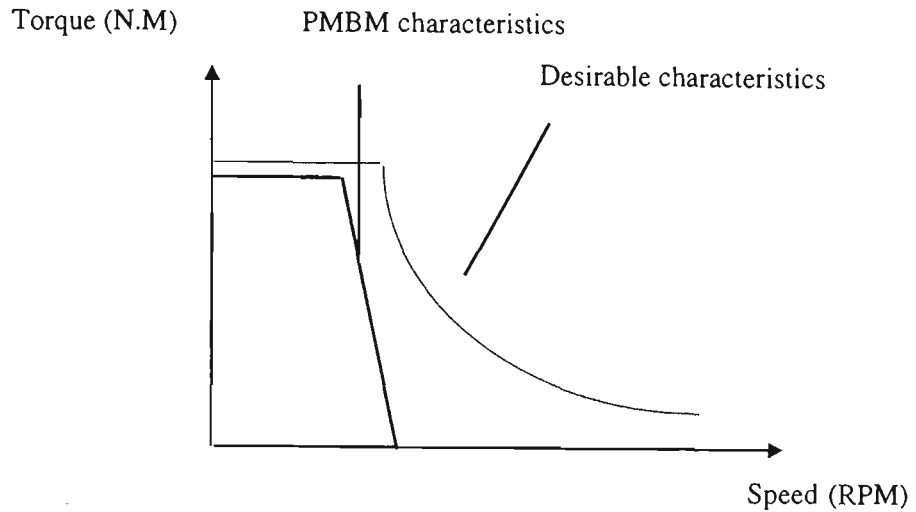


Figure 2. 7 PMBM torque-speed characteristics.

In motors with high demagnetisation flux density permanent magnets, the airgap flux can be reduced by the increase in stator current to achieve higher speeds in a PMBM. This method is only suitable for the drives which operate with field weakening control method (i.e. Synchronous Permanent Magnet Brushless Motors) [70][71].

It appears that there has not been a generalised solution for a basic problem in PMBM which is the constant airgap flux at different speeds. In dc commutator motors with field winding excitation, this problem does not exist because the field can be adjusted electrically. In series type dc commutator motor, when high torque is required, higher field current is automatically generated by the load. This increases the magnetic field intensity which increases the generated torque. In contrast, at high speeds, as the load torque decrease the armature current decreases and hence the field current is reduced. This results in less torque and less input power. This type of motor is ideal for constant power operation with a very simple control.

To match the performance of a commutator type externally excited or series excited dc motor, the static magnetic flux of the field has to be controlled. On the other hand for a low maintenance motor, a motor with no brush must be designed. These criteria were the primary reasons for the design of the Wound Rotor Brushless Motor (WRBM) in addition to reducing the cost of the motor by removing permanent magnets.

2.8.1 PMBM Sensorless Speed/Position Detection

Similar to SRM, sensorless speed/position detection is easier to achieve in a PMBM compared with IM. There have been many publications related to sensorless motor drive systems for PMBM based on the type of the motor.

French et al [72] describes the requirements of a direct torque control with sensorless detection of speed based on classification of torque in a PMBM as following:

- Cogging Torque
- Reluctance Torque
- Mutual Torque

For motors with low saliency, the first two items are negligible. Using harmonic analysis, parameters like machine parameter and rotor position can be calculated by two methods, FEA and determination of back EMF [72].

The fundamental equations are:

$$V = I.R + d\phi/dt$$

$$T = dW/d\theta$$

$$W = \int \phi di$$

Where V and I are measured parameters and R is the estimated value that can be refined in corrective loops during processing and measurements. Hence flux ϕ can be estimated from the integral of the above equation. Based on the relation between torque and co-energy direct torque control is achieved in a PMBM. The co-energy equation also incorporates the information about the position of the rotor and hence by measuring the phase voltage and current and stator winding resistance the torque and position can be calculated and controlled by control of voltage and current [72].

One method is to detect the rotor position from the back EMF voltage. In a 3-phase system only two phases conduct at the same time. During this time the third phase winding can be used to detect the position of the rotor. In the process the differentiation of current is required in this method and noise is generated. Filtering reduces the noise but introduces a phase lag that becomes problematic particularly in the field weakening operation where a phase advance of conduction angle relative to stator winding is required. Also at low speeds, back EMF approaches zero so the detection becomes even more difficult [73].

Another method to detect the rotor position similar to SRM is from variable inductance. Since the rate of change of the phase current depends on the rotor position as a result of the phase inductance, the position information is inherent in the phase current. A variant of this method is the injection of a small signal in the third winding (during non-conducting period) and measuring the variation of

current as the inductance of the winding changes with rotor position [73]. Other sensorless speed/positions methods include:

- Embedded coil winding and coil.
- Detection by conduction angle monitoring in the inverter. This method is error-prone at low speeds.
- Flux linkage measurement from measurement of voltage and current.
- Observer systems.

Observer systems by powerful DSP can estimate flux by integration and from measuring voltage and current of the windings and perform algorithms like Kalman filter in real time to compensate for the integration drift [73]. Similar method has been investigated by Ostlund et al [87]. It is important to note that sensorless position detection systems cannot detect the position at zero speed [87] for non-salient motors because the back EMF is zero. For salient motors the location of q-axis and d-axis can be found from variation of the inductance in q and d direction. However detection of d-axis cannot be obtained from machine model. The motor can be started with open loop control then the estimation control takes over but the direction of the rotation can be wrong which can be rectified by a two stage algorithm [87].

Apart from the method of bounding of the magnets on the rotor, there are many variants and types of PM motors [74][75][76]. Phase de-coupling method has been reported for the design of a fault tolerant motor similar to a SRM [76]. This motor is said to give better torque/weight ratio than a similar SRM. A doubly salient structure motor has been discussed by Liao et al [80] and it is claimed that by implanting permanent magnets in stator of a SRM better performance can be achieved in terms of efficiency, torque density and response time with a fault tolerant performance. Many axial motors have been reported that will be discussed in Section 2.10.

It is clear from literature survey that a universal algorithm and scheme is not available in sensorless detection of the position/speed in a PMBM. More importantly, the major problem seems to be the detection of the position/speed at low speed if the detection by back EMF is considered as a general method regardless of the motor type (i.e. salient or non-salient). It will be discussed that the WRBM has an absolute position detection capability regardless of the motor type that can operate at zero speed.

2.9 COMPARISON OF COMMON MOTOR DRIVE SYSTEMS

Based on the literature review so far, a summary of the benefits and shortfall of the described motor drive systems is illustrated in Table 2.1. The important factors in the comparison are, cost, low speed high torque operation, constant power operation and sensorless speed and position detection.

Table 2.1 Comparison of different motor drive systems.

TYPE	Cost of motor	Cost of drive	Low speed torque	Constant power operation	Sensorless speed/position detection	Efficiency	Suitability for EV application
<i>IM</i>	<i>Low</i>	<i>High</i>	<i>Poor</i>	<i>Excellent</i>	<i>Difficult</i>	<i>Medium</i>	<i>Good for very high power</i>
<i>SRM</i>	<i>Low</i>	<i>Medium</i>	<i>Medium</i>	<i>Difficult</i>	<i>Good</i>	<i>Medium</i>	<i>Only experimental reports</i>
<i>PMBM</i>	<i>High</i>	<i>Low</i>	<i>Excellent</i>	<i>Good for limited speed range</i>	<i>Good</i>	<i>Good</i>	<i>Excellent for low-medium power</i>

As illustrated in this table, a PMBM drive system is superior to other drive systems except in cost of the motor and its operation in constant power operation. The high cost of the motor as discussed earlier is due to the cost of the permanent

magnets and the deficiency in constant power operation is due to the constant magnetic field of the airgap. The WRBM particularly addresses these two problems by removing the permanent magnets and changing the airgap magnetic field electrically.

2.10 ELECTRIC VEHICLE (EV)

Perhaps the case of electrical vehicle is the most interesting and challenging area related to a motor drive system. With the global warming problem and foreseen energy crisis, there have been many research and publications in the field of EV. Besides, there have been many competitions for solar power cars around the world and Australia that has given rise to the level of expertise and knowledge in the field of EV. Many internet sites particularly at different universities have extensive information about the specification and performance of these solar cars and very valuable information can be collected from these sites about the suitability of a motor drive systems for EV applications.

Almost all of the solar cars observed in the internet sites used a permanent magnet motor for operation which is due to the excellent low speed torque, efficiency and ease of control. Some of the web sites regarding EV have been given in reference section.

For other types of electrical vehicles, including commercial and high power traction vehicles there have also been many reports [66][77][78][79][81].

Steimel [77] has described the methods used in Europe in electrical traction. An example is Eurostar operating at 2 x 6100kW headcars with speed of 300km/hour. This system is used in England, Belgium and France. The rotating field machine is desirable. Two methods are used, synchronous and induction machines. Permanent magnet motors are said to increase the cost of the motor by

20-30% and due to operational problem in the field weakening region are not used. SRM has only been used experimentally in one tram at the time of the report (1996). Induction motors are believed to be the most simple and robust motor drive systems for this type of application where a high power traction system is required [77]. The inverter technology has been based on GTO however smaller cars have used IGBT and BJT (up to 200kW).

Caricchi et al [78] has stated that axial-flux permanent magnet motors have high torque/weight ratio. It is stated that the torque in an axial-flux motor is ;

$$T = AR^{3.5}$$

Equation 2.1

where A is the motor parameter and R is the outer radius of the motor. The prototype motor can drive the motorcycle to a maximum speed of 50km/h. The motor has 8 poles running at 750RPM and a maximum torque of 30Nm. The permanent magnets were of Nd-Fe-B type with 1.2 T remanence flux density and 900kA/m demagnetisation field capacity. A 3 phase inverter with IGBT with 45 N.m. overload capacity resulted in 84% total efficiency at full load with a 96 volts battery voltage. The power rating of the motor was 2400W with 4.4N.m./kg motor/weight ratio.

Majority of the motors for direct drive EV applications are from Axial Flux Permanent Magnet motors (AFPM) [66][78][80][81]. The advantage of the AFPM is its high torque density for direct drive systems. An AFPM motor has also been reported with counter rotating rotors [75] for ship propulsion. This type of propulsion is said to increase the efficiency by 15%.

Despite better performance than a PM motor a AFPM has also the same problem with airgap flux and operation in field-weakening region for constant power operation. Patterson [66] reports an AFPM for a solar powered car that has a

variable airgap setting that can be changed for different speeds. Caricchi et al [81] has designed a two stage AFPM motor with two rotors that its stator winding can be phased in/out of operation by a contactor to make the motor operate at a higher speed range. The motor is water-cooled and its torque is proportional to the cube of its outer diameter similar to the Equation 2.1. Rhomboidal coil has been used as compared to trapezoidal coil to minimise end windings and hence to minimise copper losses. An efficiency of 93% has been reported with the capacity to run under 100% over load condition.

A two-stage hybrid rotor has been reported to address the constant power operation of the PM motor [79]. In this motor, the rotor has been separated axially into two sections with reluctance part and permanent magnet parts to achieve a constant power operation.

From the literature review it is obvious that the most suitable motor drive system for direct drive (no gearbox) in EV applications is AFPM motors. However, similar to a PM motor for higher efficiency at high speeds a mechanism is required to reduce the airgap flux in an efficient way. A WRBM addresses this problem by adjusting the airgap field electrically.

Before concluding the literature review, it is necessary to note that despite a large number of publications, no method similar to WRBM was found except during the patent application. In terms of inducing power from a stationary object to a rotary object that is essential part of a WRBM, no publications have been cited and the requirements for the design of the system including the motor drive systems are original. In the following chapters, particular emphasis is given to the power levels that can be transferred from a stationary object to a rotary object. The required power levels are based on the targeted specification for a suitable drive system for domestic and industrial applications.

2.11 SUMMARY

In this chapter general requirements about motors and motor drive systems were discussed. The advances in motor drive systems for domestic applications were also discussed. The importance of operation in constant power region and sensorless speed and position detection in industrial and domestic applications is being recognised in industry due to cost reduction and the need for energy efficient motors and systems.

Common motor drive systems were also discussed and more specific features of drive systems were investigated. These specific features are torque, speed, efficiency, peak torque and operation in constant power region.

In the literature survey, the most important type of motor drive systems were briefly discussed in regard to their ability to operate in constant power operation region. Although each motor drive system has its benefits and disadvantages, the quest for a motor drive system that is cost effective and can operate in different torque-speed applications continues. The comparison between the drive systems that were described has been subject of many works [11][82]. Vegati et al [82] compares IM, SRM and PM motor drive systems in a design comparison for constant power operation and spindle drive applications and concludes that the PM motors, SRM and IM generate the maximum stalled torque /volume alternatively. However, it is said that the PM motor is not suitable for spindle drive applications because of inability to operate in flux weakening region.

An Induction Motor drive system utilises a simple and inexpensive motor but a very expensive drive system. IM drive system has poor low speed torque performance and low efficiency and usually the motor and its drive system must be over sized for high torque-low speed applications.

A Switched Reluctance Motor drive system has the simplicity of an induction motor construction and relatively simpler drive system compared with an IM drive system. Although, this motor drive system has better low speed torque performance compared with an IM, its power/volume is not different with IM. SRM has a torque-speed characteristics suitable for pumps and fans. This characteristic is basically different from constant power operation characteristic and hence the operation of SRM in constant power region is not without problem.

Permanent Magnet Brushless Motor has a steeper slope of torque-speed curve compared with the slope of the desirable torque-speed characteristics of the constant power application. The result is that, at high speed the efficiency of the motor is reduced. The reason for the steep slope of the torque-speed curve is that the airgap flux of the permanent magnet is constant. Ideally, the airgap flux is required to be decreased at high speed-low torque and increased at low speed-high torque operation. The cost of the permanent magnets usually accounts for 70-80% of the cost of a PMBM. Hence, the advantage of the low cost PMBM simple drive system becomes void due to the high cost of the motor. To address the cost and high speed performance of the PMBM deficiencies, a wound rotor can be used as in commutator motors to generate a variable magnetic field. At present, a motor with wound rotor is less expensive compared with a PMBM with high performance permanent magnets for power ranges above 500 Watts. With the wound rotor, the air gap flux can be controlled hence a more suitable torque-speed torque will result compared to a PMBM. With the recent development of power electronic devices a new drive system based on the motor with wound rotor can be developed which solves the high speed deficiencies of the PMBM at high speed with reduced cost and increased performance.

CHAPTER 3

WOUND ROTOR BRUSHLESS MOTOR

3.1 THE WOUND ROTOR BRUSHLESS MOTOR CONSTRUCTION

In this chapter the construction of the WRBM and the block diagram of the drive system are described without the detailed design. The detailed design of each section will be discussed in Chapters 4 and 8.

3.2 INTRODUCTION

In Chapter 2 it was illustrated that a WRBM can address associated problems with a direct drive system that is required to operate in constant power operation. The literature review revealed that the optimum drive system is a PMBM drive system in terms of the low speed torque and the ease of drive and control. However two problems were associated with a PMBM system, the cost of the permanent magnets and the deficiency of operation at high speed due to constant magnetic field of the airgap.

A WRBM is basically similar to a PMBM but it lacks the two problems associated with a PMBM drive system. First the cost of the motor is lower because the permanent magnets are replaced with a wound rotor and second the airgap flux can be varied electrically. In fact, the WRBM is comparable with a brushed dc motor without its EMI and maintenance problems. The dc brushed motor are the best performance type of motor with ease of torque and speed control that can be configured to suit many applications and load types. However, the wearing of the brushes and the need for extensive maintenance has almost resulted in their extinction in industry. To match the performance of a commutator type externally excited or serially excited dc motor, the static magnetic flux of the field has to be

controlled. On the other hand for a low maintenance motor, a motor with no brush must be designed. With the advances in power electronics and high frequency converters, it is possible to induce the power required for the static magnetic field of the rotor from a high frequency transformer. The primary of this transformer is stationary and the secondary of the transformer is attached to the rotor and rotates with it. The power is induced into the secondary and then it is rectified to a dc voltage. This dc voltage is used to generate the static magnetic field of the rotor that can be varied by controlling the current in the primary of the high frequency transformer. Hence, a wound rotor brushless motor with characteristics similar to a separately excited dc commutator motor can be designed based on the principle of the magnetic induction of power to the rotor.

3.3 CONSTRUCTION OF THE WRBM

Construction of the WRBM motor has been illustrated in Figure 3.1.

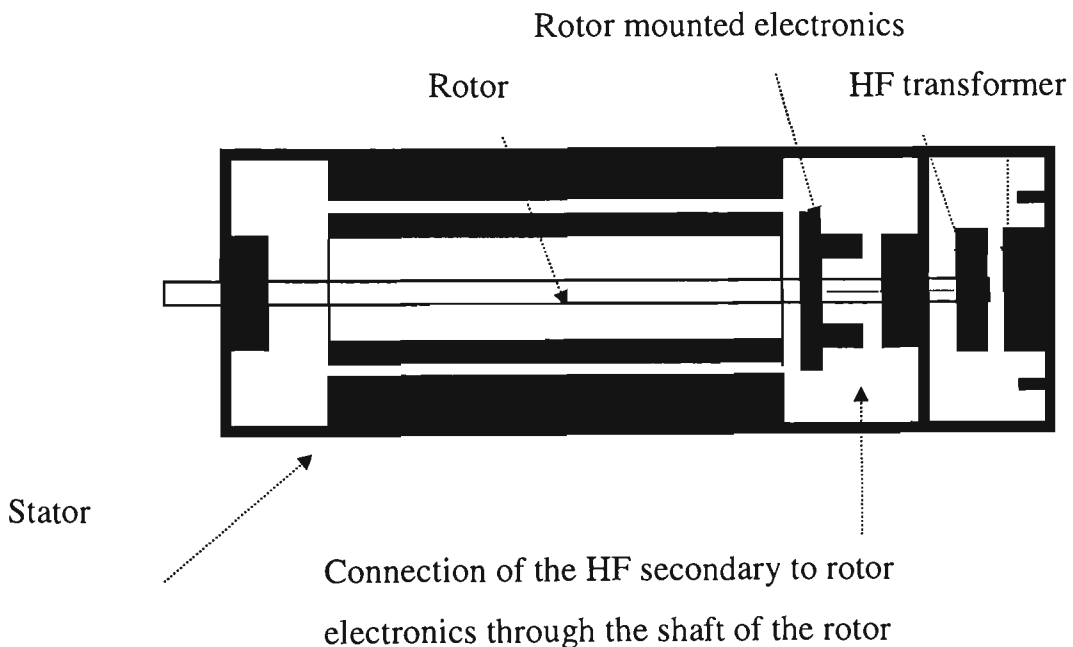


Figure 3.1 Construction of the WRBM.

As illustrated in this figure, there is no physical contact between the primary and the secondary of the HF transformer. The ac voltage generated in the stationary side by means of a switch mode power supply generates an ac voltage in the secondary side of the transformer that is attached to the rotor. The secondary winding terminal is connected to a pcb that has been mounted on the rotor. This secondary winding voltage is rectified by a bridge rectified and converted to a dc voltage that supplies the rotor winding with dc current hence generating static electric field that can be varied by controlling the primary voltage/current of the transformer.

3.4 WRBM DRIVE SYSTEM

The drive system of WRBM is similar to a PMBM drive system with the exception of the extra converter for rotor magnetic field generation. This converter can also be used for the control voltage of the drive circuit that is normally necessary.

The strength of the magnetic field without the stator winding excited, depends on the dc current in the rotor winding, the number of turns of the rotor winding turns and the magnetic reluctance of the rotor in the magnetic path inside the motor chassis. The calculation for the generated magnetic field will be discussed in Chapter 8.

The stator of the motor can be single phase or multiphase. In Figure 3.2, the stator winding of a standard 3-phase wye connection has been illustrated. The motor can be ac brushless (sinusoidal stator voltage, synchronous motor) or dc brushless (rectangular stator voltage).

Standard PMBM drive

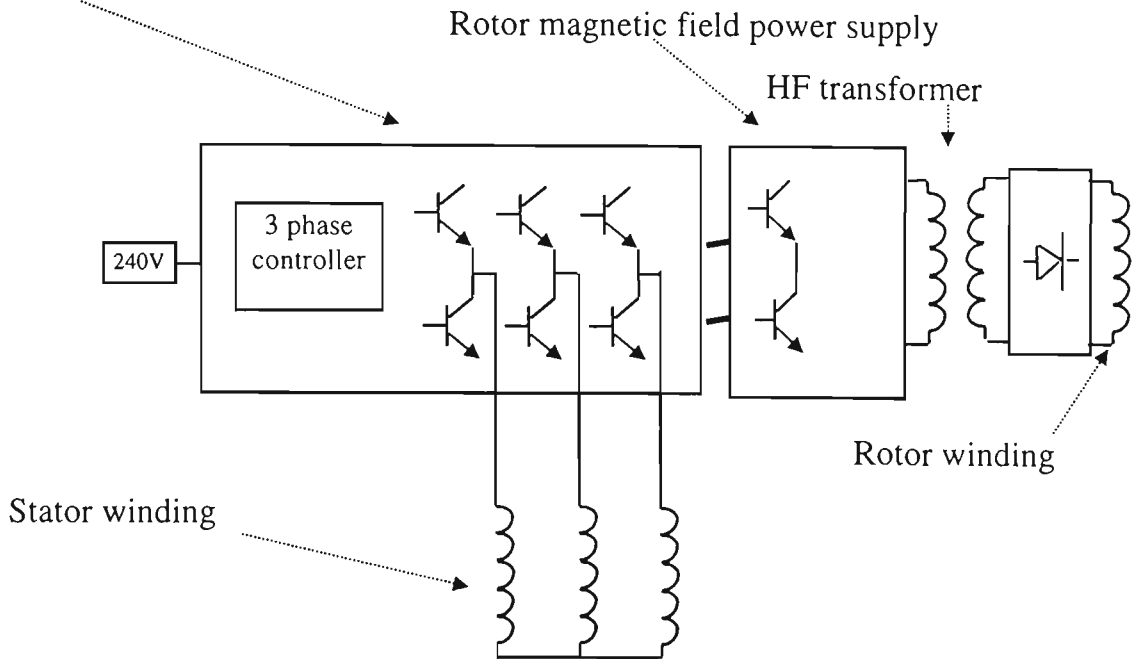


Figure 3.2 Simplified WRBM drive system.

For different motors, the rotor may include many poles. The connection of the rotor poles can be in series or in parallel. In series connection, a higher power supply voltage must be induced with less current compared with a parallel connection.

Like a PMBM a position detection mechanism is required in order to change commutation of the stator windings. Original experiment with the WRBM was performed in synchronous mode. It means that the motor speed was raised to the synchronous speed externally and then the controller changes the speed of the rotor by changing the frequency of the drive. In this mode, no position sensor was required. However, experiments performed to generate the commutation pulses with no position sensor will be discussed in the following section.

3.5 SENSORLESS DETECTION OF SPEED AND POSITION

The HF transformer used for power induction from the primary side to the secondary side has a core shape that has been illustrated in Figure 3.3.

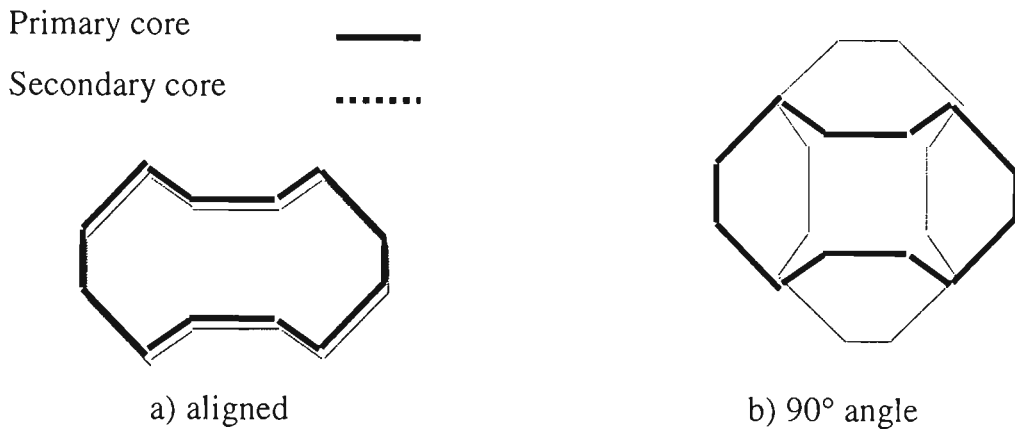


Figure 3.3 Primary and secondary of the HF transformer.

With this shape, the inductance of the primary winding varies between a maximum (Figure 3.3a) and a minimum (Figure 3.3b) value. As the secondary of the transformer spins with the rotor, the primary winding current varies slightly depending on the relative position of the primary and secondary core with respect to each other. Hence, the information about the rotor position is inherent in the primary winding current. This information can be filtered and amplified and used to identify the absolute position of the rotor, the speed of the rotor. As a result, the commutation pulses for the stator winding can be generated by measuring and processing of the primary winding current of the transformer.

The circuit for detection of primary winding current of the HF transformer has been illustrated in Figure 3.4 and its simplified model in Figure 3.7. The primary current of the transformer I_t consists of two elements I_m and I_1 (Figure 3.7). I_m is the magnetisation current of the transformer and I_1 represents the secondary winding current multiplied by the transformer turns ratio. By changing the frequency of operation the power to the rotor winding can be controlled and

variable static magnetic fields to the rotor can be obtained. As stated in previous paragraphs, I_m changes at different rotor position and hence the total transformer primary current varies slightly with a change in rotor position. This means that the information about the rotor position can be obtained from I_t and the speed can be calculated from the variation of I_t with respect to time.

The transformer current is converted to a dc voltage as shown in Figure 3.4. This circuit is basically a peak detector.

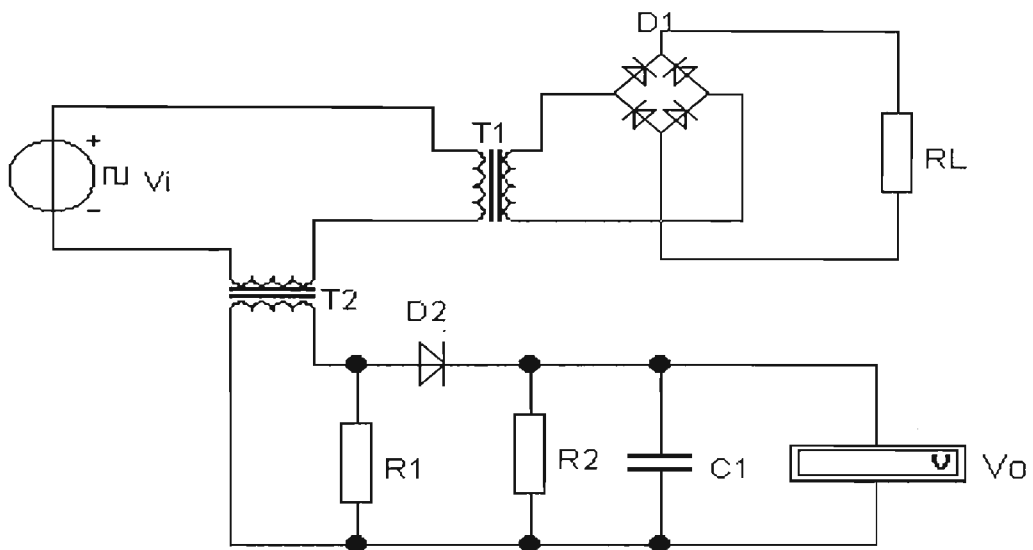


Figure 3.4 Current transformer circuit.

For a half-bridge configuration with 240V input voltage, the voltage V_i , applied to the transformer, can be defined as follows:

$$V_i(t) = \begin{cases} 153V & \text{when } 0 \leq t < 12e-6 \\ -153V & \text{when } 12e-6 \leq t \leq 24e-6 \end{cases}$$

This definition is equivalent to 153V , 42kHz frequency and 50% duty cycle pulse train.

Voltage V_o can be calculated based on the following equation:

$$V_o = [(I_{tm} \times R_l) / N_t - V_d] \quad \text{for} \quad R_2 \times C_1 \gg F_o$$

where

I_{tm} = Peak primary winding current of the transformer

N_t = Current transformer secondary turns

V_d = Diode forward voltage drop

F_o = Operating frequency

Variation of primary winding inductance can be calculated from Equation 3.1. In this equation the magnetisation inductance $L_m(\theta)$ can be defined as:

$$L_m(\theta) = \begin{cases} (L_{max} - L_{min}) \cdot [(\pi - 2\theta) / \pi] + L_{min} & 0 \leq \theta < \pi/2 \\ -(L_{max} - L_{min}) \cdot [(\pi - 2\theta) / \pi] + L_{min} & \pi/2 \leq \theta \leq \pi \end{cases} \quad \text{Equation 3.1}$$

$L_m(\theta)$ is a periodic function of θ with a period of π . $I_t(\theta)$ is also a periodic function of θ with a period of π . It means that all of the information regarding the position of the rotor can be obtained from these equations. The information about the speed of the rotor can be calculated from $dI_t(\theta)/d\theta$.

Maximum and minimum values of magnetisation inductance $L_m(\theta)$ can be calculated from Equation 3.1. If $\theta=0$, $L_m(\theta)=L_{max}$ and if $\theta=\pi/2$, $L_m(\theta)=L_{min}$.

A typical waveform of rectified $I_t(\theta)$ has been illustrated in Figure 3.5.

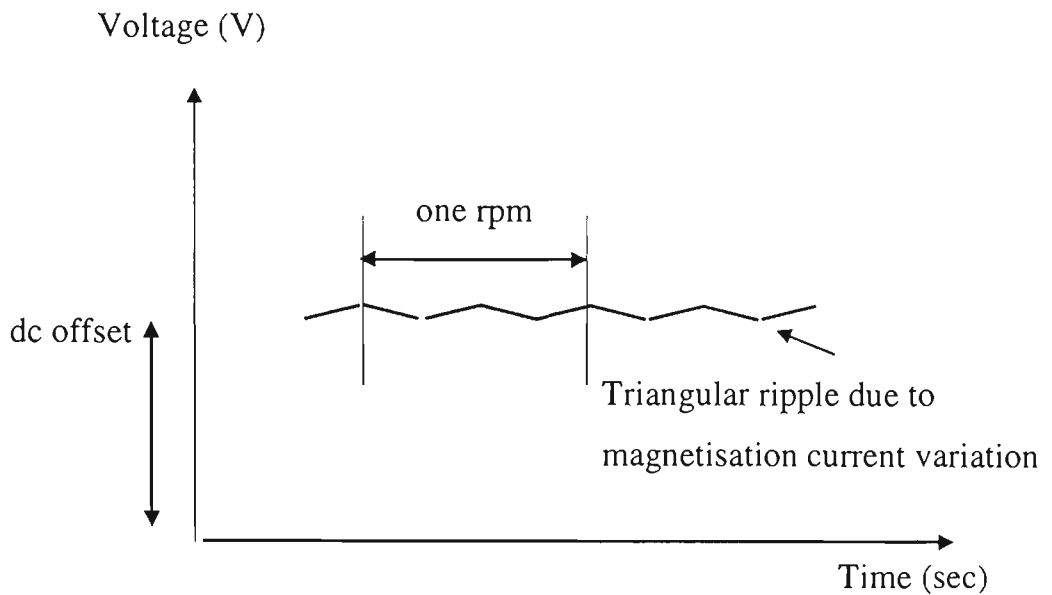


Figure 3.5 A typical voltage across R_2 in Figure 3.4.

The dc offset is due to the current in the load R_L and no information about the rotor position exists in this value. However, the triangular ripple has all of the data about the rotor position. This ripple voltage must be separated from the dc voltage and amplified for maximum dynamic range. For a drive system operating from 60 rpm to 3000 rpm, the frequency of the ripple varies from 2 Hz to 100 Hz. So a dc amplifier is required to amplify this triangular waveform. Figure 3.6 is the block diagram of the rotor position detection system based on TMS320C25 DSP.

The commutation pulses are generated from the information about the relative position of the ferrite cores and based on the position of the magnetic poles of the rotor. Depending on the detection algorithm, there could be a phase shift between the actual commutation time and the corresponding transformer primary winding current. This phase shift between the control pulses and the triangle signal can be adjusted in software.

The DSP continuously samples the transformer primary current. At the beginning a value is assumed for L_{max} and L_{min} based on the design criteria of the

transformer. These values are used to predict the transformer current. The relation between θ and current is calculated and commutation pulses are generated based on the number of phases and poles. After the motor starts, values of I_{\max} and I_{\min} corresponding to L_{\min} and L_{\max} are measured and calculated dynamically for fine tuning the commutation pulses.

To change the speed of the rotor, the frequency of the driving voltage is varied. To change the torque the magnetic field of the airgap is varied. The dc offset of the amplifier must be removed in such a way that it does not deteriorate the phase shift of the commutation pulse. Any transient in the motor operational condition must not affect the timing of the commutation pulses. An ac coupling in the amplifier could easily remove the dc offset but it generates phase shift between the commutation pulses and the triangular pulse and besides the triangular waveform frequency is very low (between 1-100 Hz). Hence the task is more difficult at different speeds different phase shifts are produced and large transient signals result as the signal is close to dc. The solution is to dc couple the amplifier and to remove the dc bias by level shifting and a subtractor that cancels out the dc offset by subtracting it from the referenced value for the speed or speed adjustment.

As in many research works studied in the literature review, many sensorless speed/position detection systems suffer from the same problem. The problem of extracting weak signals about the position and speed of the rotor in a wide variety of conditions from noisy environments.

Improper mounting of the transformers on the stator chassis and the rotor can change the performance of the system. Misalignment of the primary and secondary cores results in a distorted triangular waveform with two maximums and two minimums. To solve this problem, the high frequency transformer must be mounted on the rotor shaft in such a way that at every orientation a uniform

gap is achieved. During the experimental work and prototyping, it was noticed that a basic attention in mounting the transformer can suffice and a very high precision mechanical structure is not essential. Besides with an efficient algorithm the presence of two maximum and minimums can be solved and the accuracy of the commutation pulse timing is not hindered. The mathematical model of the speed/position detection algorithm is explained in details in Chapter 4 in the sensorless speed/position detection section.

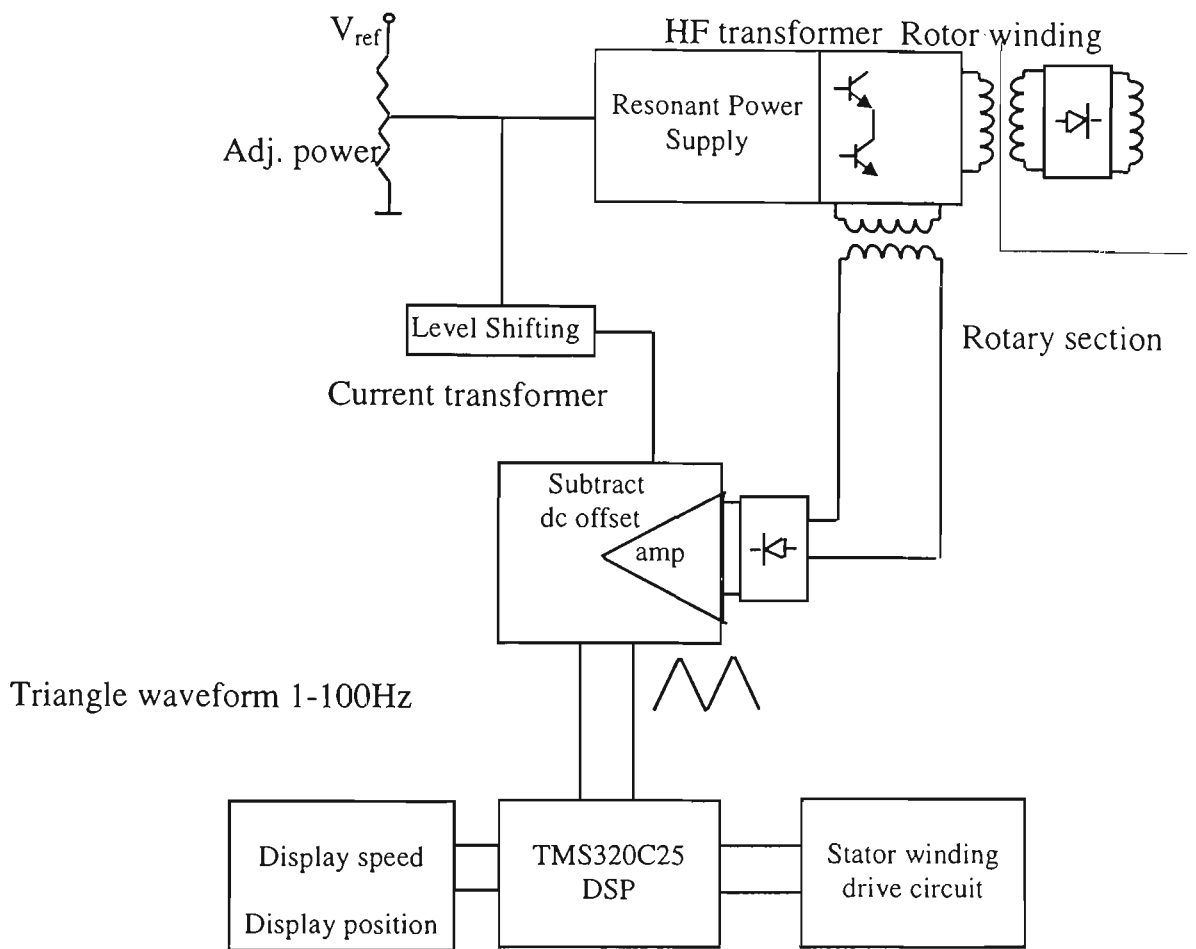


Figure 3.6 Block diagram of the WRBM controller.

The output of the amplifier signal and the input to the data acquisition section and the DSP generated commutation pulses are illustrated in Figure 3.6. It is important to note that the triangular waveform represents an absolute value for the position

of the rotor at each particular point irrespective of the motor operating condition. It means that for each point on the triangular waveform and considering its slope, there is only one position between rotor and stator poles. This is an advantage in control systems and means that the WRBM with sensorless speed/position system can be used in servo systems with closed loop control without external components. The position control can be achieved by measuring and processing the primary winding current of the HF transformer.

3.6 HIGH FREQUENCY (HF) TRANSFORMER

The most important part of the system is the high frequency transformer that is used to transfer power from the stator (stationary) to the rotor (rotary). The HF transformer has different characteristics to a standard transformer. Due to the separation of the primary and the secondary windings and cores, the leakage inductance is high and the magnetization inductance is low. For a given power, a higher supply voltage to the transformer is required if the leakage inductance is high. Also, for a given power, a higher supply current results if the magnetization inductance is low. The overall effect is that not only limited power can be converted from the primary to the secondary but also the power factor and the efficiency of operation is low compared with a standard transformer. The model of the HF transformer and the simplified circuit of the power conversion is illustrated in Figure 3.7.

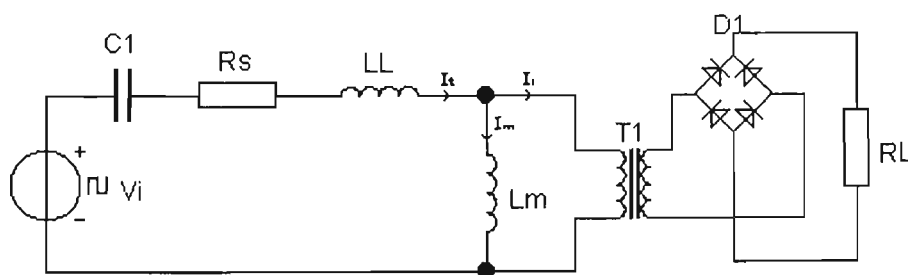


Figure 3.7 HF model and the power conversion simplified circuit.

In this figure the parameters are:

V_s = Equivalent of the half-bridge converter representation

L_L = Leakage inductance transferred to primary side

L_m = Magnetization inductance transferred to primary side

R_s = Ohmic resistance of the primary and secondary windings transferred to primary side

C_1 = Resonant capacitor

T_1 = Ideal representation of the HF transformer

D_1 = The bridge rectifier mounted on the rotor

R_L = Ohmic resistance of the rotor

From Figure 3.7 it is clearly observed that if the impedance of the leakage inductance is high and the impedance of the magnetization inductance is low, the output voltage across the rotor winding R_L is reduced.

A novel method has been implemented to counter the effect of the leakage inductance and considerable amount of power has efficiently been induced from stator to the rotor of a prototype motor. This method involves operating the converter in resonance. There are two resonant modes. One is when the resonance is between the series capacitor C_1 and leakage inductance L_L and the second resonant mode is between C_1 and an inductance equal to summation of L_L and L_m . In Chapter 4 the detailed analysis of the circuit of Figure 3.7 is discussed the advantages of operating the converter at either of these resonant frequencies are discussed. It will also be demonstrated that by adding the resonant capacitor, the only limitation in transferring power from the primary to secondary of the HF transformer is the thermal limitation of the transformer.

In Chapter 4, it will be illustrated that adding the resonant capacitor also increases the amplitude of the triangular waveform hence it will be easier to amplify the triangular waveform and remove the dc offset in the current detection circuit of Figure 3.4. The reason is that a lower gain amplifier is required and for a given supply voltage the saturation of amplifier is less likely to occur as compared with the case that the signal was weak.

3.7 SUMMARY

In this chapter the operation of the WRBM and the requirement of the drive system was discussed. The operation of the sensorless speed/position detection was also explained and the major difficulties in the operation of the system were discussed. The implementation of a WRBM requires:

1. A drive system similar to a PMBM drive system.
2. A resonant converter to reduce the effect of the leakage inductance of the HF transformer and to increase the power levels that can be delivered to the secondary.
3. A current measurement system for measurement of the primary winding current of the transformer and calculation of the position/speed of the rotor.
4. An amplifier and level shifter to generate a triangular waveform from the small variations in the primary winding current of the transformer due to changes in the magnetisation inductance.
5. A DSP or data processing unit to calculate the absolute position of the rotor from the triangular waveform and to generate the commutation pulses of the stator winding.

It is worthwhile to mention that most of the above items are available in a standard PMBM drive system and hence they do not present extra cost other than the mounting of the transformer on the rotor and stator.

The detailed discussion about the design of each sub-section is discussed in the next chapter. This discussion includes the analysis of high frequency transformer model in Chapter 4, analysis of sensorless speed and position detection in Chapter 5 and the detailed design of the WRBM in Chapter 8.

CHAPTER 4

HIGH FREQUENCY POWER CONVERSION

4.1 INTRODUCTION

In this chapter the requirements of power conversion in a transformer with stationary primary core and winding and the rotary secondary core and winding is discussed. This type of transformer is a gapped transformer and as discussed in previous chapter, such a transformer is characterised by low magnetisation inductance and high leakage inductance. The result is that, a higher source voltage is required for conversion of a given power and the efficiency and the power factor of the transformer are lower.

In the following sections, the model of the transformer is discussed and the maximum power that can be transferred to the secondary for a given supply voltage is discussed. It will be demonstrated that by driving the transformer in resonant mode the maximum power transfer can be increased dramatically. There are two different resonant modes that will be discussed in detail in terms of the advantage of each mode. The performance of the transformer is examined by circuit simulation, solution of the characteristic equation of the circuit by MATLAB and experimental tests.

4.2 TRANSFORMER MODEL OPERATING AT HIGH FREQUENCIES

The model of an ordinary transformer operating at high frequency is illustrated in Figure 4.1. There are many different topologies in switch mode power supply technologies and some of them like forward converter and fly-back converter topologies require an airgap for operation. These types of topologies can utilise the inherent gap in the transformer for transferring power to the secondary but because of poor coupling between the primary and the secondary windings, the

fly-back energy can be excessive and snubbing circuits are required to reduce the stress of the switching components. Other topologies like half-bridge and full-bridge do not require a gapped transformer and can return the energy back to the dc link by means of flywheel diodes and hence are preferred. For this reason, it is assumed that the desirable type of the transformer is a non-gapped transformer. The half-bridged topology is used because of simplicity and lower number of switching component. Although the type of topology does not affect the overall model of the transformer but the desirable values for the model vary substantially. For example, in a non-gapped transformer, a high magnetisation inductance and a low leakage inductance is required. While in gapped transformer technologies, especially fly-back, the transformer is regarded as an inductor/transformer for storing/transferring energy rather than a transformer for power conversion.

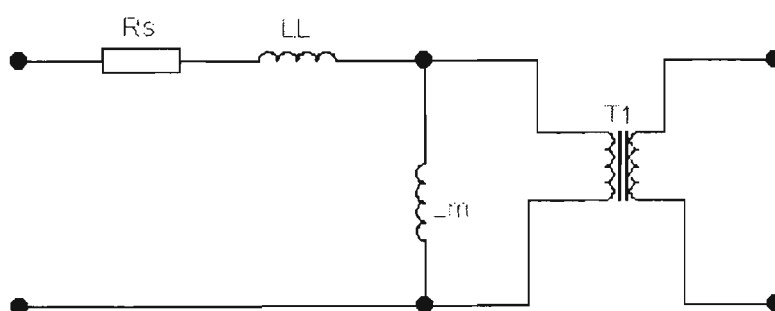


Figure 4. 1 Model of a high frequency transformer.

In this figure, T_1 is an ideal transformer, R_s is the series resistance, L_L is leakage inductance and L_m is magnetisation inductance that are transferred impedances to the primary side. The leakage capacitances are ignored.

The operating frequency considered is about 50kHz and generally a non-resonant operation is assumed although a resonant method is described later. In very high

frequencies resonant converters the effect of parasitic elements must be included in the transformer model.

With the above requirements and assumptions about the operating frequency and the type of conversion topology, the transformer of Figure 4.1 is in fact the model of a transformer operating at mains voltage and frequency. This model applies to the frequency of interest with the same design objective, to increase the magnetisation inductance and to reduce the leakage inductance. There are rare exceptions to this design objective in occasions that transients are important but at this work this design objective is used as target.

Design parameters are as following:

- Operating frequency, 50kHz
- Supply voltage, 240V
- Converter topology, Half-bridge
- Conversion power, 100-300W

The power conversion level is an estimate based on the target specification presented in previous chapter. This power level will be revised in the following chapters when the motor design is discussed.

With the basic requirements stated above, for a standard transformer, L_m is in the tens of millihenry range and L_L is in microhenry range. These values are for the case that the windings of the primary and the secondary are sandwich on top of each other and around the center pole so that the majority of the magnetic flux lines pass through both windings. Sometimes for safety reasons it is required that the primary and the secondary windings are separated in a form that is usually called split-winding method. In this case, the magnetisation inductance does not

vary considerably but the leakage inductance increases. In the following section the factors affecting the leakage inductance are discussed.

4.2.1 Magnetisation Inductance

The magnetisation inductance is defined as the primary winding inductance that is shown in the Equation 4.1.

$$L_m = \mu AN_p^2 / l_m \quad \text{Equation 4.1}$$

where L_m is the magnetisation inductance, μ is the magnetic permeability of the magnetic material, A is the cross section of the core, N_p is the primary winding turns, and l_m is the length of the magnetic path.

4.2.2 Leakage Inductance

For sandwich (concentric) winding, the leakage inductance is defined as [86]:

$$L_L = \mu_o N_p^2 V / l^2 \quad \text{Equation 4.2}$$

Where,

μ_o is the air permeability, N_p is the primary turns, V is the volume between coils of the transformer and l is the length of the magnetic path that includes the primary and secondary windings. From this equation it is clear that the leakage inductance is independent of the magnetic circuit of the transformer. For split winding this equation is not accurate because the flux and the energy stored in the airgap between the windings cannot be calculated from Ampere's Law as it has been the case for Equation 4.2. The parameters V and l are also undefined for the

split winding. Leakage inductance is related to the flux that passes through one winding and not both hence for split winding the distance between the windings and the shape of the magnetic cores are important. The analysis is complex and varies for different shape of transformers and windings.

The transformer parameters can be measured by open circuit and short circuit tests. This method is common when inductance and resistance values can be measured directly by an instrument. Using a resonant circuit, for very low values, magnetisation and leakage inductance can be measured by measuring the resonant frequency for various resonant capacitance.

For instance while measuring low values of leakage inductance, the secondary is short circuited and a resonant circuit is set up to give two frequencies (f_1 and f_2) for two different capacitances (C_1 and C_2). Then the leakage inductance is calculated from Equation 4.3 [86]:

$$L_L = \frac{f_1^2 - f_2^2}{(2\pi f_1 f_2)^2 (C_2 - C_1)} \quad \text{Equation 4. 3}$$

A direct method was used in our measurement that gives enough accuracy as the inductance values were considerably large (in the hundreds of microhenry range).

4.3 DESIGN CRITERIA REVISITED

The ratio of the magnetisation inductance to leakage inductance for a concentric winding is:

$$L_m/L_L = \mu A l^2 / \mu_0 V l_m \quad \text{Equation 4. 4}$$

From Equation 4.4 it is clear that the ratio of the magnetisation inductance to the leakage inductance is independent of the turns. It is restated that it is desirable to increase this ratio hence a transformer core with high permeability must be used. Reducing the space between the windings and spreading the winding area (increasing l) also increases the ratio while increasing the magnetic path reduces the ratio. In the following sections the effect of the low magnetisation to leakage inductance that is the characteristics of the transformer for power conversion to rotary secondary from stationary primary is discussed in details.

4.4 CHARACTERISTICS OF A TRANSFORMER WITH HIGH LEAKAGE INDUCTANCE

In previous sections the desirable characteristics of a transformer were described. In this section the characteristics of the transformer used for power conversion from a stationary (primary) core to a rotary (secondary) core are described. It is found that a transformer with high ratio of magnetisation inductance to leakage inductance is desirable for better efficiency of the transformer. For a sandwich winding, the lower the reluctance of the magnetic path the better will be this ratio. This rule is correct for the split winding although the analysis generally requires Finite Element Analysis (FEA). The dependency of length of the overlapping winding of primary and secondary that is important in sandwich winding is not meaningful in split winding.

In summary, for a split winding for conversion of the power from the stationary core to rotary core, a wider center pole, a shorter magnetic path and high permeability is desirable. It means that a core shape that is flat and wide is desirable. However, the limitation of the number of turns is also a factor that must be considered. Driving the transformer at very high frequencies is desirable in reducing the turns but there is a compromise in terms of the cost of the switches and also the radiated EMI.

The core type that was selected for the prototype was from RM series from Philips that has been illustrated in Appendix A. This type of core has another advantage in sensorless detection of speed and position that will be discussed in the subsequent chapters in details.

In general, when the windings/cores of the primary and secondary of the transformer are separated the leakage inductance is increased and if there is an airgap between the cores, the magnetisation inductance is reduced.

4.4.1 HF Transformer Model

The transformer that is used to induce power from a stationary to a rotary object is characterised by the high leakage inductance and low magnetisation inductance compared with an ordinary transformer. Figure 4.2 illustrates the simplified model of a high frequency transformer. The leakage inductance is high because the primary and secondary windings are separated and the magnetisation inductance is low because of the air gap between the cores and windings. The result is higher switching currents and a more reactive power characteristic of the transformer.

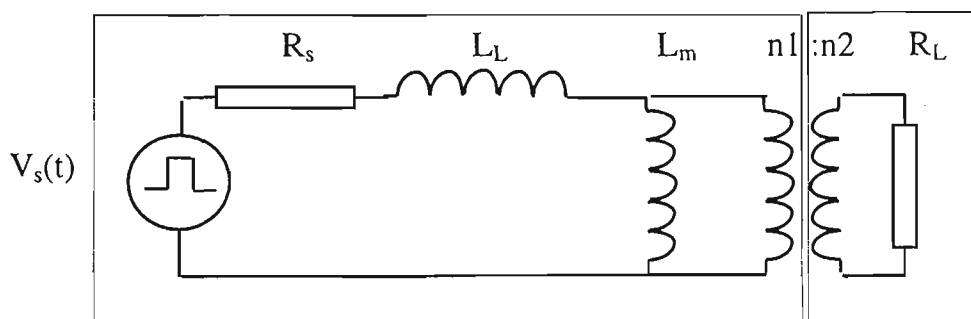


Figure 4.2 The model of high frequency transformer.

$V_s(t)$ = Equivalent pulse waveform of the half-bridge converter.

R_s = Equivalent series resistance of primary and the secondary windings that is ignored in calculations because of small value.

L_L = Equivalent leakage inductance of the primary and the secondary windings.

L_m = Equivalent magnetisation inductance of the primary.

n_1 = Primary turns.

n_2 = Secondary turns.

R_L = Load resistance

4.4.2 Non-Resonant Circuit Analysis

The transformer in Figure 4.2 is suitable for power induction from a stationary to a rotary object if the source voltage is high and the required power is low. This is illustrated by the maximum power transfer rule, which requires that the source and the load impedances must be equal. Hence,

$$\left| \frac{RL_m\omega}{R + L_m\omega} \right| = |L_L\omega|$$

or,

$$\frac{1}{R^2} + \frac{1}{L_m^2\omega^2} = \frac{1}{L_L^2\omega^2}$$

where

$$R = \left(\frac{n_1}{n_2} \right)^2 R_L$$

is the load resistance transferred to the primary.

For special case when $L_m \gg L_L$ then $R = L_L \omega$. Hence for a given transformer characteristic the maximum power transferred can be calculated.

In the experimental circuit for $L_L = 300 \mu\text{H}$, $L_m = 450 \mu\text{H}$, $F = 42 \text{kHz}$, and hence the maximum power that can be transferred from a source with 240V rms is for $R = 106.2 \text{ ohm}$. The power $P = V_R^2 / R = 147 \text{ VA}$.

The circuit of Figure 4.2 has the advantage of being inherently current limited (i.e. when $R=0$). The peak short circuit current is:

$$I_{sc} = \frac{V_s \sqrt{2}}{L_L \omega}$$

and hence $I_{sc} = 3\text{A}$.

The power and short circuit current has been calculated for a voltage source of 240V rms. In practice, depending on the power conversion topology used this value changes. For instance if the rectifier filtering capacitance is high, the dc supply voltage will be $240\sqrt{2} = 340\text{V}$. For a half-bridge converter the peak voltage of the harmonic associated with this dc voltage is $2/\pi \times 340 = 216\text{V}$ or the rms value of the fundamental is $216/\sqrt{2} = 153\text{V}$ for a nominal 240V input. Hence, the output power delivered is less, if a half bridge converter is used. In simulation study, 153V has been used because the prototype uses a half bridge converter topology.

4.4.3 Resonant Circuit Analysis

To reduce the effect of the leakage inductance a capacitor is inserted in series with the leakage inductance and the converter is operated at the resonant frequency of

the capacitor and the leakage inductance. The simplified schematic of the circuit is illustrated in Figure 4.3.

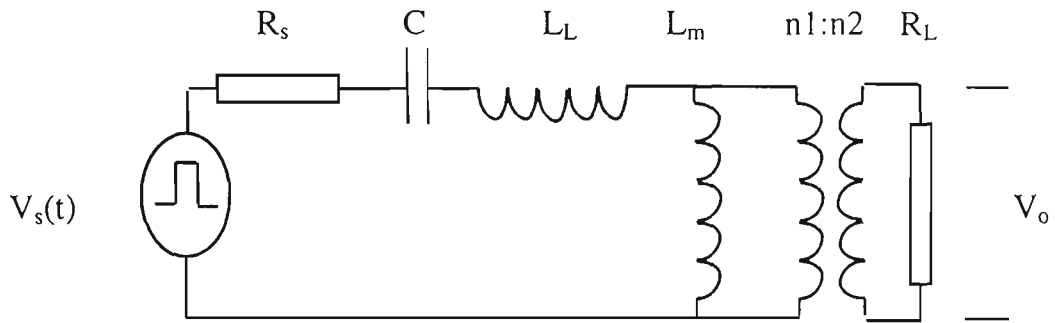


Figure 4.3 Simplified schematic of the high frequency transformer with the resonant capacitor.

The output voltage of this resonance circuit is given by Equation 4.5.

Solving the circuit of Figure 4.3 yield:

$$V_o(S) = \frac{\frac{RL_m S}{(R + L_m S)}}{\left(\frac{RL_m S}{(R + L_m S)} + L_L S + \frac{1}{CS} \right)} V_s(S)$$

or

$$\frac{|V_o(j\omega)|}{|V_s(j\omega)|} = \frac{1}{\sqrt{\left(\frac{\omega^2}{\omega_m^2} - 1\right)^2 + \left(\frac{Q\omega}{\omega_L}\right)^2}} \quad \text{Equation 4.5}$$

where

$$\omega_m^2 = \frac{1}{L_m C}$$

$$\omega_i^2 = \frac{1}{(L_m + L_L)C},$$

$$\omega_L^2 = \frac{1}{L_L C}$$

$$R = \left(\frac{n_1}{n_2}\right)^2 R_L,$$

and

$$Q = RC\omega_L$$

Equation 4.5 are solved for different Q values using Matlab programs and the results have been plotted in Figure 4.4. The source code of these programs have been given in Appendix D.

Figure 4.4 illustrates the voltage gain $|V_o(j\omega)/V_s(j\omega)|$ for different values of Q ($Q=1-5$). It can be observed that a voltage gain of 5 can be obtained for $Q>5$. From Equation 4.5 it can be concluded that if Q is low, to maximise the load power, the operating frequency must be close to ω_L . If Q is high to maximise the load power, the resonant frequency must be close to ω_t .

Running the inverter close to ω_L ensures a unity gain for $Q>0.1$. In other words, the effect of the leakage inductance L_L can be minimised if we operate the circuit at the resonant frequency of the L_L and C .

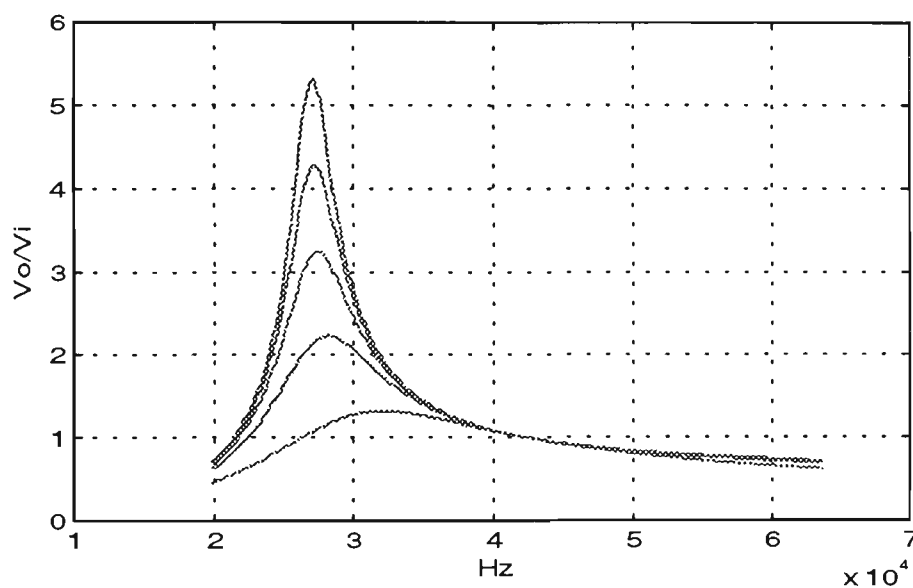


Figure 4.4. V_o/V_i ratio for different Q .

The relation between output power versus load resistance can be observed from Figure 4.5. In this figure, dual mode for maximum power transferred is clearly illustrated. If the converter is operated at ω_L for low resistance values a higher power can be converted while for high resistance loads the curves for maximum power transfer is at the vicinity of ω_t .

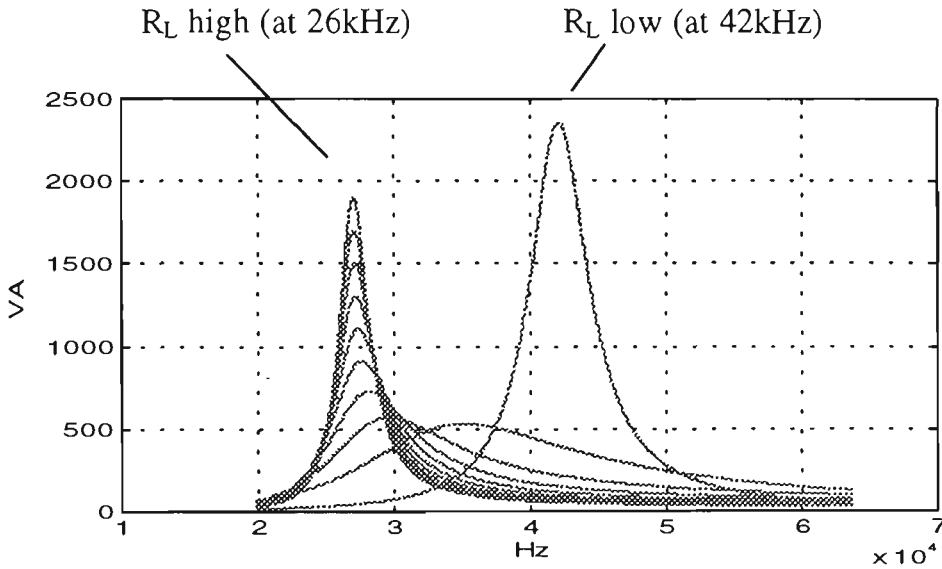


Figure 4.5 Maximum output power vs load resistance for different Q.

Circuit of Figure 4.3 does not have inherent current limit if the operating frequency is close to ω_L . It can be observed from the following equation that at $\omega = \omega_L$, the short circuit current is very high and it is only limited by resistance of the switching circuit.

$$|I_{sc}| = \frac{|V_s(j\omega)| C \omega}{\left(1 - \frac{\omega^2}{\omega_L^2}\right)}$$

Inherent current limit characteristics is sometimes desirable in converter design because the maximum converter current is limited and fast electronic circuits are not necessary to limit the peak current during a fault or at start up. It can be observed from the above equation that a small deviation from the resonant frequency can limit the short circuit current to a safe limit while considerable power transferred to the secondary.

4.5 BASIC CIRCUIT SIMULATION

Using an electronic circuit simulator, the simplified schematic of the circuit of the prototype that has been illustrated in Figure 4.6 was simulated. A sinusoidal waveform (V3) equal to 153V rms has been used for simulation that is similar to the nominal fundamental voltage of a half-bridge converter.

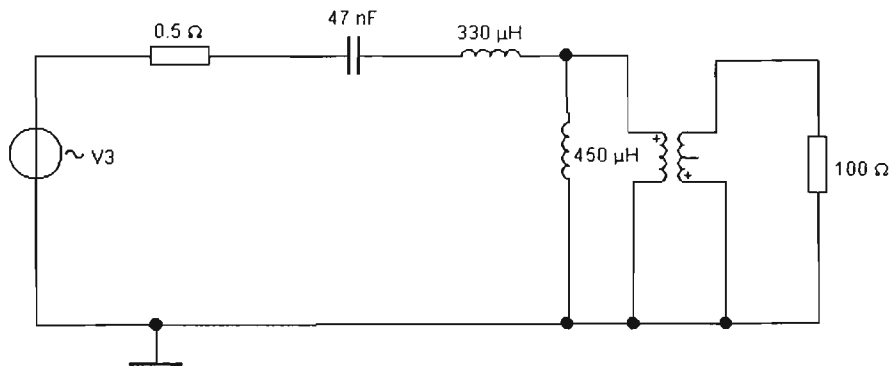


Figure 4.6 Simplified schematic of the prototype transformer.

In this figure, the model of the prototype transformer consists of an ideal transformer with $n_1:n_2$ primary and secondary winding turns ratio with the leakage inductance L_L and the magnetising inductance L_m transferred to the primary side. In the prototype $L_m=450\mu\text{H}$ and $L_L = 300\mu\text{H}$. The equivalent series resistance of the primary and secondary windings is $R_s=0.5$ ohm and the resonant capacitor is $C=47\text{nF}$.

With $n_1=n_2$, the ac analysis for $R=84-420$ ohms ($Q=1-5$) in increments of 84 ohm are illustrated in Figure 4.7 which is similar to the solution of Equation 4.5 by Matlab that has been illustrated in Figure 4.4.

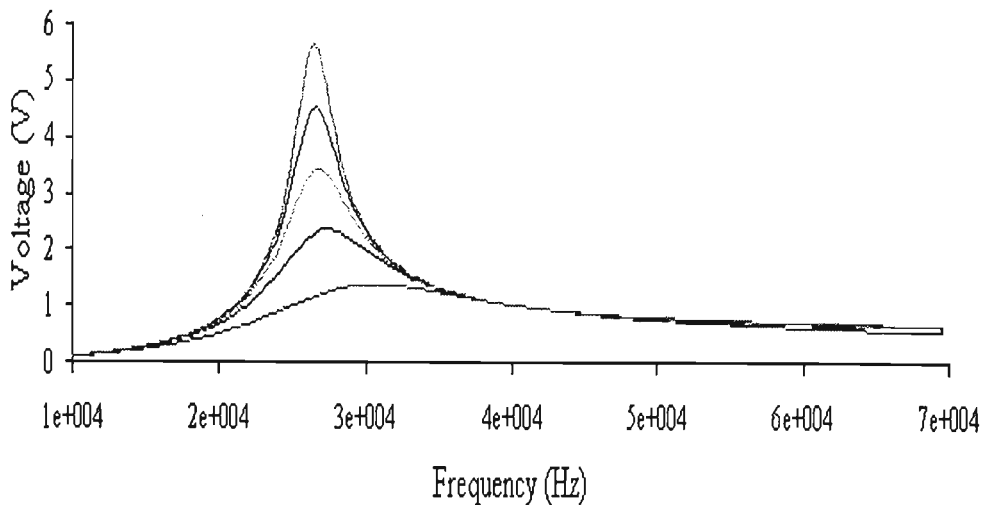


Figure 4.7 Ac analysis of the circuit of Figure 4.6 for $Q=1-5$.

The transient response for 100usec interval are illustrated in Figures 4.8-4.11 for frequencies below $f_L(\omega_L/2\pi)$, close to f_L and above f_L (25, 40 and 55kHz) and $R=8.4\Omega$ ($Q=0.1$) to $R=420\Omega$ ($Q=5$). From these figures, it can be concluded that for $Q>1$ a voltage gain larger than unity is associated with the circuit of Figure 4.6 if the operating frequency is close to ω_t . However, for low values of Q or $R<10\Omega$, a close to unity voltage gain is achieved only if the operating frequency is close to the f_L . For these Q values, operating above or below f_L results in attenuation in the output voltage. In Figures 4.8-4.11, the corresponding waveform can be found from the period or peak of the waveform (i.e. 26kHz waveform has two peaks).

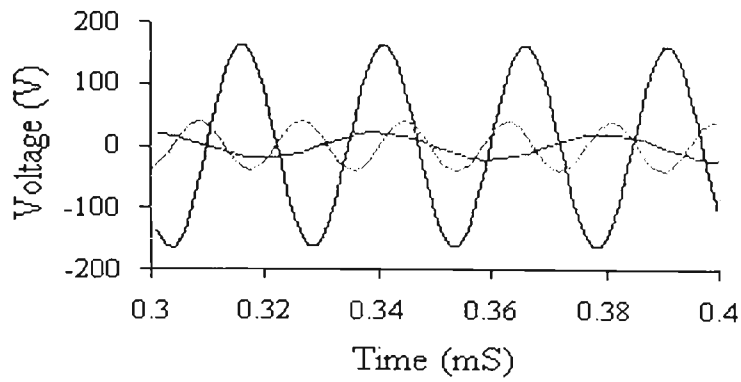


Figure 4.8 Transient response of the Figure 4.6 for $Q=0.1$ and $f_L=25, 40$ and 55 kHz.

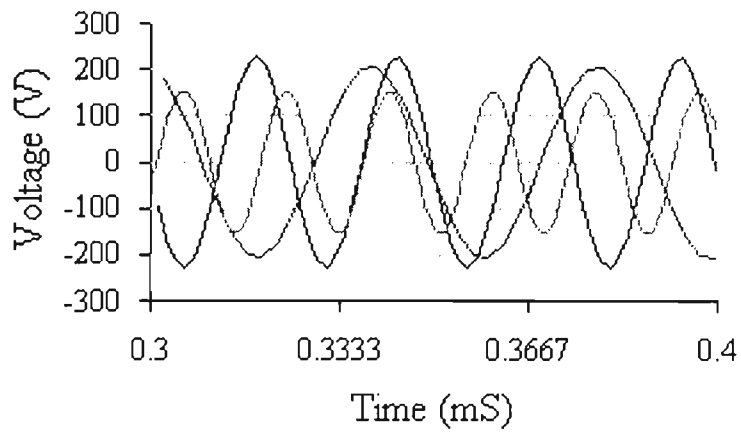


Figure 4.9 Transient response of the Figure 4.6 for $Q=1$ and $f_L=25, 40$ and 55 kHz.

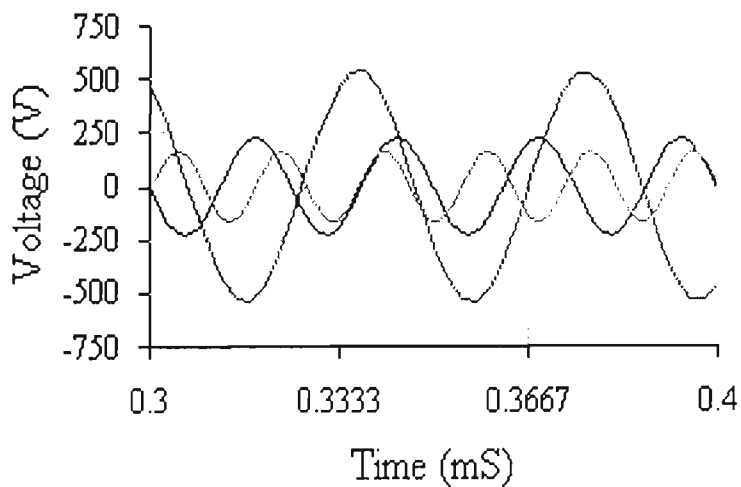


Figure 4.10 Transient response of the Figure 4.6 for $Q=3$ and $f_L=25, 40$ and 55 kHz.

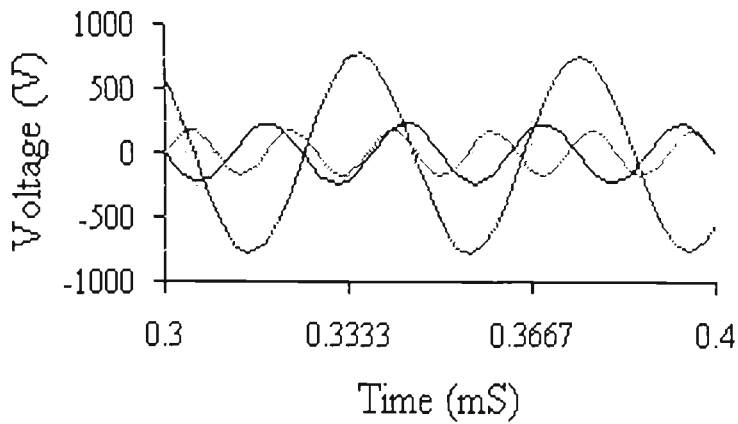


Figure 4.11 Transient response of the Figure 4.6 for $Q=5$ and f_L , 40 and 55 kHz.

4.5.1 Half-Bridge Circuit Simulation And Experimental Results

So far the simulation of the basic circuit has been based on the half-bridge converter fundamental component of the voltage and current and the effect of harmonics have been ignored. In this section the simulation of the circuit used in experiment is illustrated. The simplified circuit of the half-bridge converter is illustrated in Figure 4.12. The circuit parameters are as before but the ac voltage source is replaced with switches and dc voltage source simulating a half-bridge circuit.

For safety reasons experimental results were obtained at low voltage particularly when isolation transformer and variac were not available for isolating the electronic circuit boards from safety earth.

Simulation was unstable and 1 ohm resistor had to be used in high voltage side. Another one ohm resistor was required to measure the primary current of the

transformer in simulation. Parameters of interest are transformer current and load voltage.

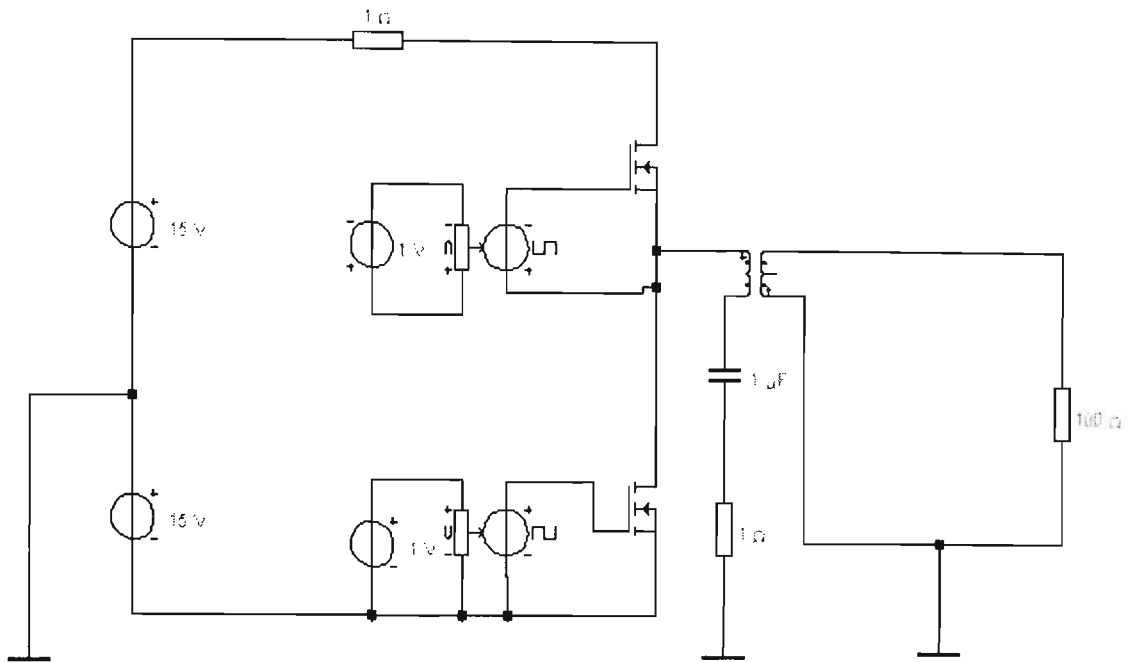
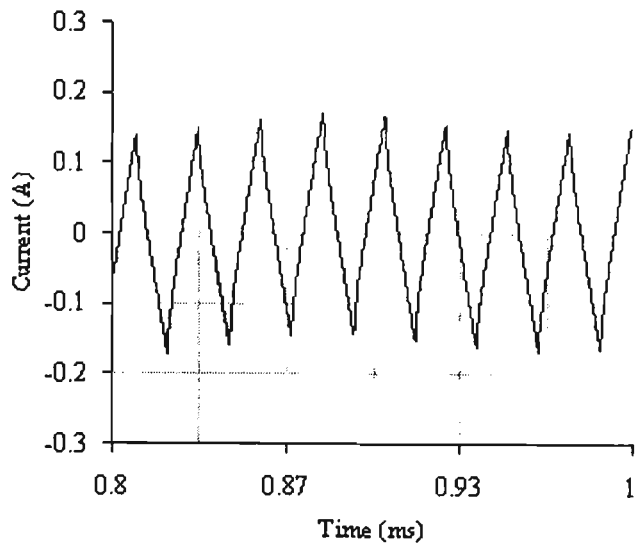


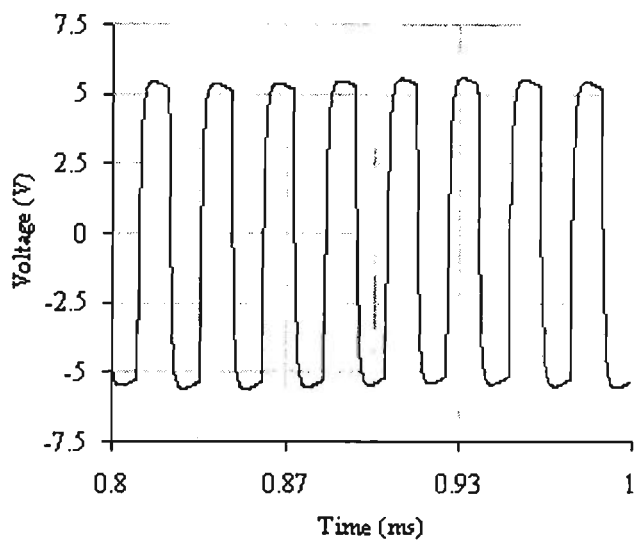
Figure 4. 12. Half-bridge circuit used in simulation.

The simulation transient analysis and the experimental results for this circuit are shown in Figure 4.12-4.16. As illustrated in these results, the waveform of the load resistance voltage is like rectangular pulses with large rise and fall time and the transformer current is triangular waveform in case of non-resonant operational mode. However, the waveforms change toward a sinusoidal shape when the circuit operates in resonant mode because of the resonant nature of the circuit.

In the resonant case, the 1 microfarad capacitor acts as a dc blocking capacitor. When its value is changed to resonant capacitor value it acts as a resonant capacitor. For the non-resonant case the value of the capacitor is increased and this capacitor only acts as dc blocking capacitor.

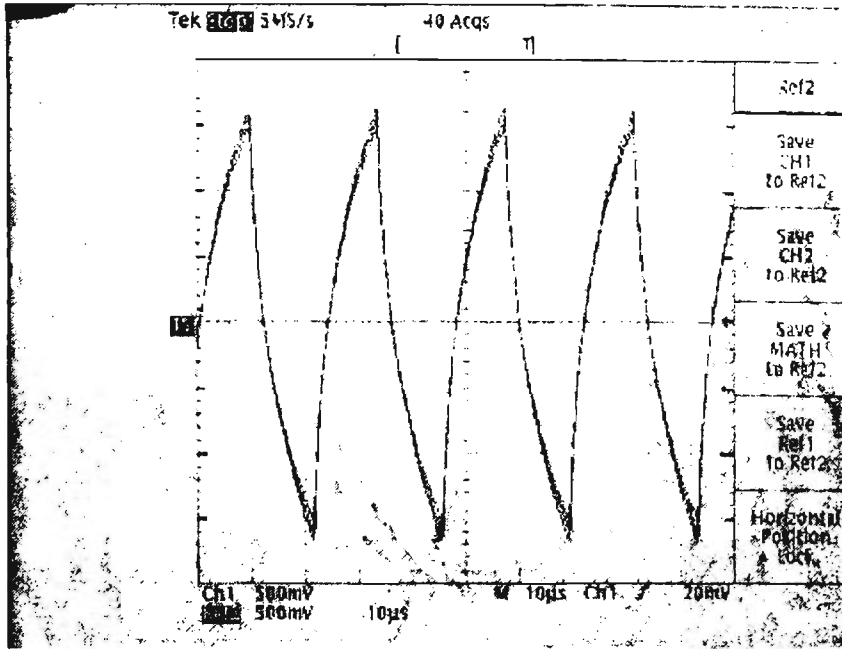


a)

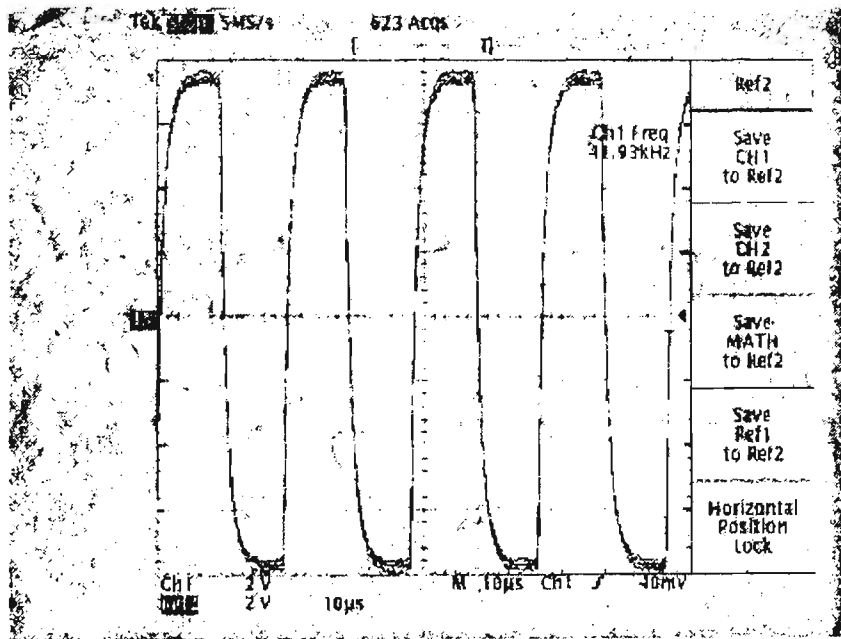


b)

Figure 4. 13. Primary winding current of the transformer a), and the load voltage b), non-resonant circuit, simulation result.

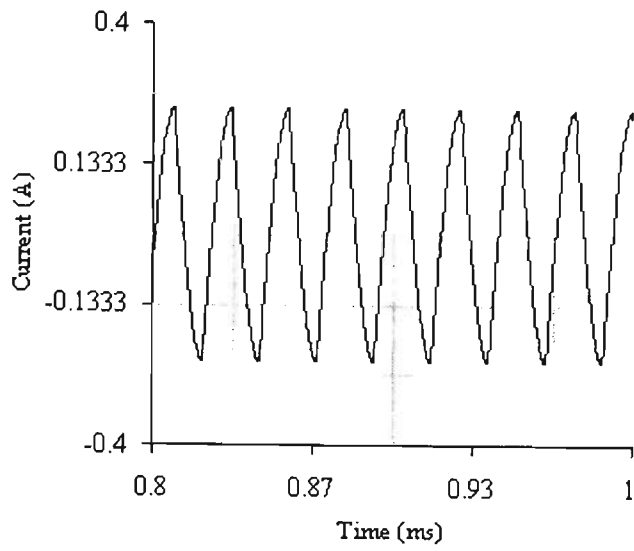


a) 85.1mA/Volts, 0.5V/Div.

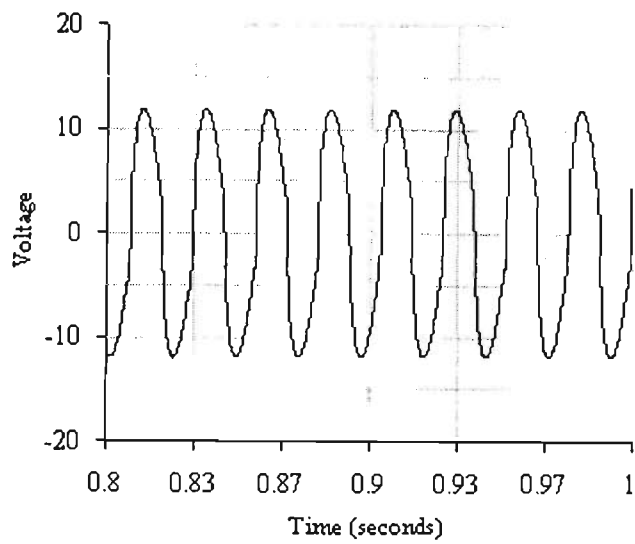


b) 2V/Div.

Figure 4.14 Primary winding current of the transformer a), and the load voltage b), non-resonant circuit, experimental result.

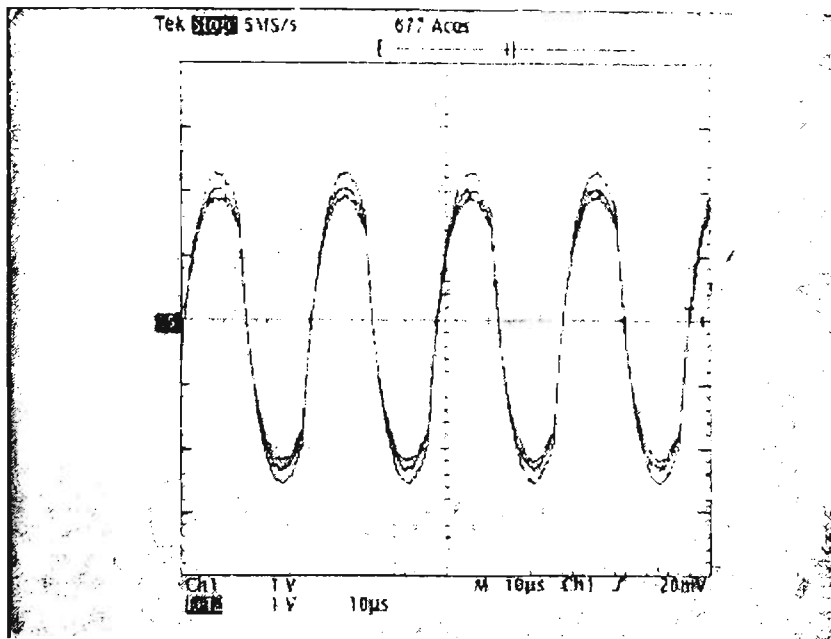


a)

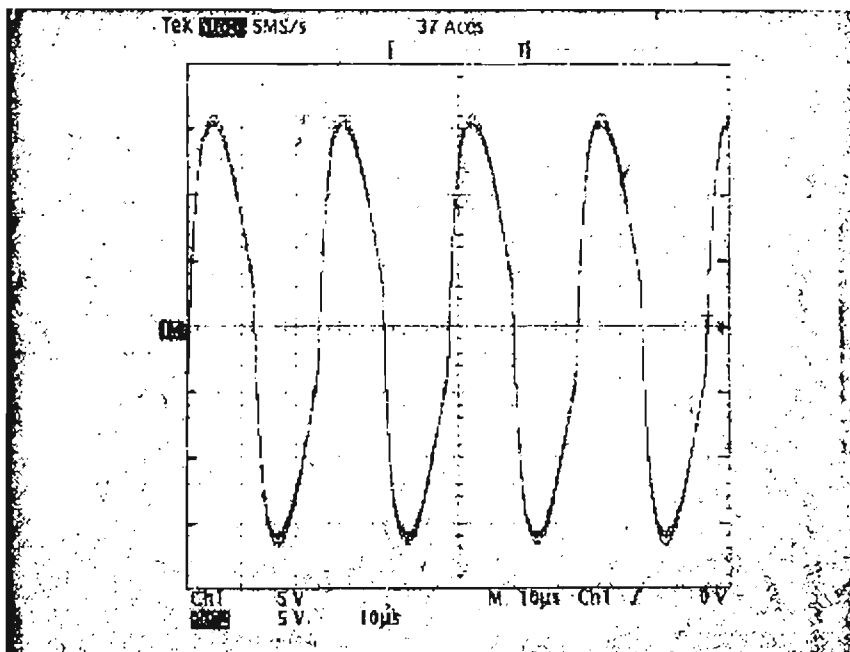


b)

Figure 4. 15 Primary winding current of the transformer a), and the load voltage b), resonant circuit, simulation result.



a) 85.1mA/V, 1V/Div.



b) 5V/Div.

Figure 4.16 Primary winding current of the transformer a), and the load voltage b), resonant circuit, experimental result.

Current of the transformer was measured with a current transformer with 1:40 ratio and across a 470 ohm resistor hence one volt across the resistor corresponds to $40/470 = 0.0851\text{A}$ or 85.1 mA transformer current. To calculate the current only multiplication of the voltage by 85.1mA is required for scaling. For example for Figure 4.14a, the peak transformer current is 1.5 Volts (3 Div.) multiplied by 85.1mA or 127.6mA that is similar to simulation value in Figure 4.13a.

These results show that the experimental results are similar to the simulation results and the circuit performance that was predicted by two method of driving characteristic equation and circuit simulation are correct. The schematics of the converter and the motor drive section have been illustrated in Appendix B.

4.6 SUMMARY

In this chapter the requirements of converting power from a stationary side to a rotary side by means of a transformer was described. Because the winding of core of the transformer are separated the leakage inductance is high and magnetisation inductance is low. Running the transformer in resonance with a capacitor reduces the effect of leakage inductance and reducing the airgap increases the magnetisation inductance.

In general, a design methodology can be employed based on the following parameter definitions:

1. Define the required power level and the supply voltage/current requirement.
2. Define the physical size of the enclosure and the cooling method.
3. Select the type of the transformer based of the estimated core and copper losses.
4. If the power levels are low, select non-resonant method.

5. If the power levels are high, select a resonant mode.
6. Select an operating frequency and fixture.
7. Select an airgap and the tolerances.
8. Estimate and measure the leakage and magnetisation inductance and the tolerances.
9. For resonant mode, select high secondary voltage and ω_r resonant frequency (high Q) or select low secondary voltage and ω_L resonant frequency (low Q). For the winding of the rotor, a high secondary winding voltage requires many turns with low current and series connection between the poles. A low secondary winding voltage requires lower turns with higher currents and parallel connection of the rotor poles. Usually, a very high current/low voltage power conversion in the secondary is more troublesome than high voltage/low current power conversion because of the transformer copper losses.
10. Change the design parameters like turns ratio and wire size to minimise core and copper losses.
11. Select the Q of the circuit and the value of the capacitance.
12. Design the variable frequency controller to change the power levels that can be transferred to the rotor winding by changing the operating frequency.

In this design procedure the details of the design have not been discussed. These details are like the fault protection circuits, the details of the cooling system, short circuit level and the type of the converter (i.e. voltage mode vs current mode).

CHAPTER 5

SENSORLESS SPEED/POSITION DETECTION

5.1 INTRODUCTION

In Chapter 4 the basic requirements of power induction from the primary to secondary of the transformer with high leakage inductance was described. In this section the method used for sensorless detection of the rotor position with respect to stator is described. In this method, by measuring and processing the transformer primary current the position of the rotor with respect to stator is calculated and from the rate of change of the angular position, the speed of the rotor is also calculated. Because the position estimation method operates based on the absolute position of the rotor with respect to stator, the commutation pulses for driving the stator winding can be generated. The principle of the operation of the sensorless speed/position detection were described in Chapter 3. In the following sections, the details of the sensorless speed/position algorithm are described.

5.2 PEAK DETECTOR CIRCUIT

The transformer used for the conversion of the power from the primary to the secondary is of RM series from Philips. The shape of this transformer has been illustrated in Figure 3.3. Because the transformer has different magnetisation inductance at different angular position between the primary core with respect to the secondary core, the position of the rotor with respect to the stator can be calculated. The magnetisation current variation results in a triangular waveform in the transformer primary winding (Figure 3.5) that can be amplified and used to detect the rotor speed and position.

In practice, the transformer current is converted to a dc voltage as shown in the circuit of Figure 3.4. This circuit is basically a peak detector. Restating the calculation of the peak-detector circuit, the transformer current can be converted to voltage V_o and is equal to:

$$V_o = \frac{I_m R_1}{N_1 - V_d} \quad \text{for} \quad R_2 C_1 \gg 1/f_o$$

where

I_m = Peak primary winding current of the transformer

N_1 = Current transformer secondary turns

V_d = Diode forward voltage drop

f_o = Operating frequency

There is a dc offset due to the current in the load R_L and no information about the rotor position exists in this value. However, the triangular ripple has all of the data about the rotor position. This ripple voltage must be separated from the dc voltage and amplified for maximum dynamic range. For a drive system operating from 50 rpm to 3000 rpm, the frequency of the ripple varies from 2 Hz to 100 Hz. So a dc amplifier is required to amplify this triangular waveform. Figure 3.6 is the block diagram of the rotor position detection system based on a high speed Digital Signal Processor TMS320C25 DSP.

The commutation pulses can also generated from the information about the relative position of the ferrite cores and based on the position of the magnetic poles of the rotor. There is a phase shift between the control pulses and the triangle signal that can be adjusted in software. During the motor operation, the DSP continuously samples the transformer primary current. At the beginning a value is assumed for L_{max} and L_{min} based on the design criteria of the transformer.

These values are used to predict the transformer current. The relation between θ , the angular position of the rotor and transformer primary winding current has to be calculated and commutation pulses will be generated based on the number of phases and poles. After the motor starts, values of I_{\max} and I_{\min} corresponding to L_{\min} and L_{\max} are measured and calculated dynamically for fine tuning the commutation pulses.

5.3 METHOD

By measuring the primary winding current of the transformer (stationary core) the position and the speed of the rotor can be detected. The equation governing the relation between the current and the magnetisation inductance $L_m(\theta)$ is $v(t)=i(t).z(\theta)$ where v is the source voltage from the converter and $z(\theta)$ is the input impedance of the circuit of the Figure 3.7 and is defined by:

$$Z(\theta) = \frac{L_L S(R + L_m(\theta)S) + RL_m(\theta)S}{R + L_m(\theta)S} \quad \text{Equation 5.1}$$

In Equation 5.1, assuming the rotor winding resistance is R_w then:

$$R = \left(\frac{n_1}{n_2} \right)^2 R_w$$

Hence,

$$I(\theta) = \frac{V(S)}{\frac{L_L S(R + L_m(\theta)S) + RL_m(\theta)S}{R + L_m(\theta)S}} \quad \text{Equation 5.2}$$

The variation of the transformer current with respect to the magnetisation inductance is:

$$\frac{dI}{dL_m} = \frac{-V(S)R^2S}{L_m(\theta)S((R + L_L S) + RL_L S)^2} \quad \text{Equation 5.3}$$

Also

$$\frac{dI}{dT} = \frac{dI}{dL_m(\theta)} \times \frac{dL_m(\theta)}{d\theta} \times \frac{d\theta}{dT} \quad \text{Equation 5.4}$$

Where T is the DSP data acquisition sampling time. Combining Equation 5.2, Equation 5.3, and Equation 5.4,

$$\frac{dI}{dT} = k \frac{-V(S)R^2S}{L_m(\theta)S(R + L_L S) + RL_L S)^2} \times \frac{d\theta}{dT} \quad \text{Equation 5.5}$$

The term $d\theta/dT$ is proportional to the angular velocity of the rotor and k is the differential of the inductance L_m with respect to θ and from Equation 3.1 is equal to:

$$k = \begin{cases} \frac{-2}{\pi}(L_{max} - L_{min}) & \text{for } 0 \leq \theta < \frac{\pi}{2} \\ \frac{2}{\pi}(L_{max} - L_{min}) & \text{for } \frac{\pi}{2} \leq \theta \leq \pi \end{cases} \quad \text{Equation 5.6}$$

In practice, dI/dT is the change in the measured current at two sampling intervals. The value of k is known and its sign can be determined at anytime because the controller can detect the rate of change of the primary winding current by

evaluating the current samples. Hence, the angular velocity of the rotor $\omega=d\theta/dt$ can be calculated by solving the following differential equation:

$$k_2 \dot{\theta} + \frac{2\Delta L}{\pi} \theta - k_1 L_{\max} = 0 \quad \text{Equation 5.7}$$

Where

$$k_1 = \frac{dI}{dT}, \quad k_2 = \frac{-V(S)R^2S}{(S^2L_L + RS + L_LSR)^2} \times \frac{2\Delta L}{\pi}, \quad \text{and } \Delta L = L_{\max} - L_{\min}$$

The term dI/dT represents the variation of the transformer current for a given load resistance R . In the DSP algorithm $dI=I_2-I_1$ and $dT=T_2-T_1$ and they correspond to the sampled current at two time intervals. Hence, the parameter dI/dT is known and Equation 5.7 becomes a first order differential equation of θ . From Equation 5.2 if $R=\infty$ then

$$I(S) = \frac{V(S)}{(L_L + L_m(\theta))S}$$

and by replacing $L_m(\theta)$ from Equation 3.1, the relation between the transformer current and the position of the rotor can be calculated from:

$$I(S) = \frac{V(S)}{[L_L + [(L_{\max} - L_{\min}) \frac{\pi - 2\theta}{\pi} + L_{\min}]]S} \quad \text{Equation 5. 8}$$

Also for special case where $R=\infty$ (no load) the variation of current is inversely proportional to the angular velocity ω . This is illustrated from Equation 5.5 when $R \rightarrow \infty$ or differentiating of $I(S)$ versus θ and combining with Equation 5.4:

$$\frac{dI}{dT} = \frac{-V(S)}{S(L_m + L_L)^2 k \omega}$$

Equation 5.9

This equation indicates that by measuring the transformer current rate of change the speed of the rotor can be calculated.

5.4 SOLUTION

MATLAB program can be used to calculate the maximum transformer current variation for different rotor position. The solution to differential equation 5.7 will not be necessary as the values for the rotor position can be obtained from a look-up table after the maximum and minimum of the triangular waveform (Figure 3.5) are obtained.

MATLAB programs for calculation of the maximum variation of the transformer current as a result of magnetisation changes are given in Appendix D. With a given transformer parameter described in Section 4.4.2 and various load resistances, the variation of the primary winding transformer current has been plotted in Figure 5.1. In this figure, for a load resistance equal to the impedance of L_L or 84 ohms, for the given transformer parameters, the variation of the transformer current with respect to the variation of the magnetisation inductance L_m is positive. For effective resistances above 84 ohms the variation of the transformer current is negative.

The higher is the variation of the transformer current with respect to variation of the magnetisation current, the better is the speed/position detection. As illustrated in Figure 5.1 the variation of the transformer current due to variation of the magnetisation inductance is very small because of low load resistance values. Later on it will be illustrated that the variation of the current is higher for higher

effective load resistance. The effective load resistance is the rotor winding resistance transferred to primary side. For instance if the rotor winding resistance of one pole is 1 ohm with 70:50 turns ratio R will be $70^2/50^2=1.96$ ohms. In practice the rotor winding is multiplied by number of poles if they are connected in series.

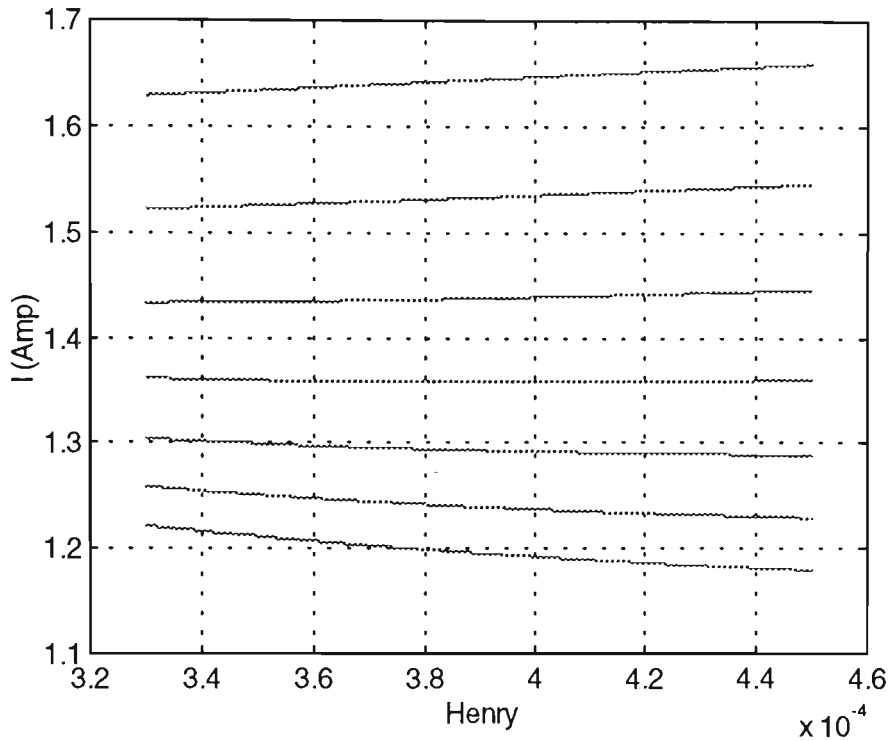


Figure 5. 1 Primary winding current vs magnetisation inductance L_m for various effective resistance from 40-100 (highest to lowest) ohms with increments of 10 ohms.

Figure 5.2-5.4 illustrates the variation of transformer primary winding current for different effective load resistances. From Figure 5.2 the variation of the transformer current with variation of L_m is $1.978-1.971=0.006A$. It means that if the current transducer has a 1:1 ratio the amplitude of the triangular waveform is about 6mA compared with 1.97A total transformer primary current. This accounts for 0.3% of the current which is small and hence an amplifier is required. If the analogue-digital converter (ADC) has a voltage range of 10 volts then for a full-

scale signal detection an amplifier with the transimpedance of $10\text{V}/6\text{mA}=1.67\text{ k}\Omega$ is required to give a peak-peak triangular waveform of 10V.

In ordinary transformers, as the magnetisation current increases, the primary winding current decreases. In non-resonant circuit the same relationship exists for high load value resistance. However, for low load resistance because of the leakage inductance the rate of change of current is positive (Figure 5.2) but the change in current is very low. In resonant case because of the shift from natural frequency of the circuit for high Q circuits, large variations in transformer current can occur with positive or negative rate of change.

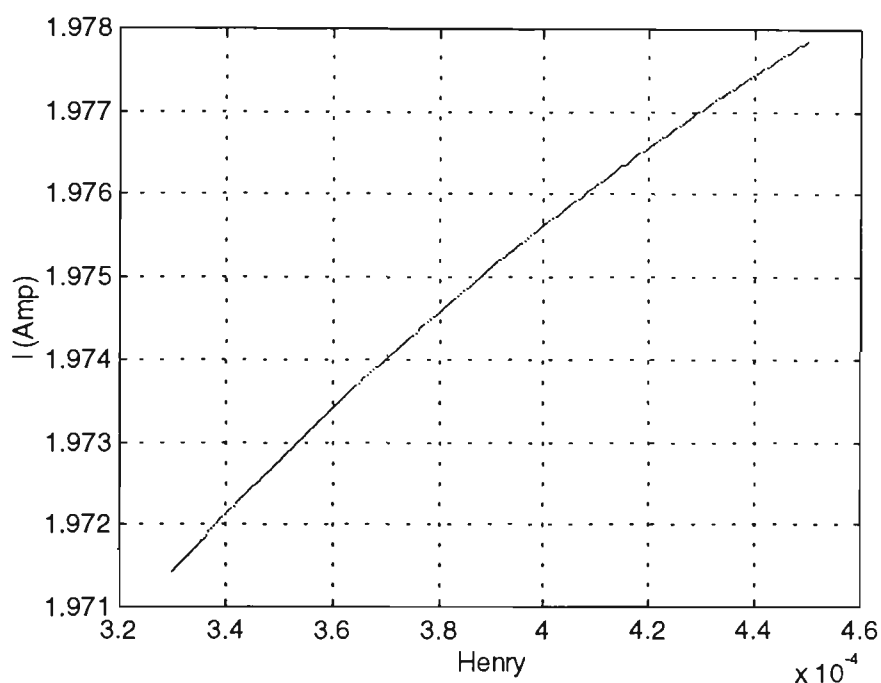


Figure 5. 2 Variation of the transformer current vs L_m for $R=10$ ohms.

In Figure 5.3, the variation of transformer current for 100 ohms effective load resistance has been illustrated. In this figure the variation of the transformer current is $1.22-1.18=0.04\text{A}$ or nearly 6.7 times more than the case when $R=10$ ohms. This current accounts for $40\text{mA}/1.2\text{A}=0.033$ or 3.3% of the total current that is 10 times the case when $R=10$ ohms. For 10V peak-peak triangular

waveform at the input of the ADC waveform the required transimpedance is only 250 ohm.

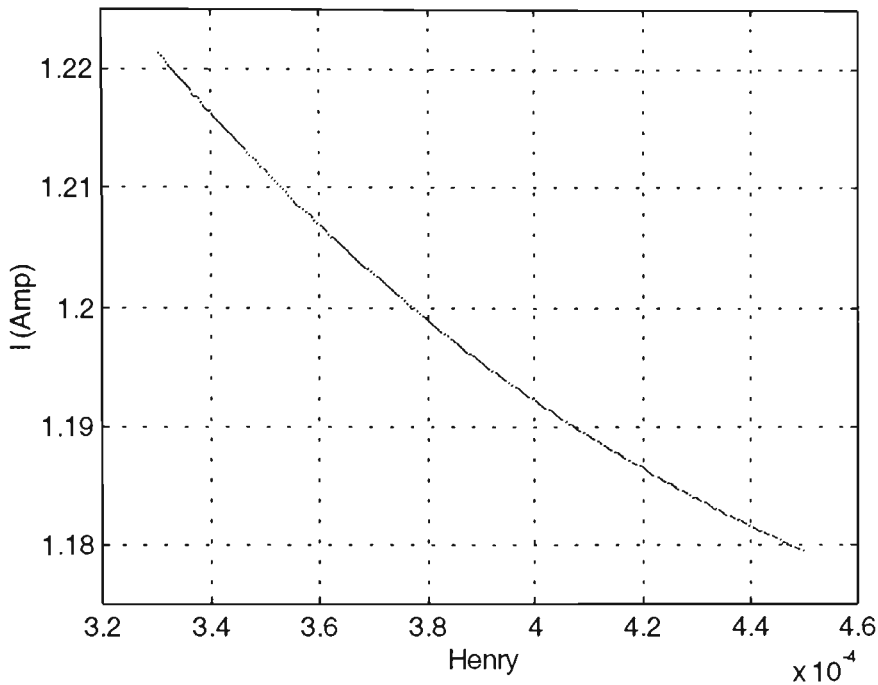


Figure 5. 3 Variation of the transformer current vs L_m for $R=100$ ohms.

Figure 5.4 illustrates the variation of the transformer current vs magnetisation inductance for $R=1000$ ohms. In this case, $\Delta I=0.18A$ or about 20% of the total current of the transformer with transimpedance of 56 ohms. This comparison demonstrates that the detection of the rotor position with detection of the magnetisation current variation is best suited when the rotor winding resistance is high. The trade off is the amount of power that is converted to the secondary that will be considerably less in the case of $R=1000$ ohms compared with the case when $R=100$ ohms. With the same transformer parameter, in Section 4.4.2 it was illustrated that for a given supply voltage when R is 106.2 ohms the maximum power is delivered to the load. Hence, in this case the choice of rotor winding selection is 106.2 ohms if the maximum power (147VA) needs to be converted to the secondary.

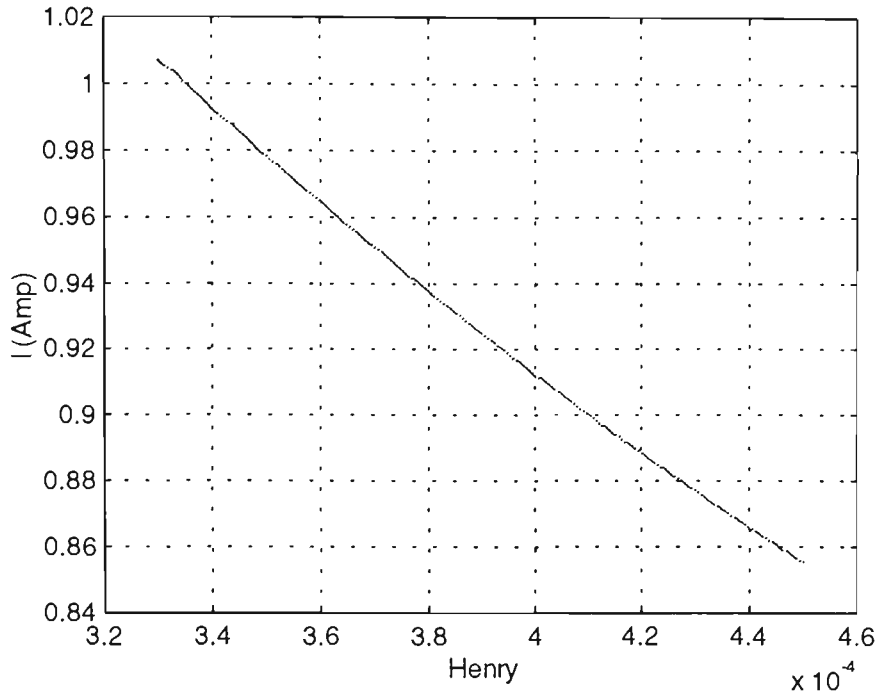


Figure 5. 4 Variation of the transformer current vs L_m for $R=1000$ ohms.

This discussion in this section is only an illustration about the sensorless operation and the values described are example and can vary for different transformer and motors. Also when a motor with an airgap flux density similar to that of a ferrite magnet is required, the maximum power conversion might not be very critical in a given design and hence higher resistance values for the rotor can be selected.

The discussion in this section can be extended to the design of a sensor based on variable inductance for detection of position when power need not to be converted. In this case replacing the effective resistance with an open circuit will give the maximum variation of the current with respect to angular rotor position.

5.5 COMMUTATION PULSE GENERATION

The variation of L_m with respect to the angular position θ is linear and hence the position detection can be simplified by re-scaling the above graphs for different

angular position. For example, for $\theta=0^\circ$, $L_m = 450\mu\text{H}$ and for $\theta=90^\circ$, $L_m=330\mu\text{H}$ hence the angular position $\theta=45^\circ$ occurs when $L_m=390\mu\text{H}$.

By measuring the transformer current and calculating the inductance value from the current, the angular position θ can be calculated. With this method, the electrical position of the rotor poles with respect to the electrical position of stator poles is identified. With pole numbers and phase numbers known in a design, the commutation pulses can be generated only by measuring the transformer current by an ADC, calculating L_m and θ , and setting the output port of the DSP.

5.6 VARIABLE TORQUE ADJUSTMENT PROBLEM

The speed of the motor can be changed by changing the frequency of the stator winding drive voltage. The torque of the motor can be separately changed by changing the magnetic field or maintaining the operating frequency and increasing the stator voltage. Changing the airgap flux can be achieved by increasing the current in the stator winding. In this case, the total current in the rotor winding is variable and the detection of the small changes of the transformer current becomes difficult. For instance, if the rotor winding current for a given torque is 2A, to double the torque the rotor winding current becomes 4A. Because the triangular ripple is only a few percent of the total current, the amplifier saturates due to a change in current that is much higher than its intended input signal (in mA range). The problem is due to the fact that the triangular waveform frequency is low (as low as 2Hz for 50rpm) and must be dc coupled to the amplifier. The current transducer cannot differentiate between the current from the load (rotor winding) and the magnetisation current. The solution to this problem is to level-shift the reference voltage that is used to adjust the rotor winding current and use the same control voltage to shift the reference of the amplifier. This method reduces if not eliminates the dc bias due to the load current variation with a dc amplifier with

variable dc offset adjustment. The schematic of the proposed circuit has been illustrated in Appendix B. Block diagram of the interconnection of amplifier with the resonant converter has been illustrated in Figure 3.6.

5.7 SPEED CALCULATION

The speed of the motor can be calculated by comparing the rate of change of the current values in two samples in a defined interval. For instance for the transformer parameters of Figure 5.3 and for two samples that have been taken in 10msec interval, if $I_1=1.18$ and $I_2=1.22A$ (maximum and minimum values).

$\Delta L=(450-330)\times 1e-6$, $\Delta I=0.04mA$, $\Delta T=1e-3$ Sec, $\Delta\theta=\pi/2$ rad, and hence from Equation 5.4, the angular velocity of the rotor can be calculated:

$$\omega = \frac{\Delta\theta}{\Delta T} = \frac{\frac{\pi}{2}}{10E-3} = 157 \text{ Rad/sec}$$

Hence the speed is $(157 \times 60)/(2\pi) = 1500$ rpm. In this example, the maximum and minimum values of L_m have been selected that results for maximum angular position difference of 90° . The gain of the amplifier will cancel out in this calculation. In practice, the values of different transformer currents for different angular positions and for a given effective resistance R (rotor winding resistance transferred to primary) can be calculated from a look-up table. Although a DSP processor has sufficient calculation power to calculate the speed and position based on the equations described in this chapter, a cheaper microcontroller can be used by aid of look-up tables for speed/position calculation.

5.8 RESONANT CIRCUIT

In this section sensorless detection of the resonant circuit of Figure 4.3 will be discussed. As discussed in Chapter 4, the resonant circuit resulted in higher power levels to be induced to the secondary by reducing the effect of the leakage inductance. It is necessary to emphasize that the discussion in this section does not take into account that the rating of the transformer for heat and saturation and the rating of the switching transistors can exceed for case studies presented. The reason is that this discussion is not limited to the type of transformer used and bigger transformers can be used which can operate in acceptable operating temperature and current.

The MATLAB programs in Appendix D are used to calculate the transformer current at different conditions. The difference with non-resonant mode of operation is that by changing L_m , the natural resonance frequency of the circuit is also changes and in most cases larger variation is obtained by variation of L_m . There is no practical way and no benefit in differentiating the variation of current due to magnetisation inductance and/or change in natural resonant frequency of the circuit that contribute to transformer primary winding variation. The reason is that the parameter of interest is the change in current vs position.

Figure 5.5 illustrates the variation of transformer current due to variation of L_m for effective load resistances between 40-80 ohms.

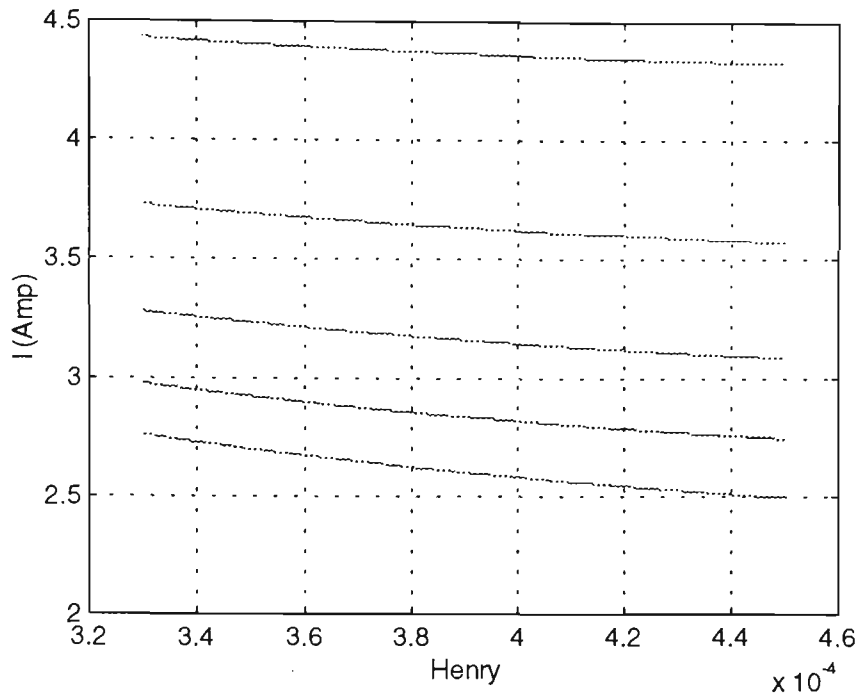


Figure 5. 5 Primary winding current vs magnetisation inductance L_m for various effective resistance from 40-80 (highest to lowest) ohms with increments of 10 ohms, resonant mode.

Comparing this figure with Figure 5.1 it can be noticed that the current levels are higher that is due to the use of the resonant method and neutralisation of the effect of L_L . Figures 5.6-5.8 illustrate the variation of the transformer current due to the variation of L_m for effective load resistance values, 10, 100 and 1000 ohms. In theses figures also the substantial increase in the transformer current is observed.

In Figure 5.6 it is illustrated that the transformer current can be increased to a level that can damage the transformer and the inverter and a current limiting is required. Also the variation of the current due to the variation of L_m has increased to 1.3% compared with 0.3% in case of non-resonant method.

The rate of change of the transformer current with respect to L_m for various operating conditions is usually negative when the effective load resistance is high. This is not a problem in the estimation of the position and speed because the

transformer parameters and the rotor winding resistance and hence the effective load resistance are usually known.

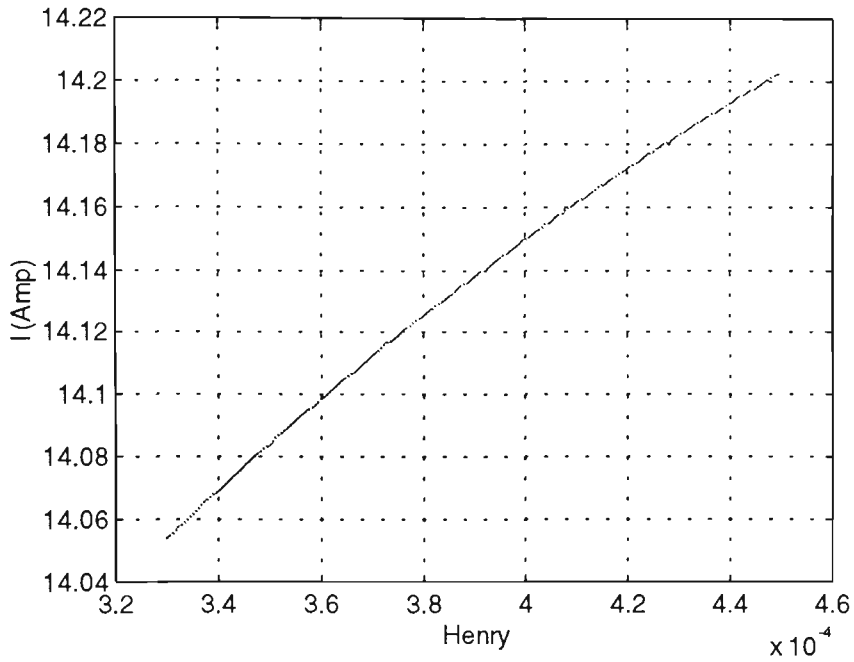


Figure 5. 6 Variation of the transformer current vs L_m for $R=10$ ohms, resonant mode.

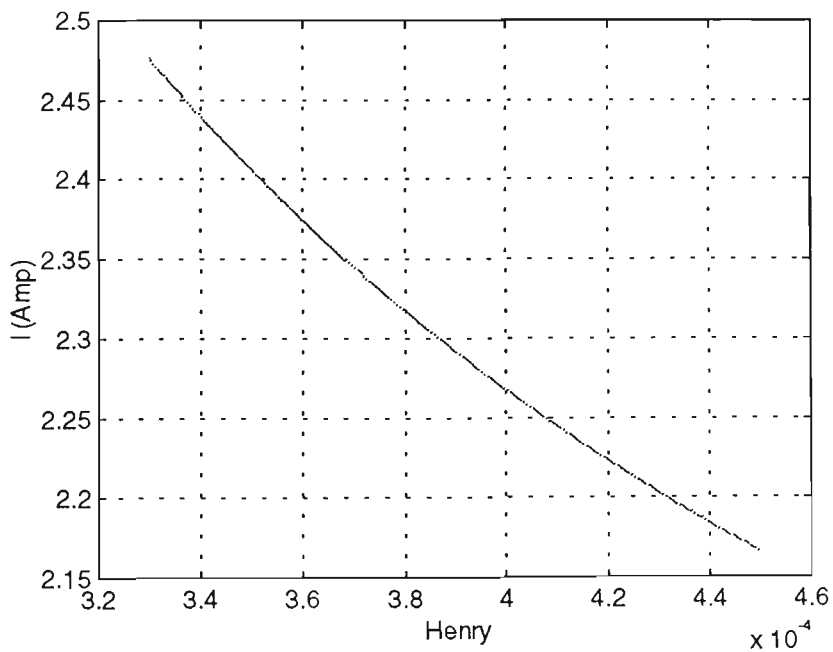


Figure 5. 7 Variation of the transformer current vs L_m for $R=100$ ohms, resonant mode.

In Chapter 4 the analysis of the resonant circuit was described in details. In that discussion it was demonstrated that there are two mode of operation in resonant mode. If the operating frequency is close to the resonant frequency ω_L , the resonant frequency of L_L and C, maximum power transfer occurs when the effective resistance R is low. In the second mode of operation, if the operating frequency is close to ω_t , the resonant frequency of C and an inductance equal to L_m+L_L maximum power transfer occurs when the effective load resistance R is high.

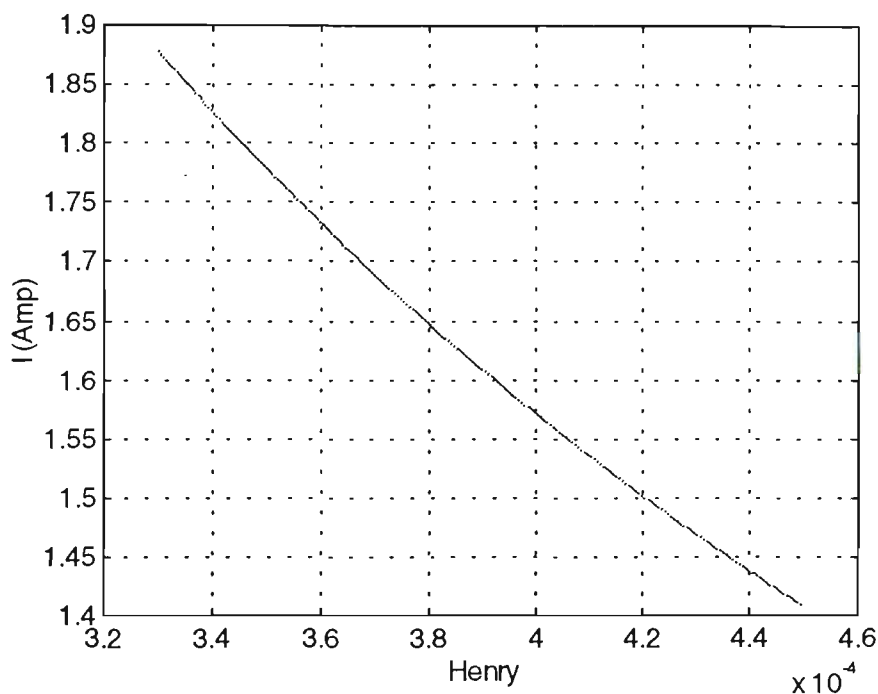


Figure 5. 8 Variation of the transformer current vs L_m for $R=1000$ ohms, resonant mode.

In Figures 5.1-5.8, the operating frequency was selected at ω_L that is 42kHz. Figure 5.9 illustrates the variation of the transformer current when the operating frequency is close to ω_t that is 26kHz. By comparing Figure 5.8 and Figure 5.9 it is illustrated that when the effective load resistance is high ($R=1000$ ohms), if the

operating frequency is ω_i , the power conversion is high. With variation of L_m , the transformer current varies approximately 6 fold when operating frequency is close to ω_i compared to only 0.35 when the operating frequency is close to ω_L . Higher converted power confirms the discussions in Chapter 4 about the operating frequency of the inverter for maximum power conversion.

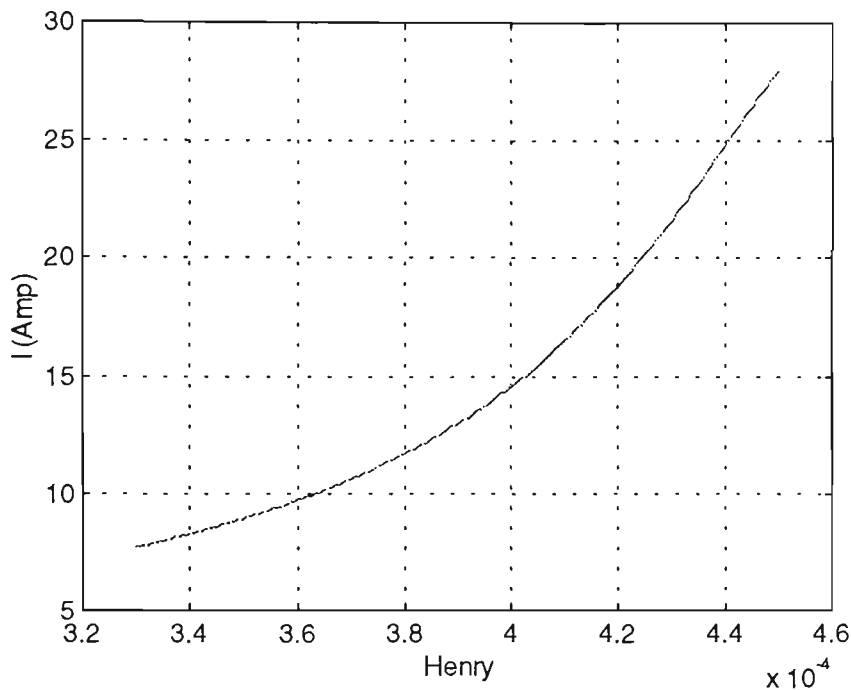


Figure 5. 9 Variation of the transformer current vs L_m for $R=1000$ ohms, resonant mode, operating frequency of 26kHz.

5.9 SUMMARY

In this chapter, the fundamental of sensorless speed and position detection was described. The calculation by MATLAB program indicates that operating at higher load resistance values result in higher variation of transformer primary current. The variation of the primary winding current of the transformer in all but one operational condition is minor and does not cause any ripple in the torque. But it generates enough variation that can be used to detect the position and speed of

the rotor. The exception is when the operating frequency is close to total resonant frequency ω_t in this case the variation of current in transformer current can be 6 times when L_m changes from minimum to maximum value. In this mode also the power delivery is maximum and a voltage higher than the supply voltage can be obtained that is not generally required in application related to the WRBM.

A variable rotor winding current with wide dynamic range is not generally desirable because the amplifier is a dc amplifier and any change in dc offset results in saturation of the amplifier. This is particularly problematic if the commutation pulses are generated by sensorless operation. This problem can be solved by simultaneous torque and amplifier adjustment to change the amplifier dc offset whenever the torque is changed.

The experiments regarding sensorless detection of speed were simulated by a triangular waveform and the commutation pulses for a 2-phase motor was generated with the DSP controller. The program for finding the maximum and minimums and commutation pulse generation has been illustrated in Appendix C.

CHAPTER 6

MOTOR DESIGN METHODS

6.1 INTRODUCTION

In this chapter, the fundamentals of Permanent Magnet Brushless Motor (PMBM) design are discussed. Two methods are common, Classical Method (CM) and Finite Element Analysis (FEA) method [63]. In CM, the electromagnetic equations related to the motor are calculated from the mechanical dimension of the motor by approximation. In FEA method, a graphical tool is used to draw exact motor dimension. The motor drawing is divided in sections called mesh and electromagnetic equations are applied to each mesh, then the overall performance of the motor is calculated by processing vector mathematics on the meshes.

In this chapter, each method is described in regard to the design of PMBM and then a particular motor lamination is selected that will be used throughout this work to compare the performance of a PMBM and a Wound Rotor Brushless Motor (WRBM).

6.2 COMMON DESIGN OBJECTIVE

There are design methodologies common in CM and FEA. In one design, the torque-speed requirement of the motor and an approximate enclosure is given, then the mechanical and winding specification are required to realise the motor design. In another approach, the lamination dimension is known and general rough design illustrates if the motor can be designed to comply with the required torque-speed specification. Then the number of poles, the rotor shape and the rotor winding are calculated. This method is generally the preferred method, because existing induction motor laminations that are produced in large quantities can be

used in order to reduce the cost of the design. This method is used throughout this chapter and next chapters so that:

- An existing lamination is used for low cost commercialisation.
- A design-based comparison can be made between different designs
- The cost of prototyping is minimised.

Following the above requirements, a single-phase induction motor (Figure 6.1) was selected with the following dimensions:

Stator inside diameter, ID = 82 mm

Stator outside diameter, OD = 140 mm

Number of slots, SN = 36

Depth of Slots DS = 17 mm

Width of slots WS = 8 mm

Teeth space TS = 2 mm

Teeth width = 5 mm

Length of lamination stack, L_{stk} = 30 mm

Lamination type = Commercial grade

In the prototype, the cage rotor of the motor was removed and a set of metal bars were welded. The shaft was machined to make the necessary route for the connection of the power conversion transformer to the rotor mounted electronics and winding. The objective of the prototyping was to evaluate the power induction from the stationary side to the rotary side and to investigate the performance in an environment with high permeability. The details of the motor and particularly the high frequency transformer construction will be described in Chapter 8.

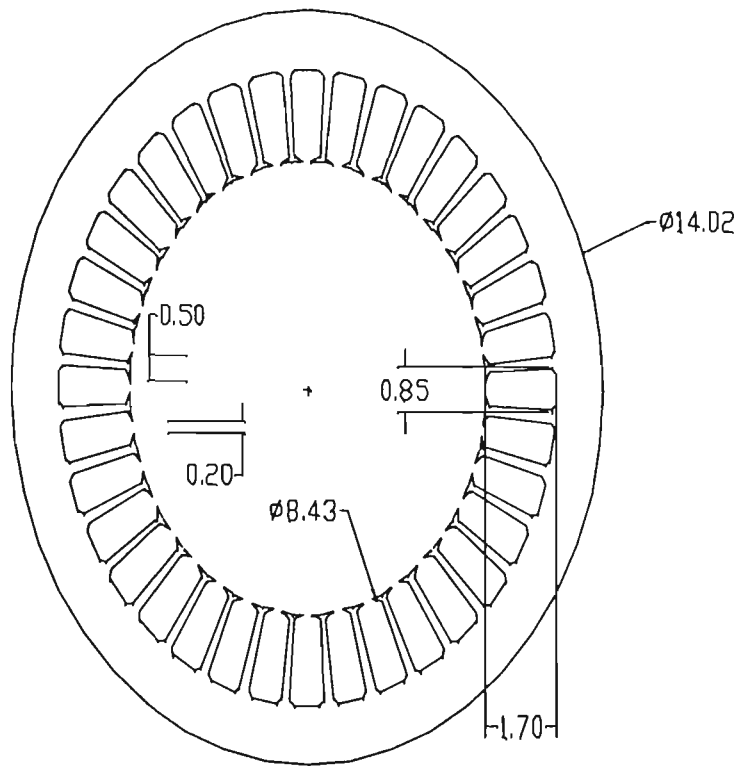


Figure 6. 1 Stator dimensions (in centimeter) for design of PMBM.

This stator will be used in all design steps discussed hereafter in order to meet the objectives that was discussed earlier in this section.

6.3 CLASSICAL DESIGN METHOD

Software programs have been developed for design of the PMBM motors that do not necessarily use FEA although they include FEA [63][85]. In these programs the main engine of the program is a calculator with graphical user interface. SPEED¹ is a program that is used to perform the motor design similar to an interactive calculator. It is supported by a database of different shapes that makes the design and development faster. But the annual subscription to access the database is relatively expensive.

¹ SPEED is the registered name of a software developed by Galskow University for motor design.

In this section, a step by step design procedure is explained that has been researched and developed by referring to publications in this field [63] [87]. During the design, the following subjects are discussed:

- The requirements of the motor drive system for domestic applications are restated and a specification is written as target specification.
- Properties of permanent magnets and different magnetic materials are discussed.
- The dimensions of the stator in Figure 6.1 are used to estimate the suitability of this motor to comply with the specification (it is also called sizing).
- Step by step procedure is introduced to design the winding, rotor and pole numbers with a given permanent magnet type.

The detailed design of the motor is given in Chapter 7 based on a permanent magnet selection and airgap flux. Then the rotor with the permanent magnet is replaced with a rotor with wound rotor of a WRBM. After the motor is designed with CM, the same design will be evaluated by FEA.

6.3.1 Motor Specification

In this section, the target specification is discussed. The objective of this work was to find an alternative for the existing motor drive system that is high performance and low cost for domestic and industrial applications.

In Chapter 2 the requirements of the ideal motor for use in domestic environment in particular and in industry in general was summarised. Although there are many applications with higher power than 500-1000W in household goods, this range was select for ease of prototyping and in order to compare different motor designs (i.e. PMBM and WRBM).

The requirement of the motor is tabulated in Table 6.1. This table basically represents the same findings that were presented in Chapter 2 without the details in order to proceed with approximate design first.

Table 6. 1 Preliminary specification of the variable speed drive system for domestic applications.

		Description
1	Power	Power rating 500-1000W
2	Drive type	Direct drive preferably, use different pulley ratio to increase torque
3	Torque	12 N.M. direct drive, 1 N.M. with pulley ²
4	Speed	50-1200 rpm direct drive, 800-12000 rpm with pulley ²
5	Efficiency	Above 80%
6	Cost	Comparable or less than PMBM

If the direct drive system cannot be achieved with the mechanical dimension outlined in Figure 6.1 a pulley can be added to increase the low speed torque. This matter will be discussed in details during the design, but at this stage having a direct drive is not assumed to be essential. Especially, when by adding pole numbers the ratio of the low speed torque and high speed can be changed at the expense of higher manufacturing cost.

² Refer to Table 2.1

6.3.2 Permanent Magnet Materials

In the design of PMBMs, different types of permanent magnets can be selected depending on the minimum torque requirement, the diameter of the motor, the operating temperature, the locked rotor condition and more important the cost of the motor.

Following are the parameters of a permanent magnet that need to be considered in design of a PMBM:

6.1.1.1 Remanence B_r

The value of flux density with no applied external field ($H=0$) is called remanence. Under identical parameters that will be discussed in the following sections, the higher is the B_r the better is the permanent magnet. Typical values for B_r are 1-1.3 Tesla for sintered N_d-F_e-B (Neodymium-Iron-Boron) at high levels to 0.35-0.43 Tesla at low levels for ferrite. Other materials like Alnico at 0.6-1.35 Tesla and sintered S_m-Co (Samarium-Cobalt) at 0.7-1.05 Tesla. Considering other parameters like temperature variation, coercive force, and maximum operation temperature, it seems that N_d-F_e-B is the most suitable magnet for motor applications despite that N_d-F_e-B is inferior to other types in some aspects. Another disadvantage of the N_d-F_e-B is its cost in comparison with Ferrite permanent magnets is high.

6.1.1.2 Temperature

Temperature affects permanent magnets by changing its magnetic remanence and/or intrinsic coercivity. Ferrites tend to irreversibly demagnetise at their lowest temperature limit and the N_d-F_e-B at their highest temperature limits. Samarium-

Cobalt (S_m -Co) can operate at temperatures up to 250°C. Alnico magnets operate even at higher temperatures. Curie Temperature is the temperature at which the magnetisation is reduced to zero. In case of N_d - F_e -Co and S_m -Co, the Curie temperature is lower than the temperature that these magnets change their characteristics. Hence, beyond the Curie temperature these magnetic materials lose their magnetisations permanently.

6.1.1.3 Magnet Energy Product

The value of $B_r H_k$ that is referred to $(BH)_{max}$ is sometimes used to evaluate permanent magnets. The $B_r H_k$ product is the value of remanence B_r multiplied by the knee value of the magnetising force and is a measure of flux generating with strength to withstand an external Magneto Motive Force (MMF).

In the design of PMBM, BH value must be considered in calculation of the maximum field that can be generate in any condition (usually fault condition) in order not to demagnetise the magnets.

6.1.1.4 Selection Of Magnets

Depending on the torque-speed requirement, assuming parameters like Curie temperature and demagnetisation are acceptable, magnets with different remanence can be selected to suit the design. For instance, if a direct drive system is designed and the outside diameter of the motor cannot be increased then a magnet with high remanence (N_d - F_e -B) is required. However, if the motor is required to operate at higher speeds and the torque at low speed is increased with the aid of pulley or gearbox, then a Ferrite type magnet can be used. In cases that large axial motors can be used, also Ferrite magnets can be used due to their low cost. As illustrated in Table 6.1, two choices of design exist to achieve the target specification, direct drive and pulley. For this reason, the choice of magnet

selection will be explored better when the detailed design of the motor is described in the following sections.

6.4 SIZING

Sizing is referred to the estimation of the motor dimension approximately for a given torque-speed requirement. Sizing is usually the first step in designing a motor or motor drive system. Due to saturation of iron at high magnetic field within a volume of iron, the maximum amount of torque generated in a motor depends on the diameter of the motor and the length of the lamination stacks. Also due to the temperature rating of insulation and Curie temperature of the permanent magnets, the amount of heat generated in a motor also depends on the volume of the motor and the rate of heat dissipation. Hence, two common terms have been defined in regard to motor design to quantify the amount of flux and heat generated in a motor, that is basically core/copper losses. The term used for estimation of the maximum flux is called magnetic loading and the term used for the maximum heat is called electric loading. A universal equation is used to define the torque generated in a motor based on its relation with electric and magnetic loading. This methodology has been used both in textbook references [63][85] and also journal publications [19] for design of PMBM. This method has been adapted and developed here to design the PMBM motor and WRBM with the same dimensions.

It is generally accepted that for micro-power to 20MW motors the following formula applies when calculating the maximum torque that can be delivered by a motor [19][63]:

$$T = \frac{\pi}{2} D_r^2 L_{stk} M_L E_L \quad \text{Equation 6. 1}$$

where

T = Output mechanical torque

D_r = Rotor diameter

L_{stk} = Rotor stack length

E_L = Electric loading

M_L = magnetic loading

6.4.1 Electric Loading

Electric loading is a measure of how much current a given motor can carry in its copper without exceeding the temperature rating of the motor and insulation.

Electric loading is expressed in terms of Amp/Meter and is:

$$E_L = \frac{\text{Total - amp - conductors}}{\text{Airgap - circumference}} = \frac{2mN_{ph}I}{\pi D_r} \quad \text{Equation 6. 2}$$

where:

m = Number of phases

N_{ph} = Number of conductors in a phase winding

I = Phase current

A typical E_L value for a small motor is about 10-20 kA/m.

6.4.2 Magnetic Loading

Magnetic loading M_L is a measure of how strong the airgap flux can be before saturation occurs in iron and is [19]:

$$M_L = \frac{\text{Average - flux}}{\text{Rotor - circumference}} = \frac{B_r}{1 + \mu_r \frac{L_g}{L_m}} \quad \text{Equation 6. 3}$$

Where

B_r = Permanent magnet remanence

μ_r = Recoil permeability

L_m = Magnet thickness

L_g = Airgap thickness

Typical values for μ_r is 1-2 and the ratio of L_m/L_g is about 4-8 that results in a typical magnetic loading 0.7-0.8 of the remanence flux density. The higher the ratio of L_m/L_g , the higher is the airgap flux but the more expensive is the cost of magnets.

A typical M_L value for small motor is about 0.5-1 Tesla. In slotted motors, the flux density in the teeth is twice as the airgap. Hence, to prevent the saturation of the iron, the airgap flux density is limited to 0.9T.

As an example, assuming $E_L=15000$ A/m and $M_L=0.7$ T, the torque generated by the motor with dimension illustrated in Figure 6.1 is:

$$T = \frac{\pi}{2} \times 0.082^2 \times 0.03 \times 15000 \times 0.7 = 3.3 \text{ N.M.}$$

It illustrates that with the motor dimensions selected, the motor cannot achieve 12 N.M. torque without the aid of pulley or gearbox.

Sizing can be achieved by similar method with different definitions:

TRV = Torque per unit rotor volume.

σ = Airgap shear stress that is the tangential force/unit of rotor surface area.

In general, Equation 6.1 can be re-written as:

$$T = K D_r^2 L_{stk} \quad \text{Equation 6. 4}$$

where K is the output co-efficient [63].

By definition,

$$TRV = \frac{\text{Torque}}{\text{Rotor - Volume}}$$

Hence as T in Equation 6.4 is proportional to the rotor volume, then:

$$TRV = 2\sigma \quad \text{and} \quad K = \frac{\pi}{2}\sigma \quad \text{and} \quad K = \frac{\pi}{4}TRV$$

Different types of motors, depending on their cooling have different TRV, K or σ .

Table 6.2 illustrates some typical values for different types of motors with different *TRV* values.

Table 6. 2 TRV values for different motors [63].

MOTOR TYPE	TRV, KN.m./m ³
<i>Small, totally enclosed (Ferrite)</i>	7-14
<i>Totally enclosed (N_d-F_e-B)</i>	14-42
<i>Integral-hp Industrial motors</i>	7-30
<i>High-performance servomotors</i>	15-50
<i>Aerospace machines</i>	30-75
<i>Large liquid-cooled machines</i>	100-250

With the values in Table 6.2, using ferrite and mid-point (10.5 kN.m./m³) *TRV* for small motors result in a motor with a torque equal to:

$$T = 0.785 \times TRV \times 0.082^2 \times 0.03 = 1.7 \text{ N.m.}$$

Using N_d-F_e-B and the mid-point (28 kN.m./m³) *TRV* results in a torque equal to:

$$T = 4.4 \text{ N.m.}$$

That is relatively similar to 3.3 N.m. calculated earlier. These figures are approximate and illustrate the best torque that can be achieved with a given rotor dimension. It is important to note that increasing the rotor diameter can increase the torque substantially due to square power of the diameter in the torque equation. In Chapter 2 it was illustrated that the torque generated by axial motors is proportional to the 3.5 power of the diameter. Hence, for many direct drive applications, an axial type motor is used.

It is clear that the motor selected cannot be used in a direct drive system to supply 12 N.m. torque. However, with a pulley, enough torque for a top-loading washing machine or other household appliances can be produced. Using pulley to increase torque is a cheap alternative for direct drive PMBM because ferrite permanent magnets can be used that are cheaper than Nd-F_e-B magnets.

6.4.3 Current Density

Another measure of how a motor is capable of current conduction without overheating is the current density. Current density J is defined as:

$$J = \frac{E_L}{\text{Fill_factor} \times \frac{\text{Slot_width}}{\text{Slot_pitch}} \times \text{Slot_dept}}$$

The current density simply illustrates the amount of current that can be packed in the slots. Fill-factor is constant that is related to how packed the winding are in slots. Different motors have different current densities. Table 6.2 illustrates typical current densities:

Table 6. 3 Typical current densities.

<i>TYPE</i>	<i>A/mm2</i>
<i>Totally enclosed</i>	<i>1.5-5</i>
<i>Air-over Fan-cooled</i>	<i>5-10</i>
<i>Liquid Cooled</i>	<i>10-30</i>

As an example, the current density for the motor in Figure 6.1 assuming electrical loading of 10A/mm, fill-factor of 0.4, 17mm slot depth and 2mm/5mm slot-width/slot-pitch (Figure 6.1), the current density is:

$$J = \frac{10}{0.4 \times 0.4 \times 17} = 3.7 \text{ A/mm}^2$$

The details of the case study motor design including the detailed calculation and description of different fill factors will be discussed in Chapter 7.

6.5 FINITE ELEMENT ANALYSIS (FEA)

Finite Element Analysis is a method used in calculation and design of problems that cannot be solved by classical methods due to the complexity of the geometry and parameters involved in the design. FEA is used in many engineering fields like, electromagnetic, electrostatic, fluid mechanic, thermodynamics and structural engineering.

In the field of motor design, FEA is well established method and can generate accurate calculation of the motor parameters like torque, flux, current and inductance. FEA method involves division of the motor cross-section into smaller sections called finite elements. Each element is solved depending on the type of problem with solution of differential equations and from Maxwell, Laplace, Poisson and Helmholtz equations in terms of a vector potential. The complete solution of the problem involves vector solution of individual elements in final part of the solution (post-processing phase).

Every FEA consists of three sections, preprocessing, solution and post-processing that will be described in the following sections.

6.5.1 Preprocessing

Preprocessing is the phase that the problem is presented in a model or geometry with characteristic of each section of the model defined. In general, preprocessing consists of:

- Problem definition
- Geometry definition
- Property definition
- Mesh generation

In problem definition, the type of analysis is usually specified. For instance, the solution of static magnetic field in an iron core, or solution of a system involving electrostatic.

In geometry definition, a graphical editor is used to draw and define the exact dimension of the design. FEA can be 2D or 3D and hence the graphical editor is 2D or 3D. The geometry of the design is divided into enclosed sections that have different property. For instance, the iron in a motor lamination and the airgap are enclosed geometries that have different properties. The geometry definition includes definition of vertex, edge, area or volume (in 3D) that could have different properties at boundaries of each section.

Property definition involves assignment of electrical or magnetic property to each section defined in the geometry definition phase. Vertex, edge, surface and volumes (3D) are assigned a property that includes parameters like, permeability, resistivity, vector potential, and current density.

In the mesh generation phase, the geometry of design is divided in elements that have the property of the material that are enclosed in a boundary. These elements are solved for different parameters like magnetic flux and the complete solution is obtained by vector solution of individual elements in the solution phase.

Figure 6.2 illustrates a screen capture of the QuickField FEA software material property generation in an example of field analysis of a permanent magnet. In this figure, in the left hand side of the window, the attributes to each geometry section (surface) that has been illustrated in right hand side is highlighted.

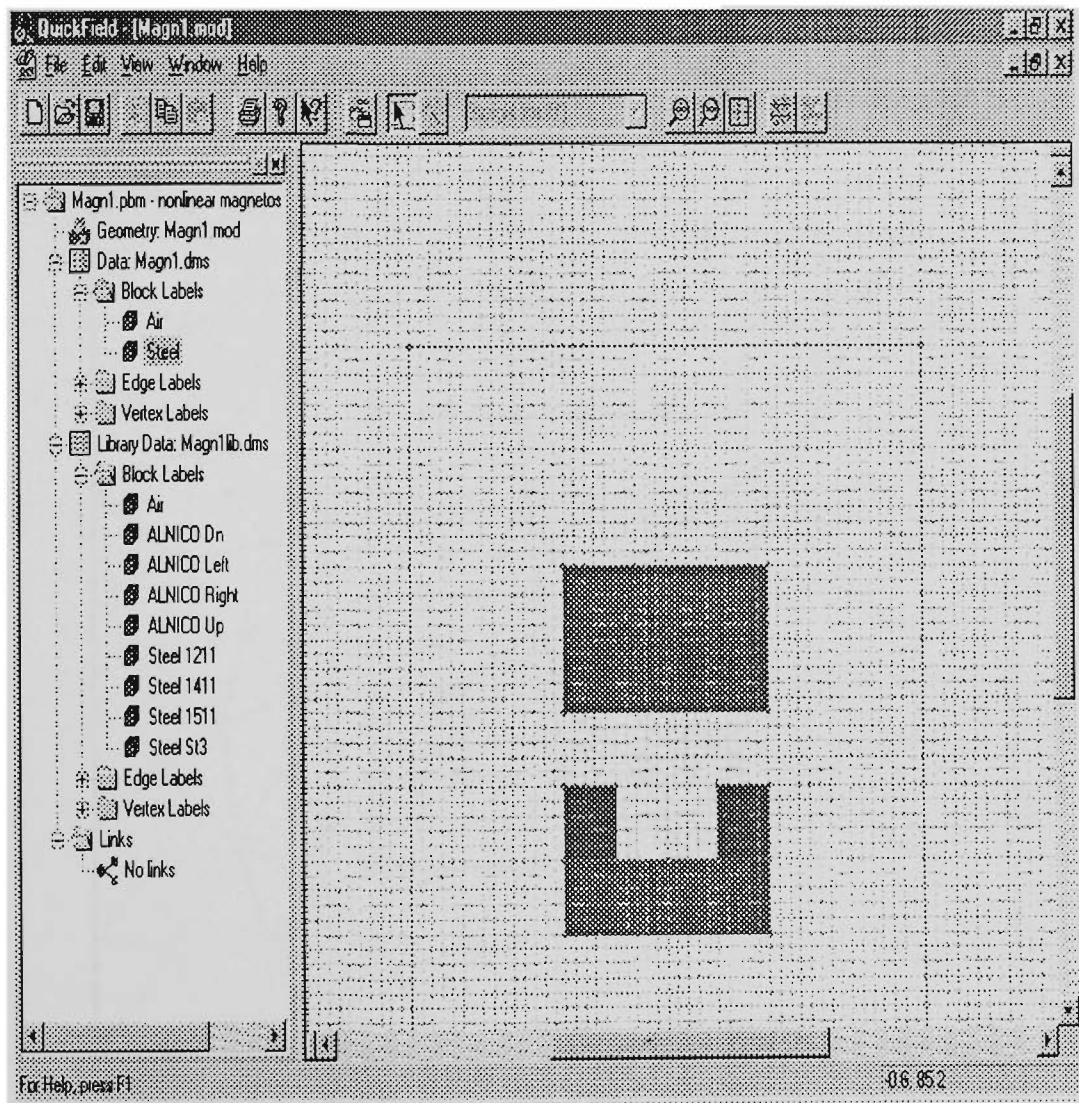


Figure 6. 2 Assignment of material property in model generation

In the left hand window of Figure 6.2 different geometric properties are illustrated. These properties include Body label (2D surface), Edge label (line) and Vertex label (point) that could have different material properties like magnet, air or steel.

Figure 6.3 illustrates the mesh presentation of the example in Figure 6.2. In this figure, the outside mesh property is air (i.e. relative permeability of 1) and the surfaces included in this figure are permanent magnet and steel. The stimulating force is the magnetic flux of the permanent magnets.

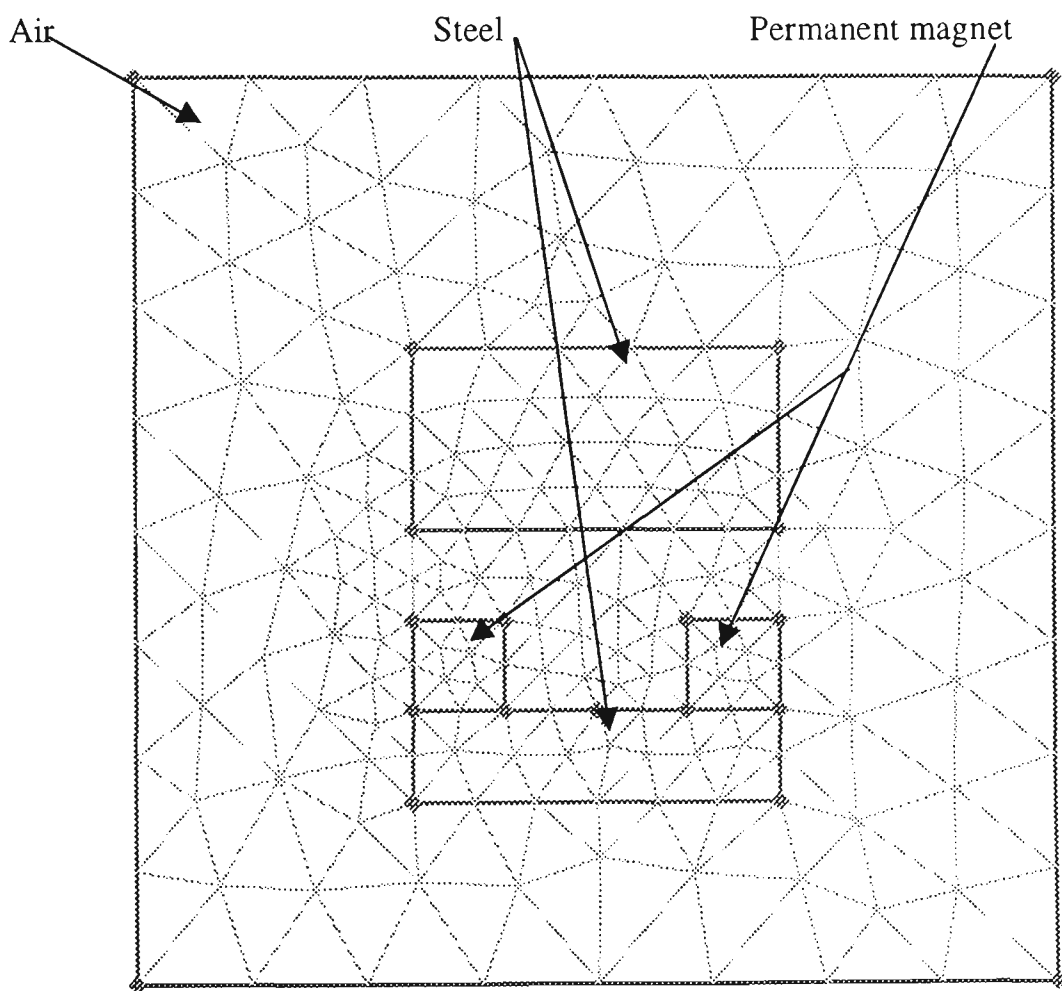


Figure 6. 3 Mesh generation for Figure 6.2 example.

6.5.2 Solution

In this phase the solution of the design is obtained from the solution of the partial differential equations generated in the mesh generated phase. The algorithm is based on minimisation of the energy function that is the stored potential energy in the field [63]. This solution is usually transparent to the designer and involves complex mathematical algorithms like Newton-Raphson to solve a set of nonlinear algebraic equations about the parameter of interest. The solution is usually in terms of array of data that can be plotted and analysed in the post-processing phase.

6.5.3 Post-Processing

In the post-processing phase, the data collected in the solution phase is displayed in a graphical presentation that enables the design engineer to visually observe the area of the design that have potential problems. The type of graphical data that can be observed are like, flux plots, flux densities, vector plots of flux, contour plots of the flux, calculation of torque, force and inductance.

FEA is usually a timely process and in many cases the increased accuracy of the result compared to classical methods may not justify the cost and time. In particular, a FEA is usually performed on a particular design and geometry while the classical methods or interactive programs that operate based on classical methods can be used with any geometry. However, the FEA are becoming more versatile and user friendly and the gap in development time is being reduced. Figure 6.4 illustrates a contour plot of the flux in the permanent magnet problem in Figure 6.2 and Figure 6.5 illustrates the magnetic field intensity plot of the same example.

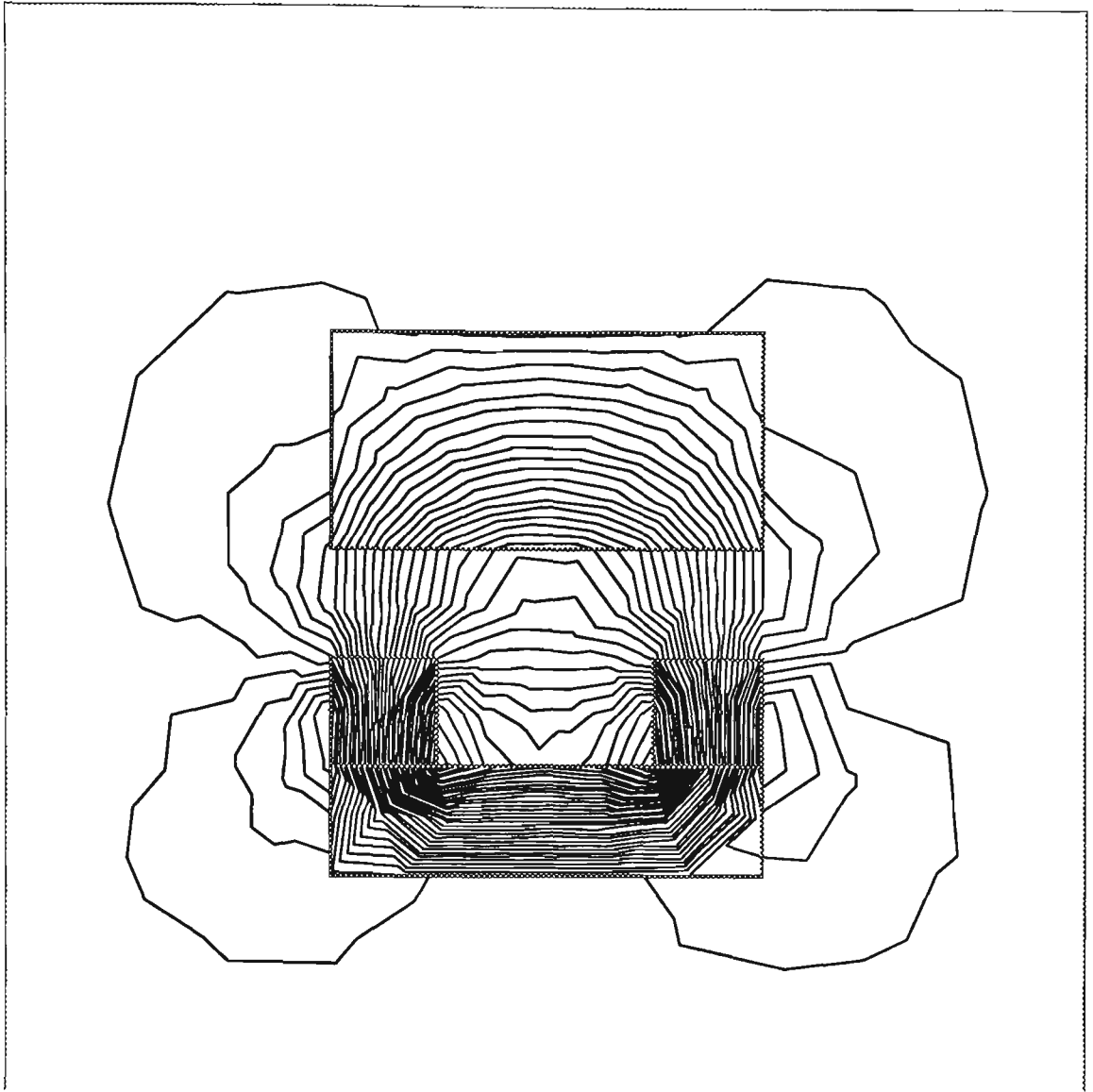


Figure 6. 4 Post-processing contour plot of Figure 6.2 example.

Further to these plots, the post-processing is usually equipped with software tool to measure the field intensity at any point or calculate the inductance of a winding and other parameters that are of interest in a design.

Graphical representation makes it easier to identify the problem area quickly and to change the design parameters if necessary before a complete analysis is performed.

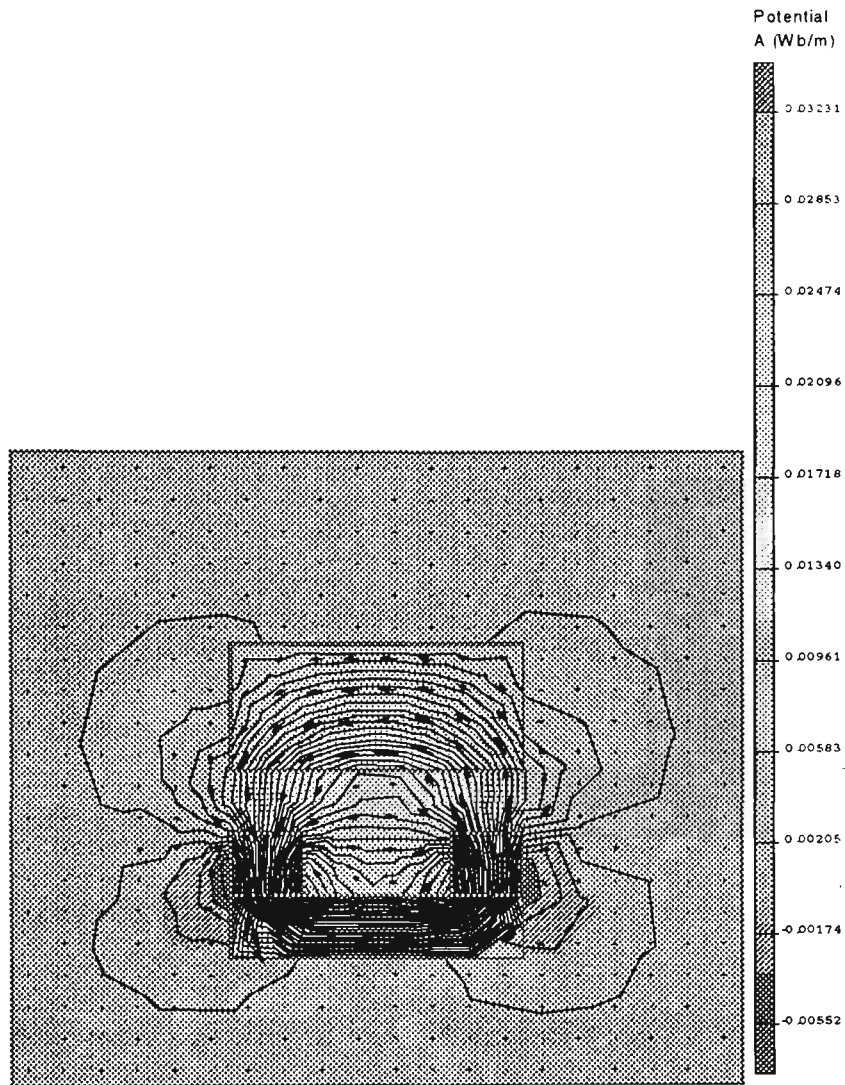


Figure 6. 5 Magnetic field intensity plot of Figure 6.2 example.

6.5.4 FEA Software

ANSYS is a FEA software that is capable of analysis in different field of engineering. Although its graphical editor can perform 3D model generation, due to its generalised design, the learning time for the features was more than other FEA programs.

QuickField is another FEA program that was evaluated on a personal computer and was found to be more specific and easier to work with.

In QuickField, the graphical editor is basic but the program accepts the import of complex graphics in dxf (AUTOCAD) format. This feature made it easy in generating the geometry of the design with versatile programs in minimum time.

6.6 SUMMARY

In this chapter the basic methods used in motor design were described. The methods described are the Classical Method (CM) and Finite Element Analysis (FEA) method. In classical methods, the sizing of the motor was described that enables the designer to estimate the suitability of a lamination and motor body to provide the required torque output.

The basics of the FEA was described in this chapter and despite adequate accuracy of the classical method in one design, FEA can be used to further verify or enhance a design. FEA is usually used for detailed design of a motor and hence, the analysis for the motor that has been selected in the prototype will be performed in the following chapters where the detailed design is described.

In the sizing that was performed on the motor of Figure 6.1 which has been selected for the prototyping, it was found that the motor cannot supply the required torque set out in the specification of the target motor. The target torque in the specification was 12 N.m. and the torque that could be achieved by the motor of the Figure 6.1 was about 3-4 N.m.. This does not contradict with the objective of this study and as it had been proposed, the prototype for evaluation purposes of a system could deliver better performance over conventional motors as described in the target specification. In this chapter it was illustrated that by doubling the diameter of the motor, output torque can be increased 4 times. Hence, the design

objective can be made with selection of different lamination. But designing the motor based on the lamination of Figure 6.1 will continue for a number of reasons:

1. By adding a pulley that is relatively cheaper alternative to increasing the motor diameter, the required 12 N.m. Torque can be obtained.
2. Although the losses were not included in the sizing, the sizing has been selected based on the lowest performance category of the motors. By selecting different rotor lamination and slightly higher flux density and more efficient cooling, a higher output torque might be achieved. This will be revealed in the detailed design.
3. The objective of the design in this chapter is a generalised investigation of different suitable alternatives to the present systems like SRM and PMBM and the issues related to commercialisation shall be commenced after the completion of this work.

The detailed design with the lamination of the stator in Figure 6.1 will be discussed in the following chapters.

CHAPTER 7

MOTOR DESIGN WITH LOW AIRGAP FLUX DENSITY

7.1 INTRODUCTION

In chapter 6 the basic motor design method and sizing was described. In this chapter and Chapter 8 two cases are discussed in regard to the specific requirements of the motor for domestic and industrial applications. In this chapter first a PMBM motor is designed that operates with lower airgap flux density and can be used with a pulley to provide the required 12 N.m. torque. Then a WRBM is designed that provides the same torque and the performances are compared for important parameters like peak torque, speed range and efficiency. A design similar to the design with the low airgap flux is described with exactly the same stator lamination but with higher airgap flux density that can operate at higher torque and lower pulley ratio as a comparison. The objective of this design methodology is to investigate the suitability of the WRBM in regard to the airgap flux density.

The motor design in this chapter and Chapter 8 based on Classical Method is reinvestigated by a simplified FEA, both for low and high airgap flux densities. The designs described in this chapter and Chapter 8 are not by any means a design that can lead to a production unit but they are rather designs for investigation to discover the advantages and disadvantages of the WRBM. The detailed design that is usually used in a motor design requires further analysis in line with experiments that are beyond the scope and resources of this work.

7.2 PERMANENT MAGNET (PM) MOTOR DESIGN

7.2.1 Sizing

In Chapter 6, it was found that the maximum torque that could be achieved with a motor similar to that of Figure 6.1 was 3.3 N.m. and that a pulley was required to increase the torque to 12 N.m. that had been specified in our target specification. That design was based on the maximum magnetic flux that we could assume in the airgap in order not to saturate the teeth of the stator lamination.

Assuming that the pulley ratio is 1:10, we can design a motor with lower airgap flux density that uses ferrite for its rotor. In Table 6.2 it was illustrated that with the motor of Figure 6.1, using Ferrite for the magnets, a PMBM can be designed to supply 1.7 N.m. torque. With 1.7 N.m. and a pulley ratio of 1:10 there is enough margin to obtain 12 N.m. torque. Later on it is necessary to change this ratio because if the ratio is high, the motor speed is increased and the core and inverter switching losses increase. This iteration procedure is normal during any design and is discussed here to clarify the steps that are taken and trades off exist in selecting the suitable motor parameters.

With 1:10 ratio, and 1200 rpm for spin, the motor highest speed must be 12000 rpm. Later on, it is illustrated that this frequency is high and switching and core losses can increase. However because the airgap flux is low and the motor operates in constant power region, we proceed with 1:10 ratio and 12000 rpm speed.

7.2.2 Phase Numbers

Phase numbers are usually a compromise between the cost of the drive and the utilisation of the rotor winding for a given supply voltage. Motors with phase numbers higher than 3 have advantages in torque ripple, conductor utilisation and efficiency but they cost more because of the complexity of the drive. Common motor drive systems are usually 3-phase and 2-phase. Our prototype is a 2-phase motor to test power induction concept and simplicity but the design of motor is based on a 3-phase system.

Using a single-phase system, with rms value of 240V, the nominal voltage of the dc link is approximately $V_s=340$ volts with sufficient filtering. Depending on WYE or DELTA connection, there are different line and phase voltage and current values for the 3-phase motor. For sinewave motors depending on type of PWM modulation a voltage between 0.612-0.78 of V_s can be achieved [63]. For square-wave motors the maximum available voltage is about 0.75% V_s .

7.2.3 Pole Numbers

Number of poles is usually selected inversely proportional to the rotor speed because as the rotational speed increases the driving frequency is increased and the stator losses and the switching losses in the inverter transistors are increased. During a design procedure when a standard lamination is not selected for the design, with increasing the number of poles the yoke diameter can be reduced for a given magnetic and electric loading.

Increasing the pole number has the following advantages:

- Lower torque ripple
- Lower end winding inductance of stator
- Lower magnetic imbalance that results in lower bearing current
- Higher low speed torque

The disadvantages of higher pole number are:

- Higher switching losses in inverter
- Higher core losses
- Higher winding cost

For these reasons, generally 4-pole and 8-pole motors are the most common motors due to the trade off between the advantages and disadvantages described.

For a given stator lamination, there could be limitation in number of pole selections due to the pitch size of the windings. If the pole numbers are reduced, the end turn inductance is increased for a lamination with high number of slots or winding pitch size. Stator inductance is generally not desirable because it reduces the power factor of the motor although there are exceptions in industry.

For this design an 8-pole motor was selected because the slot numbers is relatively high (36) and the flux is relatively low due to the use of ferrite permanent magnet.

7.2.4 Winding Configuration

When the number slots/pole is an integer, the winding is called integral-slot winding and it is usually avoided in practice because of cogging torque, although there are exceptions in industry. The winding pitch can be the closest integer of slots/pole. Based on the lamination of Figure 6.1, number of phases, poles and slots the winding pitch will be 6 and the coil span is 5. It means that the start of winding 1 of phase 1 will be at slot 1 and the end winding will be at slot 6 if we number the slots from 1 to 36.

Stator can be wound differently depending on the ease of winding with winding machinery. Lap winding and concentric windings are examples and a detailed description of their advantages and disadvantages are described in reference [63] and will not be covered in this work. For this motor a Lap winding is selected.

In Lap winding start and end of the coils of one pole are in adjacent slots. For example if the start of coil one is in slot 1 the start of coil 2 of the same phase is in slot 2. The end of coil 1 is in slot 5 and end of coil 2 is in slot 6.

Table 7.1 illustrates the summary of the motor parameters. The commutation frequency is obtained from the following equation for a six-step drive operation [63]:

$$f_c = 6x \frac{rpm}{60} x \frac{poles}{2} \quad \text{Equation 7. 1}$$

Table 7. 1 Stator winding parameters.

Number of slots	36
Number of phases	3
Number of poles	8
Number of stator coils	36
Winding pitch	6
Commutation frequency at 12000 rpm	4800
Airgap	0.8mm

The pole numbers for the operating frequency seems high but due to the use of ferrite for permanent magnet and constant power operation (low torque at high speed) the core loss can be acceptable. The airgap length is an experimental value and is usually 0.8 mm for motors with ferrite permanent magnets [63].

7.2.5 Magnet Material And Rotor Dimension

A ferrite is assumed for this motor that has $B_r = 0.4T$ with a $H_c = 3200$ Oersted (O_e). The data for this magnet has been extracted from reference [63]. A thickness of 10 times the size of the airgap is selected for the magnets. With the stator ID and OD dimensions that described in Chapter 6. The dimension of the rotor can be calculated from the dimension of airgap and magnet thickness and is summarised in Table 7.2:

Table 7. 2 Rotor dimensions.

<i>Rotor outward diameter</i>	D_r	$82 - 2 \times 0.8 = 80.4mm$
<i>Magnet thickness</i>	L_{mag}	$10 \times 0.8 = 8 mm$
<i>Rotor yoke diameter</i>	D_y	$80.4 - 2 \times 8 = 64.4mm$

For a 6 step square-wave drive that is cost effective with DELTA connection a pole arc of 2/3 of one pole-pitch ($360/8=45^\circ$) or 30° will be sufficient. For a full-pitch or 45° magnet arc, WYE connection has to be used. Full-pitch magnet in DELTA connection results in excessive third harmonic current in the stator winding.

7.2.6 Calculation Of Flux

The magnet pole area is calculated from:

$$A_p = \frac{\pi D_y L_{stk}}{Poles} = 758.30 \text{mm}^2 \quad \text{Equation 7. 2}$$

This value (758.39mm^2) in Equation 7.2 is for full-pitch magnet arc. For 30° magnet arc this value is 505.5mm^2 .

With estimation of the airgap flux B_m from B_r in Equation 6.3, the flux per pole is equal to:

$$\phi = B_m A_p = 0.364 \times 758.5 \text{e} - 6 = 2.76 \text{e} - 4 \text{W}_b$$

For short arc magnet the flux is $2.76 \text{e} - 4 \times 2/3 = 1.84 \text{e} - 4$ Webber.

7.2.7 Number Of Turns Per Coil

To calculate the number of turns, first the EMF constant K_E must be calculate from the speed of the motor. A nominal speed of 80% of no-load speed has been suggested for ferrite and 90% for rare earth magnet [63].

Assuming a no-load speed of 80% of 12000 rpm, the angular velocity is:

$$\omega_{nl} = \frac{2\pi}{60} \times \frac{rpm}{0.8} = 1570 \text{ rad / sec} \quad \text{Equation 7. 3}$$

With a dc link of 350 volts from a 240V system and assuming no losses, the EMF constant is:

$$K_E = \frac{E}{\omega} = \frac{350}{1570} = 0.216 \text{ v.S/rad} \quad \text{Equation 7. 4}$$

Because $K_E = K_T$ hence the torque constant K_T is also 0.216 N.m. (or v.s/rad) It can be proved that [63] for a WYE 3 phase machine:

$$K_E = \frac{2}{3} \frac{Z\phi p}{a\pi} C \quad \text{Equation 7. 5}$$

In this equation Z is the total conductors of the motor (3-phase), a is number of parallel paths into which the phase winding is divided. C is a constant that depends on pole arc and windings. For DELTA connection $2/3$ is replaced by $1/3$. With $a=1$ and $C=0.9$ and pole-pair of 4, Z is calculated and is:

$$Z = \frac{3 a\pi K_E}{2 \phi p C} = \frac{3 \times 1 \times 3.14 \times 0.216}{2 \times 2.76e - 4 \times 4 \times 0.9} = 1025 \quad \text{Equation 7. 6}$$

For a magnetic pole arc of 30° , $Z = 3/2 \times Z = 1536$.

Because there are $36/3 = 12$ coils per phase and each coil has two side conductors, the coil turn is $1025/(2 \times 12) = 43$ turns for full-pitch size and $1536/(2 \times 12) = 64$ turns for 30° magnet arc.

The next step is to calculate the wire gage that has been described in the next section.

7.2.8 Wire Size

Although there are equations for calculating slot area [63], for the Figure 6.1, the slot area can be approximated by one 2×17 mm rectangle and two 3×17 mm triangle that results in total area of 85.0 mm^2 .

The wire diameter that can be filled in the stator slot is:

$$D_w = \sqrt{\frac{A_{slot} \alpha_f}{N}} \quad \text{Equation 7.7}$$

where α_f is the slot fill factor that varies for different types of winding and is assumed 0.4 in this case and N is the number of conductors in one slot. Because there are total of 36 coils, there will be double winding in each slot as the number of slots is 36. Hence, the diameter of wire $D_w = 0.56 \text{ mm}$ (actual size 0.629 mm) for full-pitch arc and 0.5 mm (actual size 0.515 mm) for 30° magnet arc that are the next lower standard wire gage to the D_w value.

7.2.9 Coil Total Length

Total length of coil is used to calculate the copper losses. The average length of one turn of the coil wire is twice the stack length plus twice the winding pitch plus the allowance for the end turns curvature. The distance is calculated from the center of the slot opening. Hence, the average length of one turn is:

$$L_{wm} = 2(L_{stk} + \text{winding_pitch} + C_f) \quad \text{Equation 7.8}$$

The winding pitch is 5 that based on stator ID of 82mm and slot depth of 17 mm and 8 poles can be calculated:

$$\text{winding_pitch} = \pi \frac{ID + \frac{\text{Slot_depth}}{2}}{\text{slots}} \quad \text{slot_pitch} = \pi \frac{82 + 8.5}{36} \times 6 = 47.3 \text{mm} \quad \text{Equation 7.9}$$

With curvature factor of the end turns $C_f = 30\%$ of stack length, from Equation 7.8, the length of one turn is $L_{wm} = 2(30 + 47.3 + 0.3 \times 30) = 172.60 \text{mm}$. The total length of the coil wire is $43 \times 172.6 = 7.4$ meter and the total length of the coils in one phase is $12 \times 7.4 = 89.2$ meters. For 30° magnet arc motor the total length is $1.5 \times 89.2 = 133.9$ meters. With 0.56mm wire diameter that has 6.9 ohms/100 meters, the coil resistance is $6.9 \times 89.2 / 100 = 6.15$ ohm for full arc magnet. With 8.8 ohms/100 meters for 0.5mm diameter wire for 30° arc magnet motor the coil resistance is $8.8 \times 133.9 / 100 = 11.67$ ohms.

7.2.10 Torque Calculation

Assuming the speed of 12000rpm the back EMF is:

$$E = Speed(rpm) \times \frac{2\pi}{60} K_E = 12000 \times \frac{2\pi}{60} \times 0.216 = 271.3 \text{ V} \quad \text{Equation 7. 10}$$

With the supply impedance of $R_s=1$ ohm, the total impedance of two phases each with $R_p = 6.15$ ohms , a dc link voltage of $V_s=340$ volts and $V_{inv}=2$ volt drop across the inverter the nominal stator current is calculated:

$$I_s = \frac{V_s - E - V_{inv}}{R_s + 2R_p} = \frac{340 - 271.3 - 2}{1 + 2 \times 6.15} = 5.0A \quad \text{Equation 7. 11}$$

This value will be tested for current density and compared with the values that are tabulated in practice for different types of motors.

The torque generated can be obtained from:

$$T = I_s K_E = 5 \times 0.216 = 1.08 \text{ N.m.} \quad \text{Equation 7. 12}$$

For the motor with 30° magnet arc the stator current is:

$$I_s = \frac{V_s - E - V_{inv}}{R_s + 2R_p} = \frac{340 - 271.3 - 2}{1 + 2 \times 1.67} = 2.74A$$

The torque for this motor is $T=2.74 \times 0.216=0.59 \text{ N.m.}$. The torque value that has been obtained for the motor with full magnet arc is lower than what was predicted

in sizing in Section 7.2.1 (maximum achievable torque of 1.7 N.m.) because a TRV of mid point of 7-14 K.N.m./m³ had been selected. If the TRV of 7 K.N.m./m³ is selected (for small motor) the maximum torque from sizing will be 1.11 N.m. that is very close to the value predicted in Equation 7.12.

The target torque specification of 1.2 N.m. is almost met only with the full-magnet arc motor (1.1N.m.). If both could supply the required torque, and if the current densities for these designs were acceptable in terms of temperature increase, a 30° arc magnet is a cheaper design.

7.2.11 Current Density Calculation

In Chapter 6, typical current densities for different motors have been given in Table 6.3. Because the motor operates at relatively high speed, with integral fan in the motor enclosure a fair degree of cooling is provided and hence if the second row of Table 6.3 is considered for the motor, a current density between 5-10 (i.e. 7.5) A/mm² is assumed. For full-pitch motor, the current density is the stator current divided by the area of the wire and will be:

$$J_s = \frac{I_s}{\frac{\pi D^2}{4}} = \frac{5.0}{\frac{3.14}{4} 0.55^2} = 21 \text{A/mm}^2 \quad \text{Equation 7. 13}$$

With the wire diameter of 0.5mm and 2.7A stator current, the current density for the motor with 30° magnet arc is 13.8A/mm². Both exceed acceptable value of 7.5A/mm² and the motor operates at lower torque that is 1.2 N.m.. The stator current at this torque is $1.2/1.1 \times 5 = 5.45\text{A}$ for full-pitch and $1.2/0.59 \times 2.7 = 5.4\text{A}$ for 30° magnet arc. Hence, both motors operate at the same current for 1.2 N.m. (as expected because of similar torque constant) but the full-pitch motor has lower stator winding resistance and hence is more efficient. At this current the current

density for full-pitch is 22.9A/mm^2 and for the 30° magnet arc the current density at 5.4A is 27.6A/mm^2 . This illustrates that the motor with 30° magnet arc is not only less efficient but also has higher copper losses and its current density is higher than the acceptable level.

7.2.12 Losses Calculation

7.2.12.1 Stator Copper Losses

At low speed, stator losses can be approximated by ignoring the core losses and calculating only the copper losses due to current in two phase windings and it is:

$$P_{cu} = 2I_p^2 R_p = 2 \times 6.15 \times 5.0^2 = 307.5\text{W} \quad \text{Equation 7.14}$$

For the motor with 30° magnet arc, the copper loss is $P_{cu}=170.5\text{W}$ for 0.59N.m. torque. Phase current at 1.2 N.m. is 5.4A and from equation 7.14 copper losses can be calculated. At 1.2N.m. , copper losses are 386W for full arc and 705.3W for the 30° magnet arc motor. These losses are clearly too high and are not acceptable at least for the motor with the 30° magnet arc length. The reason for the high losses is the fact that the magnets are ferrite and the airgap flux is low and the rotor diameter is small. This matter will be discussed when the motor with higher remanence flux is used in the design.

7.2.12.2 Stator Core Losses

Core losses are calculated at high speed (12000rpm) and consists of hysteresis losses that are proportional to $B^{1.6}f$ and eddy current losses that are proportional to B^2f^2 [63]. The operating frequency f at 12000rpm is:

$$f = 12000/60 \times \text{pole_pairs} = 800 \text{ Hz}$$

Equation 7. 15

Assuming a flux density of 0.72T in the steel that is twice the airgap flux, the total core losses can be calculated from a comparison of the losses for a typical lamination at 1.5T and 60 Hz. The core loss for 0.025" (24Gauge) M-19 is 4.6W/kg. Assuming magnetic field of 0.72T in the iron (twice the magnetic field of the airgap), at 800 Hz the core losses is mostly due to eddy current losses and is [63]:

$$P_{co} = \left\{ \frac{f_1}{f_f} \times \left(\frac{B_1}{B_2} \right)^{1.6} + \left(\frac{B_1 f_1}{B_2 f_2} \right)^2 \right\} \times 4.6$$

$$= \left\{ \frac{800}{60} \times \left(\frac{2 \times 0.36}{1.5} \right)^{1.6} + \left(\frac{2 \times 0.36 \times 800}{1.5 \times 60} \right)^2 \right\} \times 4.6 = 207.4 \text{ W / kg}$$

Equation 7. 16

The volume of the stator is:

$$\text{Volume} = L_{stk} \left(\frac{\pi}{4} \times (OD^2 - ID^2) - \text{Total_slot_area} \right)$$

$$= 30 \times \left(\frac{\pi}{4} \times (140^2 - 82^2) - 36 \times 85 \right) = 21143 \text{ mm}^3$$

Equation 7. 17

With steel density of 7750 kg/m³ and 21143mm³ volume, the weight of the iron is 1.64kg. Hence the total core losses are 207.4x1.64x0.55 =187W. The value of 0.55 is due to the fact that the core loss curves are expressed in dc and hence the dc value of flux must be used.

7.2.13 Efficiency

The efficiency of the motor is usually maximum at full load and can be calculated from the motor output mechanical power and losses. The mechanical power is:

$$P_m = 2\pi \frac{\text{rpm}}{60} x T = 2\pi \frac{12000}{60} x 1.2 = 1507.2W$$

Equation 7. 18

Ignoring the bearing losses, total electrical losses are the summation of core loss and copper loss. These losses are $386+187=573W$ for the motor with full magnet arc and $705.3+187=892.3W$ for the motor with 30° magnet arc. Hence the efficiency of the motor is $1507.2/(573+1507.2)=72.5\%$ for the full arc magnet motor and 62.8% for the motor with 30° magnet arc. The efficiency figures are less than typical efficiencies (85%) for permanent magnet motors and are higher compared with induction motor of the same size that have 60-70% efficiency. These efficiency figures are given in order to describe the calculation procedure and obviously the motor with 30° magnet arc cannot be used at 1.2 N.m., because there is not sufficient EMF and even if a higher supply voltage is used the motor overheats.

The mechanical power of the motor seems high for this motor but the reason is that a higher current density was allowed in the design due to the fact that the motor runs at high speed and has considerable integral fan cooling.

7.2.14 Motor Parameter Summary

The motor parameters of the two designs described in previous sections have been outlined in Table 7.3. It is worthwhile to compare the performance of this motor in terms of the target specification that was described in Chapter 6. The motor with full magnet arc can provide the necessary torque and speed that is required.

Table 7. 3 Summary of the designed motor parameters.

<i>Motor parameter</i>	<i>Full arc magnet motor</i>	<i>30 arc magnet motor</i>
<i>No. Of coils /phase</i>	12	12
<i>Coil # turns</i>	43	64
<i>Resistance of the phase coils</i>	6.15 ohms	11.67 ohms
<i>Core loss</i>	187W	187W
<i>Copper loss at 1.2N.m.</i>	386W	705.3W
<i>Maximum Output power</i>	1356.4W at 1.08 N.m.	741W at 0.59 N.m.
<i>Output power at 1.2N.m., 12000rpm</i>	1507W	1507W ¹
<i>EMF voltage</i>	271.3V	271.3V
<i>No-load speed</i>	12000 rpm	12000 rpm
<i>EMF constant</i>	0.216 V.S/Rad	0.216V.S/Rad
<i>Maximum Torque</i>	1.08 N.m.	0.59 N.m.
<i>Stator current at maximum torque</i>	5.0A	2.7A
<i>Phase current at 1.2 N.m.</i>	5.45 A	5.45 A
<i>Current density at maximum torque</i>	21 A/mm ²	13.76 A/mm ²
<i>Efficiency at 1.2N.m.</i>	72.5%	62.8%

¹ The motor cannot deliver 1.2 N.m. and this value has been written for comparison of two motors and other designs in the following sections.

7.3 PERFORMANCE TEST

In this section the performance of the motor design for the case of washing machine is evaluated. Restating that the motor required 550 rpm minimum speed at 1.2 N.m. and 12000 rpm at 0.2 N.m. based on 1:10 pulley ratio and the torque-speed requirement of Table 1.1.

7.3.1 Low Speed Power Calculation

At 550 rpm and 1.2 N.m, from Equation 7.18 the mechanical power is $P_m=69W$. Losses at low speed are mainly due to copper loss that is 386W and hence the efficiency is 15.1%. The efficiency at low speed for the 30° magnet arc is 8.9% that is very low (copper loss of 705.3W).

7.3.2 High Speed Power Calculation

At 12000 rpm and 0.2 N.m., similar to the calculation in previous section, the mechanical power is 251W. Core losses are similar to Table 7.3 and because the phase current is $0.2/1.2 = 0.1667$ times the current at 5.4 A, the copper losses are 0.0278 times or 36 times less. Hence, the copper loss is $386/36=10.7W$ for full arc magnet and $705.3/36=19.6W$ for 30° magnet arc motor and the total losses are 197.7W and 206.6W respectively. The efficiency is $251/(251+197.7) = 55.94\%$ for full arc and $251/(251+206.6)=54.85\%$ for full arc and 30° arc magnet motors.

Table 7.4 outlines the performance of the motors designed in regard to the target specification.

Table 7. 4 Comparison of the motor parameter vs the target specification.

	<i>Required parameter</i>	<i>Full arc magnet motor</i>	<i>30 arc magnet motor</i>
Power at high speed	12000 rpm- 0.2N.m.-251W	457.6W, Electrical power	448.7W, Electrical power
Efficiency at high speed		55.94%	54.85%
Power at low speed	550 rpm, 1.2 N.m. 69W	455W, Electrical power	774.3W, Electrical power
Efficiency at low speed		15.1%	8.9%
Peak Torque	200% desirable	1.08 N.m., 90% of 1.2N.m.	0.59 N.m., 49.17% of 1.2 N.m.
Stalled phase current	Calculated from Equation 7.11 by E=0	25.4A	13.89A

In Table 7.4, the stalled current is referred to the locked rotor current and must be limited by the drive controller otherwise the magnets can be demagnetised permanently. The calculation of current that results in demagnetisation of magnets is discussed in details in reference [63]. The current limiting to prevent the demagnetisation of magnets is not required in a WRBM and hence a higher peak torque can be generated if saturation of iron does not occur and if the inverter is protected.

From this table, it is clear that the efficiency of the motor is reduced at high speed low torque to values below 60%. The efficiency of low speed operation is low as well due to the fact that the airgap flux was low (use of ferrite) and higher number of turns were required to generate the required torque. It also illustrates that if cooling is provided for the motor at low speed, the full arc motor almost meets the requirements of the washing machine specification that was described in Chapter

6. Although the torque at low speed is slightly lower (1.08 compared with 1.2 N.m.), the belt ratio can be increased to produce higher drum torque at low speed at expense of lower drum speed at high speed that is a conservative value (1200 rpm).

7.4 FEA OF THE MOTOR

A finite element analysis was performed to observe magnetic flux density distribution around the motor lamination and airgap. The value for the coercive magnet field intensity H_c was selected at 256kA/m with 0.3 T magnetic flux density and relative permeability μ_r of 1 from data sheet. Figure 7.1 illustrates the flux lines. Only a portion of the motor was simulated due to limitation on the software and complete analysis should change the result in terms of the symmetry of the flux lines.

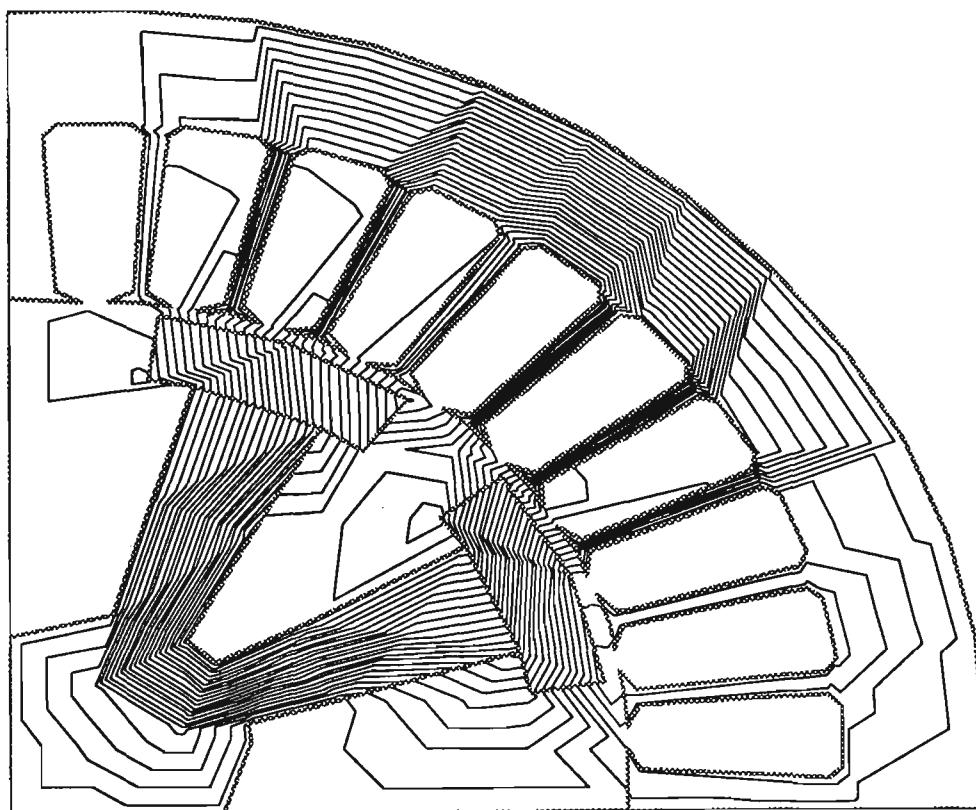


Figure 7. 1 FEA of the motor with Ferrite permanent magnet.

In this figure, the measured magnetic flux intensity at iron was 0.7T, in airgap its almost uniform at 0.15T and 0.23 at the magnet. This is somehow close to what we assumed in our design for the flux density in iron. Although the airgap flux is less than what we assumed but the airgap dimension is slightly higher than 0.8 mm due to the limitation in FEA package mesh generation.

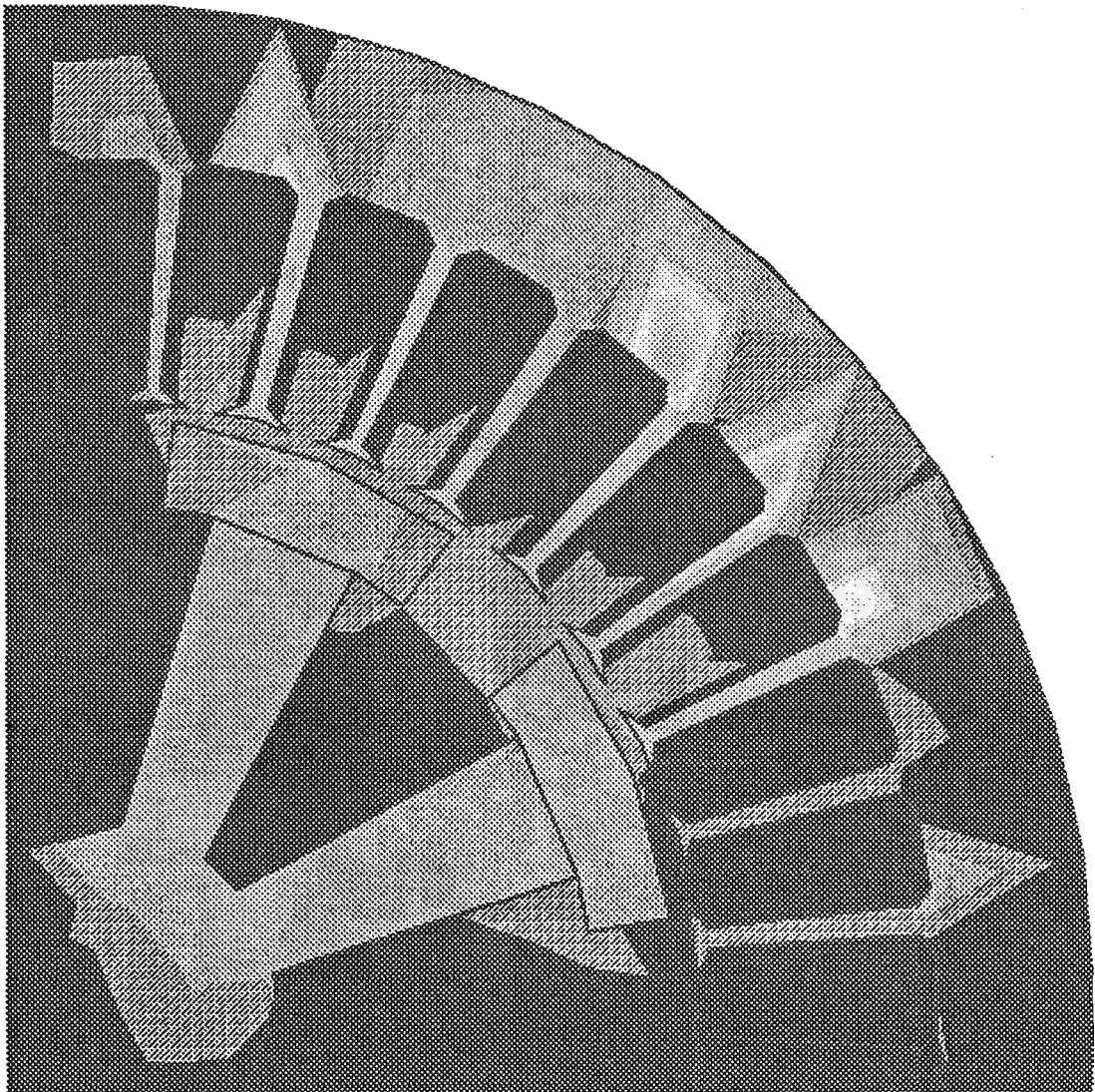


Figure 7. 2 Magnetic field intensity of the motor with Ferrite magnet.

Magnetic field intensity has been illustrated in Figure 7.2. In this figure the areas that are subject to saturation due to high flux density can be identified for the design of lamination (bright area). In this design, the maximum flux density is about 0.7T and hence the saturation does not occur assuming a saturation level of

1.2T in iron that is a conservative value (usually selected at 1.8T for rare earth magnet motors).

7.5 CONCLUSION

The permanent magnet motor design that was presented in this chapter indicated that by using a pulley ratio of 1:10, the required 12N.m torque of the target specification cannot be met with both motors. In the case of the motor with full arc magnet, the torque is close to target but the current density exceeds specification. At low speed, this motor runs at 550rpm and there is considerable cooling hence a higher current density can be acceptable. Using ferrite permanent magnets for the design, resulted in a cheaper design but the efficiency of the motor is relatively lower than standard permanent magnet motors. Using a permanent magnet with higher B_r results in reduction of the winding turns and hence a more efficient motor can be designed. However, within the specified lamination of Figure 6.1, a direct drive system cannot be achieved and a pulley is required to increase the low speed torque.

Using full magnet arc design (45°) results in a more efficient motor and the maximum generated torque is almost twice as the motor with 30° magnet arc. However, a 30° magnet arc is a cheaper design because it uses less magnets.

Because the airgap flux is low in a motor with ferrite, a higher peak torque ratio can be achieved because the saturation in iron occurs at higher flux intensities. However, one must make sure that there is enough supply voltage to generate the required EMF and sufficient margin to prevent the demagnetisation of the magnets. Stalled torque phase current is a good indication of the peak torque levels. This current must be limited by the controller to prevent the inverter from damage and the permanent magnets from demagnetisation.

The design of the motor in this chapter is not ideal for the given lamination parameters. A more efficient motor can be designed if some of the parameters are varied. For example, the diameter of the wire for the full arc motor was selected at 0.56mm (although exists but not common) while the calculated wire size was 62.88mm. The next wire diameter is 63mm but adding the insulation thickness the wire size exceeds the limit and coils will not fit. But if flux is increased and the turns are reduced so 63mm wire is used, the efficiency will improve. To some extent we followed this procedure to balance the design parameters but the objective has been to compare different designs within a motor chassis and the detailed design that can increase efficiency is not required at this stage.

Next chapter describes the design of a motor with high B_r and the designs are compared in order to find out the best design for a WRBM.

CHAPTER 8

HIGH AIRGAP FLUX PERMANENT MAGNET AND WOUND ROTOR BRUSHLESS MOTOR DESIGN

8.1 INTRODUCTION

In this chapter, the motor that was designed with ferrite permanent magnet is redesigned with a magnet with high remanence flux density. In Chapters 6 and 7 we illustrated that to obtain a motor with higher torque at low speed a high airgap flux density is required. The disadvantages of a motor with high airgap flux were high-speed inefficiency and high cost of the motor.

In this chapter, the detailed design and analysis of the motor shown in Figure 6.1 with high airgap flux is described and the result will be compared with the motor design with ferrite permanent magnet. It will be demonstrated that with the given motor parameter of Figure 6.1, the ferrite motor has higher efficiency at high speed compared with the rare earth magnet motor while at low speed the opposite is true. The comparison between these motors verifies the need for a motor with variable airgap flux such as the Wound Rotor Brushless Motor that will be designed next.

8.2 DESIGN PROCEDURE

The procedure of the permanent magnet motor design that was followed in the design of motor with ferrite magnets is described in this section. By using MATLAB program in Appendix D, the motor parameters are calculated for a motor with high remanence flux density and the results will be compared with

the motor with ferrite permanent magnets. The summary of the design procedure is as follows:

1. Tabulate the motor mechanical dimensions like rotor and stator diameters and stack length.
2. Verify the sizing of the motor if it is adequate for the application, Equation 6.4 and Table 6.2.
3. Calculate the optimum coil numbers and poles based on estimation of torque/speed requirements.
4. Select magnetic material by cost, low speed torque and sizing of the motor.
5. Calculate magnet pole area, Equation 7.2.
6. Calculate airgap flux.
7. Calculate no-load speed and EMF constant, Equation, 7.3-7.5.
8. Calculate number of coils and coil turns, Equation 7.6.
9. Calculate wire diameter, Equation 7.7.
10. Calculate coil average length and pitch, Equation 7.8-7.9.
11. Calculate EMF, Equation 7.10.
12. Calculate phase current, Equation 7.11.
13. Calculate torque, Equation 7.12.
14. Check if the torque is acceptable, if not change the motor parameter.
15. Calculate the current density, Equation 7.12.
16. Check if the current density is acceptable by referring to Table 6.3.
17. Calculate copper losses, Equation 7.14.
18. Calculate core losses, Equation 7.16-7.17.
19. Calculate mechanical power, Equation 7.18.
20. Calculate efficiency from mechanical power and losses.
21. Check if the motor operating condition is acceptable.
22. Calculate efficiency at low and high speed.
23. Use FEA to verify the design by checking the airgap flux, magnetic field intensity and other parameters like torque and winding inductance.

The above design procedure is by no means a complete design for a motor but it includes sufficient calculation to obtain the suitability of a lamination or a type of motor for a particular application and perhaps prototyping. The motor parameters that have been described in the above procedure can be used to calculate some of the parameters that were described. For example, the maximum torque is a good measure when calculating issues related to high inertia loads and acceleration.

8.3 MOTOR DESIGN WITH HIGH REMANENCE FLUX MAGNET

The procedure for design of the motor with a magnet with high remanence flux is exactly the same as the procedure described in Chapter 7 with only changing B_r from 0.4T to 0.9 T and the magnet constant for calculation of EMF constant from 0.8 to 0.9. A rare earth magnet with $B_r=0.9$ Tesla is assumed for this motor. Based on the MATLAB program in Appendix D, the motor parameters are summarised in Table 8.1. In this table, the design of the motor for full magnet arc and 30° magnet arc are described.

As illustrated in this table compared with the motor with ferrite permanent magnet (Table 7.3) the core losses are higher and copper losses are lower. The reason is that lower number of turns are required to generate the required torque so the ohmic resistance of the stator winding is lower and hence the copper losses are less than the motor with ferrite magnets. Core losses are higher in the motor with high B_r because the flux is higher and eddy current and hysteresis losses are higher. At maximum required torque-speed, that is 1.2N.m.-12000RPM, the efficiency of the motor with high B_r is lower than the efficiency of the motor with ferrite magnet.

Table 8. 1 Motor parameter with a high remanence flux magnet.

DESCRIPTION	FULL ARC MAGNET	30° ACR MAGNET
EMF Magnet Constant	0.9	0.9
Magnet Remanence Flux Density	0.9000 Tesla	0.9000 Tesla
Pole Numbers	8	8
RPM	12000.00 RPM	12000.00 RPM
Required Torque	1.2000 N.m.	1.2000 N.m.
Supply Voltage	339.4113 Volts	339.4113 Volts
Stator Slots	36	36
Slot Area	85.0000 mm ²	85.0000 mm ²
Stator OD	0.1400 meter	0.1400 meter
Stator ID	0.0820 meter	0.0820 meter
Stack Length	0.0300 meter	0.0300 meter
Stator Volume	2.1158e-004 meter ³	2.1158e-004 meter ³
Stator Weight	1.6398 Kg	1.6398 Kg
Rotor OD	0.0804 meter	0.0804 meter
Rotor ID	0.0644 meter	0.0644 meter
Airgap	0.0008 meter	0.0008 meter
Magnet Thickness	0.0080 meter	0.0080 meter
Magnet Pole Area	0.0008 m ²	0.0005 m ²
Maximum Airgap Flux Density	0.8182 Tesla	0.8182 Tesla
Approximate Flux	6.2075e-004 Webber	4.1404e-004 Webber
Commutation Frequency	4800.0000 Hz	4800.0000 Hz
No Load Speed	1396.26 Rad/sec	1396.26 Rad/sec
EMF Constant	0.2431 V.S/Rad	0.2431 V.S/Rad
Total Number Of Conductors	512.60	768.90
Coil Numbers	12	12
Actual Wire Diameter	0.8997 mm	0.7289 mm
Wire Diameter	0.8000 mm	0.7000 mm
Wire Pitch Size	0.0474 meter	0.0474 meter
Mean Coil Length	0.1728 meter	0.1728 meter
Coil Wire Length	3.6282 meter	5.5287 meter
Total Coil Length	43.5384 meter	66.3442 meter
Total Coil Resistance	1.4803 Ohm	2.8528 Ohm
EMF	305.4701 Volts	305.4701 Volts
Stator Phase Current	8.0647 Ampere	4.7633 Ampere
Torque	1.9604 N.m.	1.1579 N.m.
Current Density	16.0442 A/mm ²	12.3773 A/mm ²
Maximum Operating Frequency	800.00 Hz	800.00 Hz
Copper Loss	192.5562 W	129.4572 W
Core Loss	941.3034 W	941.3034 W
Mechanical Power	2463.5243 W	1455.0610 W
Total Loss	1133.8596 W	1070.7606 W
Efficiency	68.48%	57.61%

Table 8.1 Motor parameter with a high remanence flux magnet, continued.

DESCRIPTION	FULL ARC MAGNET	30° ACR MAGNET
Stalled Stator Current	85.1917 Ampere	50.3178 Ampere
Stator Current At Required Torque	4.9365 Ampere	4.9365 Ampere
Copper Loss At Required Torque	72.1483 W	139.0421 W
Current Density At Required Torque	9.8209 A/mm ²	12.8273 A/mm ²
Mechanical Power At Required Torque	1507.9645 W	1507.9645 W
Efficiency At Required Torque	59.81%	58.26%

The main inefficiency of the motor with high B_r is due to the high airgap flux at high speed and in constant power operation this flux (torque) is not required although contributes to very high core losses. This problem was discussed in the abstract of this work and in literature review and was the basis for our work to design a motor with variable airgap flux for operation in constant power where a high airgap flux is not necessary. From Table 8.1 it is also observed that, the stalled current is much higher than the motor with ferrite permanent magnets because the winding resistance is less.

The maximum torque of 1.96 N.m. for full arc and 1.16N.m. for 30° magnet arc meet the torque requirement of 1.2N.m. of the target specification. The core loss for this motor is about 941W that is very high and is the main source of this motor inefficiency. The operation of the motor within the limits of the target specification results in a lower copper losses while the core losses do not change unless the airgap flux is reduced at high speed.

8.3.1 Constant Power Operation

Referring to the target specification in Table 1.1, at 550 rpm the required torque is 1.2 N.m. and at 12000 rpm the required torque is 0.2 N.m.. Hence similar to Table 7.4 the performance of the motor with high B_r can be summarised in Table 8.2.

The stator current at 0.2N.m. is $0.2/1.2 \times 4.94A = 0.823A$. Copper loss can be calculated from the square root of the current ratios and is only 2 watts for full arc and 3.9W for the motor with 30° magnet arc. The core losses at low speed can also be calculated from Equation 7.16 but because the operating frequency is only 37 Hz (at 550rpm) the losses does not exceed a few watts (4.8 watts for motor with high B_r). Electrical power is the sum of the mechanical power, core and copper losses. For example for the case of the motor with full arc magnet the electrical power at high speed is equal to $251+941+2=1194W$. Usually the copper losses are ignored at high speed low torque and core losses are ignored at high torque low speed operation.

Table 8. 2 Comparison of the motor performance vs the target specification for the motor with high B_r .

	<i>Required parameter</i>	<i>8.3.1.1 Full arc magnet motor</i>	<i>30° arc magnet motor</i>
Power at high speed	12000 rpm, 0.2N.m.-251W	1194W Electrical power	1196 Electrical power
Efficiency at high speed		21%	21%
Power at low speed	550 rpm, 1.2N.m. 69W	145.8W Electrical power	212.8W Electrical power
Efficiency at low speed		47.33%	32.42%
Peak Torque	200% desirable	1.96 N.m., 163% of 1.2N.m.	1.158 N.m., 96.5% of 1.2 N.m.
Stalled phase current	Calculated from Equation 7.11 by $E=0$	85.2A	50.3A

Copper losses at low speed and rated torque are 72W and 139W for the full arc and the motor with 30° arc magnet. Adding copper loss and core loss of 4.8 W to the mechanical power at 1.2N.m. and 550 rpm results in electrical input power.

By comparing Table 7.4 that summarises the motor performance for the ferrite motor with Table 8.2, the quantitative presentation of the problem with permanent magnets are described. As expected, the efficiency of the motor at high speed is low and the efficiency of the motor at low speed is high for the motor with high B_r compared with the motor with low B_r . The problem is that if a permanent magnet is designed to operate at low speed, it is inefficient at high speed and if a permanent magnet is designed to operate at high speed, it cannot produce high torque at low speed. The reason to this problem is constant airgap flux and as illustrated permanent magnet motors cannot be operated in a wide speed range at high efficiencies. Next section the comparison between the design parameters for two motors with high B_r and low B_r are described.

8.3.2 Comparison Of Motors With High And Low B_r

Table 8.3 further illustrates the difference between two motors designed in Chapter 7 and in Chapter 8. In this table the design parameters of the motors with low B_r and high B_r for full arc and 30° arc magnet are summarised. It is evident that the motor with high flux density is suitable for low speed operation while the motor with low flux density is suitable for operation at high speed. The required torque is only generated with the motors with high airgap flux density and their current densities do not exceed the acceptable levels. This means that the copper losses and the wire diameter is acceptable and if the operating speed of the motor is reduced so that the core losses are reduced, the motors with high B_r are good designs that meet the requirements that were setup in the target specification.

Table 8. 3 Motor design parameter comparison.

DESCRIPTION	LOW B _r	HIGH B _r	LOW B _r , 30°	High B _r , 30°
EMF Magnet Constant	0.8	0.9	0.8	0.9
Magnet Remanance Flux Density	0.4000 Tesla	0.9000 Tesla	0.4000 Tesla	0.9000 Tesla
Pole Numbers	8	8	8	8
RPM	12000.00 RPM	12000.00 RPM	12000.00 RPM	12000.00 RPM
Required Torque	1.2000 N.m.	1.2000 N.m.	1.2000 N.m.	1.2000 N.m.
Supply Voltage	339.4113 Volts	339.4113 Volts	339.4113 Volts	339.4113 Volts
Airgap	0.0008 meter	0.0008 meter	0.0008 meter	0.0008 meter
Magnet Thickness	0.0080 meter	0.0080 meter	0.0080 meter	0.0080 meter
Magnet Pole Area	0.0008 m2	0.0008 m2	0.0005 m2	0.0005 m2
Maximum Airgap Flux Density	0.3636 Tesla	0.8182 Tesla	0.3636 Tesla	0.8182 Tesla
Approximate Flux	2.7589e-004 Webber	6.2075e-004 Webber	1.8402e-004 Webber	4.1404e-004 Webber
No Load Speed	1570.80 Rad/sec	1396.26 Rad/sec	1570.80 Rad/sec	1396.26 Rad/sec
EMF Constant	0.2161 V.S/Rad	0.2431 V.S/Rad	0.2161 V.S/Rad	0.2431 V.S/Rad
Total Number Of Conductors	1025.20	512.60	1537.81	768.90
Coil Numbers	12	12	12	12
Actual Wire Diameter	0.6288 mm	0.8997 mm	0.5154 mm	0.7289 mm
Wire Diameter	0.5500 mm	0.8000 mm	0.5000 mm	0.7000 mm
Wire Pitch Size	0.0474 meter	0.0474 meter	0.0474 meter	0.0474 meter
Mean Coil Length	0.1728 meter	0.1728 meter	0.1728 meter	0.1728 meter
Coil Wire Length	7.4292 meter	3.6282 meter	11.0574 meter	5.5287 meter
Total Coil Length	89.1500 meter	43.5384 meter	132.6884 meter	66.3442 meter
Total Coil Resistance	6.1514 Ohm	1.4803 Ohm	11.6766 Ohm	2.8528 Ohm
EMF	271.5290 Volts	305.4701 Volts	271.5290 Volts	305.4701 Volts
Stator Phase Current	4.9525 Ampere	8.0647 Ampere	2.7053 Ampere	4.7633 Ampere
Torque	1.0701 N.m.	1.9604 N.m.	0.5845 N.m.	1.1579 N.m.
Current Density	20.8455 A/mm2	16.0442 A/mm2	13.7779 A/mm2	12.3773 A/mm2
Maximum Operating Frequency	800.00 Hz	800.00 Hz	800.00 Hz	800.00 Hz
Copper Loss	301.7571 W	192.5562 W	170.9117 W	129.4572 W
Core Loss	190.7484 W	941.3034 W	190.7484 W	941.3034 W
Mechanical Power	1344.7598 W	2463.5243 W	734.5634 W	1455.0610 W
Total Loss	492.5056 W	1133.8596 W	361.6602 W	1070.7606 W
Efficiency	73.19%	68.48%	67.01%	57.61%
Stalled Stator Current	25.3641 Ampere	85.1917 Ampere	13.855 Ampere	50.3178 Ampere
Stator Current At Required Torque	5.5536 Ampere	4.9365 Ampere	5.5536 Ampere	4.9365 Ampere
Copper Loss at Required Torque	379.4463 W	72.1483 W	720.2702 W	139.0421 W
Current Density At Required Torque	23.3754 A/mm2	9.8209 A/mm2	28.2843 A/mm2	12.8273 A/mm2
Mechanical Power At Required Torque	1507.9645 W	1507.9645 W	1507.9645 W	1507.9645 W
Efficiency At Required Torque	72.56%	59.81%	62.34%	58.26%

For the motor with high airgap flux, to minimise copper losses, as discussed in Chapter 7 the wire diameter size can be reduced by changing the motor parameter. For example the actual wire diameter is 0.8997mm for the case of full arc magnet motor with high B_r . The next higher size is 0.9mm while the MATLAB program has selected 0.8mm. By changing the motor parameter a few turns from the winding can be reduced to fit a wire with a bigger diameter (i.e. 0.9mm compared with 0.8mm) and a more efficient motor is obtained. In Table 8.2 some of the parameters like stator dimensions that are common in all designs have been omitted for clarity.

In Table 8.3, after the maximum achievable torque is calculated (like 1.96N.m.), the motor parameters are calculated for the operation of the motor at the 1.2N.m. required torque. As in permanent magnet motors the torque is directly proportional to the stator current, the stator current is calculated by multiplying the torque ratios. Hence the efficiency of the motor and the current density of the motor at required torque can be calculated. For example the current density of the motor with full arc at 1.2 N.m. is $9.82\text{A}/\text{mm}^2$ that is acceptable for a motor with air-cooled based on Table 6.3. This current density at maximum torque of 1.96 N.m. is $16\text{A}/\text{mm}^2$, that exceeds the rating of the motor. However, in some specifications the motor is required to operate for a limited time at 125% or 150% of the full-load and hence the overload condition can be satisfied if the rated torque is 1.2N.m..

In terms of efficiency of the motors, the efficiency of the ferrite motor at required torque is higher than the efficiency of the motor with rare earth magnet. The reason is that the motor is operating at high speed. Table 8.4 illustrates the efficiency of two motors at constant power operation.

Table 8. 4 Efficiency comparison between the rare earth and ferrite magnet motors for constant power operation.

<i>Operation</i>	<i>High B_r</i>	<i>Low B_r</i>
High Speed	21%	55.94%
Low Speed	47.33%	15.1%

Low speed efficiency of 47.33% is an acceptable efficiency and similar to efficiencies with designs reported by some of the references in literature review [19]. However, high speed efficiencies are very low and is due to the airgap flux. A reasonable level of core loss is about 70-100 Watts that corresponds to a maximum speed of 3000 rpm for the rare earth magnet and 7500 rpm for the ferrite motor despite the fact that at very high speed the integral fan of the motor provides an effective cooling. With 100W of core loss at 12000rpm-0.2N.m. and 69W of copper loss at 550rpm-1.2N.m., the motor efficiency at full load (12000rpm-1.2N.m.) is about 89.9% that is very good for a small motor. This efficiency cannot be achieved at 12000 rpm-0.2N.m.. However, because the rare earth magnet can supply a maximum of 1.96N.m. or 163.3% the required torque, a lower pulley ratio can be selected. This pulley ratio will result in a high speed limit of $12000/1.63=7362$ rpm that is acceptable in terms of core losses. This process illustrates the trade off and changing design parameters to obtain the best design.

From the above discussion, it is clear that a Wound Rotor Brushless Motor should operate at efficiencies similar the low speed operation of the rare earth magnet and high speed operation of the ferrite magnets assuming the converter loss and the rotor winding losses are ignored. In the following sections a quantitative analysis of the WRBM efficiencies will be presented.

8.3.3 FEA Of Motor With High B_r

The FEA of the motor with high B_r generates the same contour of the flux lines as illustrated in Figure 7.1 and 7.2 with higher flux density values. In this analysis it is assumed that the iron has uniform saturation properties that is not true for high magnetic field intensities. Due to limitation of the FEA software in mesh generation the ratio of airgap flux to B_r was lower than what was predicted by Equation 6.3. But at the vicinity of the teeth of the stator the flux is almost twice as the B_r that is what had been expected and is evident by high concentration of flux lines in Figure 6.3.

8.4 WOUND ROTOR BRUSHLESS MOTOR (WRBM) DESIGN

In this section the design procedure for a WRBM is described. From previous sections it was found that a permanent magnet motor with ferrite magnet has higher efficiency at high speed compared with a motor with high remanence flux density while at low frequency the opposite is true. If a WRBM is designed that has an electrically generated airgap flux similar to a permanent magnet motor with high B_r , the wire diameters can be increased due to reduction of coil turns. This results in an efficient motor similar to a permanent magnet with high B_r . At high speed the airgap flux can be reduced electrically to make the motor similar to a ferrite motor that has less core losses due to the reduction of flux. This is the basis for the design of the WRBM. Hence, assuming $B_r=0.9$ T, the motor parameter is the same as the motor described in Table 8.1 for the full arc magnet motor without the losses at high speed. With this introduction, the design of a WRBM is basically the design of a motor for low speed torque and the design of the rotor winding to generate the same magnetic flux density as a permanent magnet with high B_r . The design is divided in three sections, static magnetic field generation, low speed and high speed calculations that will be described in the next few sections.

8.4.1 Static Magnetic Field Generation

At this stage it is assumed that the rotor winding are supplied with a dc voltage or current source and it is required to generate a magnetic flux density equal to B_r within the physical dimension of the motor of Figure 6.1. The input to the problem is the dimension and the required B_r and the solution is the amp-turns required to generate this magnetic flux density at expense of rotor copper losses. It is obvious that the worst case condition in terms of the copper losses is at maximum B_r and when the current is reduced in the rotor winding to generate a lower flux at high speed the copper losses are less.

8.4.1.1 Approximate solution:

A simplified calculation can be performed by assuming that the reluctance of the iron is negligible compared with the reluctance of the airgap. Hence, all of the amp-turn that is required to generate a magnetic field equal to B_r in the airgap is determined by the airgap reluctance and is calculated from Equation 8.1. Because in a complete magnetic path the airgap reluctance consists of two airgaps a factor of 2 is required.

Assuming equal area for the airgap and the rotor poles and ignoring the reluctance of iron, the total magneto-motive force NI_r can be approximately calculated from Equation 8.1.

$$NI_r = \frac{B_r}{\mu_0} 2xg = \frac{0.9T}{4\pi \times 10^{-7}} \times 2 \times 0.8e^{-3} = 1146.5AT \quad \text{Equation 8.1}$$

This simplified equation states that to generate a $B_r=0.9$ Tesla a coil is required with amp-turns of 1146.5. If we select $I_r=1A$ then the coil has 1147 turns. Using 80mm average length of a 0.5 mm diameter wire ($2 (stack\ length + pole\ width)$) with a resistance of $8.8ohm/100meter$, total resistance of the coil is 8 ohms/pole that results in only $8W/pole$ of copper losses from $P_{rcu}=I_r^2 \times R_r=8W/pole$. Hence, the extra copper loss that result in generating a magnetic flux density similar to a permanent magnet is $8 \times 8=64W$. However, when the current in rotor winding is reduced to generate a flux similar to a ferrite magnet, (i.e. 0.4T) the copper losses in rotor is only $(0.4/0.9)^2 \times 64 =12.6W$ while the motor core losses reduced from 941.3 W to 190.7W (Table 8.3). This approximate calculation was described to illustrate how the WRBM outperform a permanent magnet motor at high speed at the expense of acceptable losses at low speed operation. This outcome is what we predicted throughout this work. In practice, a much higher wire diameter can be selected so the losses can be reduced. Although the efficiency of the converter that induces the power to rotor is low and must be accounted for, excellent performance of the motor at high speed and in constant power operation is a good trade off for most of applications.

In above example it was assumed that the airgap flux is equal to B_r while in permanent magnet design the airgap flux density is B_m that is lower than B_r and requires less amp-turns than B_r . It is also concluded that a motor with smaller airgap is more suitable for WRBM. In the following section a detailed design of the static magnetic field is described.

8.4.2 Calculation Of The Rotor Winding Area

Figure 8.1 illustrates the cross section of a motor with wound rotor. In this motor the rotor winding area consists of a triangle with the dimension of D_r and half of the distance between the edges of poles. In this figure the rotor pole area is similar to a permanent magnet motor but can be reduced in thickness so that the winding

area is increased. If the arm of the rotor that connects to the pole has an area half of the pole the intensity of the flux density can be twice that of the airgap. If the arm width is large, winding area is reduced and if the arm width is small the iron can saturate.

Assuming a maximum flux density of 0.9T for the airgap, the flux density in the arms can reach to the saturation level and magnetomotive force must not exceed this level although determining exact value for magnetic flux density requires a FEA.

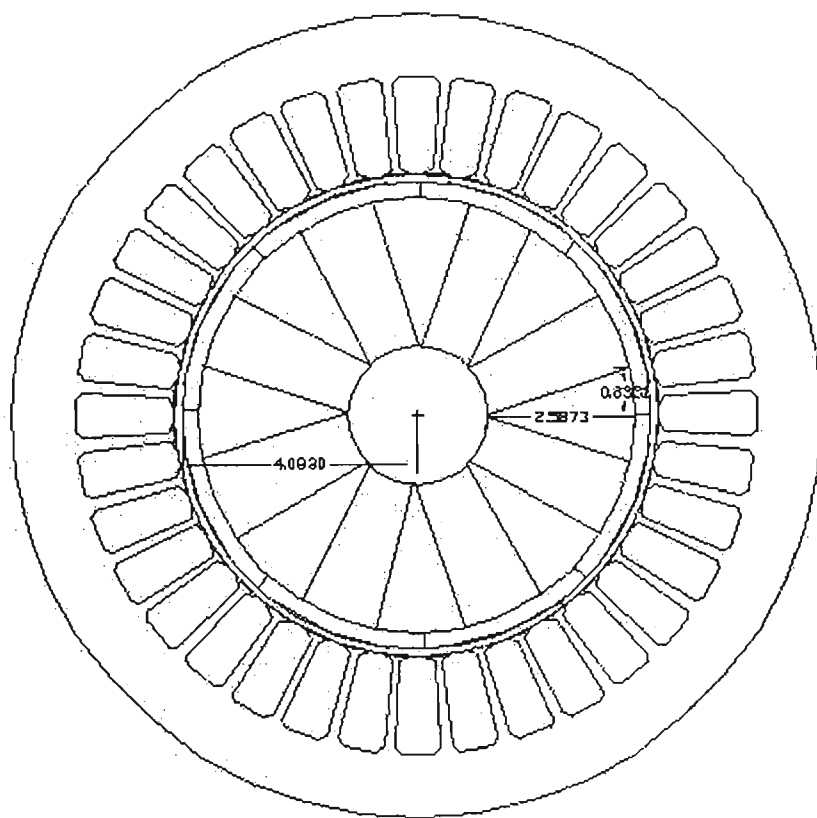


Figure 8. 1 Cross section of a WRBM.

The distance between 2 adjacent poles can be approximated by:

$$Pole_width = \frac{\pi D_y}{poles} = \frac{3.14 \times 64.4}{8} = 25.3mm$$

If the arm that connects the pole to the shaft of the motor has a width of one third of the pole width, the area of the rotor pole (25.3/3=8.4) to the area of the arm will be one third. The winding area can be calculated by approximating to a triangle area from:

$$\begin{aligned} Winding_Area &= \frac{pole_width - arm_width - pole_space}{2} \times \frac{D_y - shaft_Dia}{2} \times \frac{1}{2} \\ &= \frac{25.3 - 8.4 - 0.7}{2} \times \frac{72.4 - 20}{2} \times \frac{1}{2} = 106mm^2 \end{aligned}$$

This area can also be measured by utilities available in engineering drawing software packages. Reducing the arm area will further increase the winding area as illustrated in Figure 8.4. Using the software utility to measure the area, the area was measured at 152mm² for the rotor design in Figure 8.4.

8.4.3 Wire Diameter

Equation 7.7 can be used to estimate the diameter of the wire that can be fitted in rotor slots. With single wire winding the fill factor of 0.75 is selected hence to fit 1147 turns the wire size is 0.30mm that is smaller than 0.5mm predicted in previous section and results in high losses.

The airgap flux is $B_m = B_r / 1.1 = 0.818T$ that results in reduction of amp-turns to 1043. Increasing the current to 4A and reducing the turns to 1043/4=261 with an area of 152 mm² (Figure 8.3), 0.63mm diameter wire can be used that has

5.4ohm/100 meters. Hence total rotor winding resistance per pole is $261 \times 0.08 \times 0.054 = 1.13$ ohms and the losses will be $4^2 \times 1.13 = 18W$ per pole and 144W total in the rotor. Considering a converter with 80% efficiency total power losses are 180W. This power is relatively high and one way to reduce it as discussed earlier is to reduce the airgap. Reducing the airgap to 0.5mm the total amp-turn to generate 0.818T in the airgap becomes $0.5/0.8 \times 1043 = 652$ turns. Wire diameter of 0.4mm with specific resistivity of 13.5 ohm per 100 meters (13.5ohms/100m) can be used. Total winding resistance will be $652 \times 0.08 \times 0.135 = 7$ ohms and total loss of 7W per pole and 56W total. With a converter efficiency of 80% total rotor losses is 70W that is acceptable with total rotor winding resistance of 56 ohms.

8.4.4 Low Speed Operation

With rotor copper loss of 70W, total stator and rotor copper losses are $192.5 + 70 = 262.5W$ for the motor with 0.5mm airgap, and $192.5 + 180 = 372.5W$ for the motor with 0.8mm airgap.

The torque generated in the motor is similar to the maximum torque of the motor with high B_r or 1.96N.m. and if 1.2 N.m. is required, the torque constant can be reduced by reducing flux or the stator winding current is reduced by reducing supply voltage or PWM techniques. If the flux or stator current is reduced to $1.96/1.2 = 1.63$ total losses is reduced. If the stator current is reduced by square root of 1.63 (1.277) and if the airgap flux is also reduced by the same proportion, the copper losses will become 228.4W. The method to calculate the losses is by reducing (K_e that is the same as K_t) and I_s by 1.277 times so that the torque T and K_e are reduced by 1.63 times from 1.69 to 1.2N.m.. Copper losses due to 8.07A stator winding current is 192.5W and the rotor copper loss is 180W. The new losses will be $192.5/1.63$ and $180/1.63$ and total losses will be 228.4W for the motor with 0.8mm airgap and 161W for the motor with 0.5mm airgap.

8.4.5 High Speed Operation

At 0.2N.m., torque constant of 0.243 and the stator current is reduced by $1.96/0.2=9.8$ times. The airgap flux can be reduced by square root of 9.8 or 3.13 and stator current with the same amount to give 9.8 times less torque. This results in rotor winding current of approximately $1/3.13=0.32$ A for an airgap flux of $0.9/3.13=0.287$ T that gives a torque constant of $K_e=K_t=0.078$ N.m./A. The Stator current is also reduced from 8.07A (Table 8.3) to $8.07/3.13=2.58$ A. Rechecking the torque again:

$$T=K_t I_s=0.078 \times 2.58=0.2 \text{ N.m.}$$

The stator core losses can be calculated from Equation 7.16 at $B_r=0.287$ (with the MATLAB program in Appendix D) and it is 99.5W. Stator copper losses are 9.8 times less than the losses for maximum torque because the current is 3.13 time less hence the stator copper loss is $192.5/9.8=19.6$ W.

For the motor with 0.8mm airgap the rotor copper loss reduce 9.8 times to $180/9.8=18.37$ W. It is assumed that the converter has constant efficiency at every load for simplicity of calculation. This in not usually the case but because power converted is low, the losses are low and the error will be negligible. Total losses are the sum of the copper losses and core loss and will be $99.5+19.6+18.37=137.5$ W compared with 941W of the motor with high B_r (Table 8.3) and 190.35W for the motor with ferrite permanent magnet. For the motor with 0.5mm airgap, total loss is $99.5+19.6+7.1=126.2$ W. This is a power saving of in excess of 800W compared with the motor with high B_r and power saving of 56W compared with the motor with low B_r . This result is what we had anticipated that the major benefit to the WRBM is operation at constant power region with power saving at high-speed operation.

8.4.6 Current Density

Using Equation 7.13 the rotor current density for one amp rotor current and 0.4mm wire diameter is $8A/mm^2$, that is acceptable (Table 6.3) especially because of the rotor rotation some cooling is provided.

8.4.7 Efficiency

In Table 8.5 efficiency of the WRBM and permanent magnet motors with high B_r and low B_r are illustrated. The efficiency of the WRBM with 0.8mm airgap at low speed is $69/(228.4+69)=23.2\%$ and $251/(137.5+251)=64.6\%$ that is excellent results as the efficiency exceeds the permanent magnet with low B_r at high speed. The efficiency for the motor with 0.5mm airgap is $69/(161+69)=30\%$ at low speed and $251/(126.2+251)=66.54\%$ at high speed.

Table 8.5 Comparison of the efficiency of the WRBM with permanent magnet motor.

<i>Operation</i>	<i>WRBM 0.8mm airgap</i>	<i>WRBM 0.5mmairgap</i>	<i>PMBM High B_r</i>	<i>PMBM Low B_r</i>
High Speed, 12000 rpm, 0.2N.m., 69W	64.6%	66.54%	21%	55.94%
Low Speed, 550 rpm, 1.2N.m., 251W	23.2%	30%	47.33%	15.1%

This table quantitatively describes what had been anticipated throughout this work and agrees with general observation that a WRBM has higher efficiency at high speed and lower efficiency at low speed compared with a permanent magnet motor.

8.4.8 FEA

Due to the limitation of the FEA software, accurate results could not be obtained however the flux lines and relative measurement of the flux densities confirmed that the arm of the rotor flux densities are higher than the airgap. Figure 8.2 illustrates FEA of a rotor similar to Figure 8.1. To increase the winding area the rotor shape was changed to that of Figure 8.4.

The main problem with WRBM is the lack of winding area for the rotor when the magnetic flux density is high. As illustrated in Figure 8.2-8.4, the concentration of the flux lines in the arm of the rotor is high and in simplified term the flux density in the arm is twice the flux density of the pole if the area of the pole is twice the area of the arm. This flux is the result of static magnetic field and does not generate any loss but can saturate the iron and the amp-turns to generate the required flux density increases. At 2.2T the permeability of iron is equal to that of air due to saturation hence care must be taken in design of the rotor.

As illustrated in Figure 8.2 there is some leakage of flux between rotor poles and they must be separated with a minimum distance. A FEA analysis can identify leakage area and the areas that have high magnetic field intensities.

Bright areas in Figure 8.3 illustrate the areas that the concentration of magnetic field is high and particularly when the saturation characteristics (i.e. BH curve) of iron is used in FEA, the effect of saturation can be quantified. In one analysis, iron permeability is assumed constant and in second analysis the proper BH curve is used and hence by checking the flux density and magnetic field intensity the effect of saturation can be identified. Unfortunately, in this work there were difficulties in using the FEA because of the limitation of the student version and hence only

interest in FEA was the observation of the flux lines although almost all of the motor parameters can be found in professional version of the FEA software.

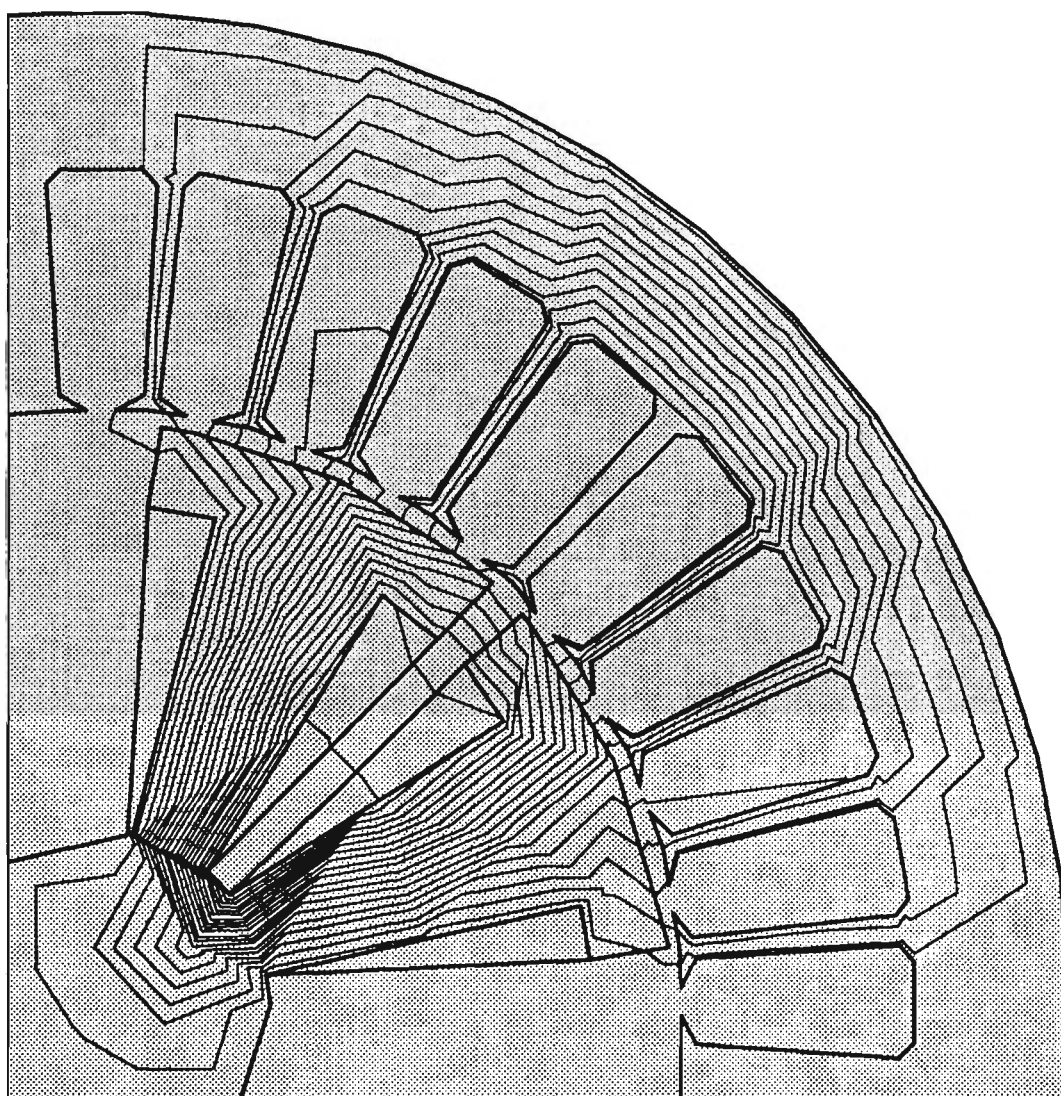


Figure 8. 2 Contour of the magnetic flux density of WRBM.

In terms of the design, the main objective in the design of the rotor in WRBM is to increase the winding in order to increase the diameter wire of the rotor winding without reducing the width of the arm. Figure 8.4 is another design that has bigger winding area (152mm^2) compare with 107mm^2 in Figure 8.1. The calculation of the area is not always straightforward and does not have a particular rule. Drawing packages and FEA software have utilities that calculate the area of an enclosed entity and this was found more practical to define equations for calculation of the

winding area. However, simple estimation by equations that was defined in Section 8.4.1.2 can be used as guideline for a suitable winding.

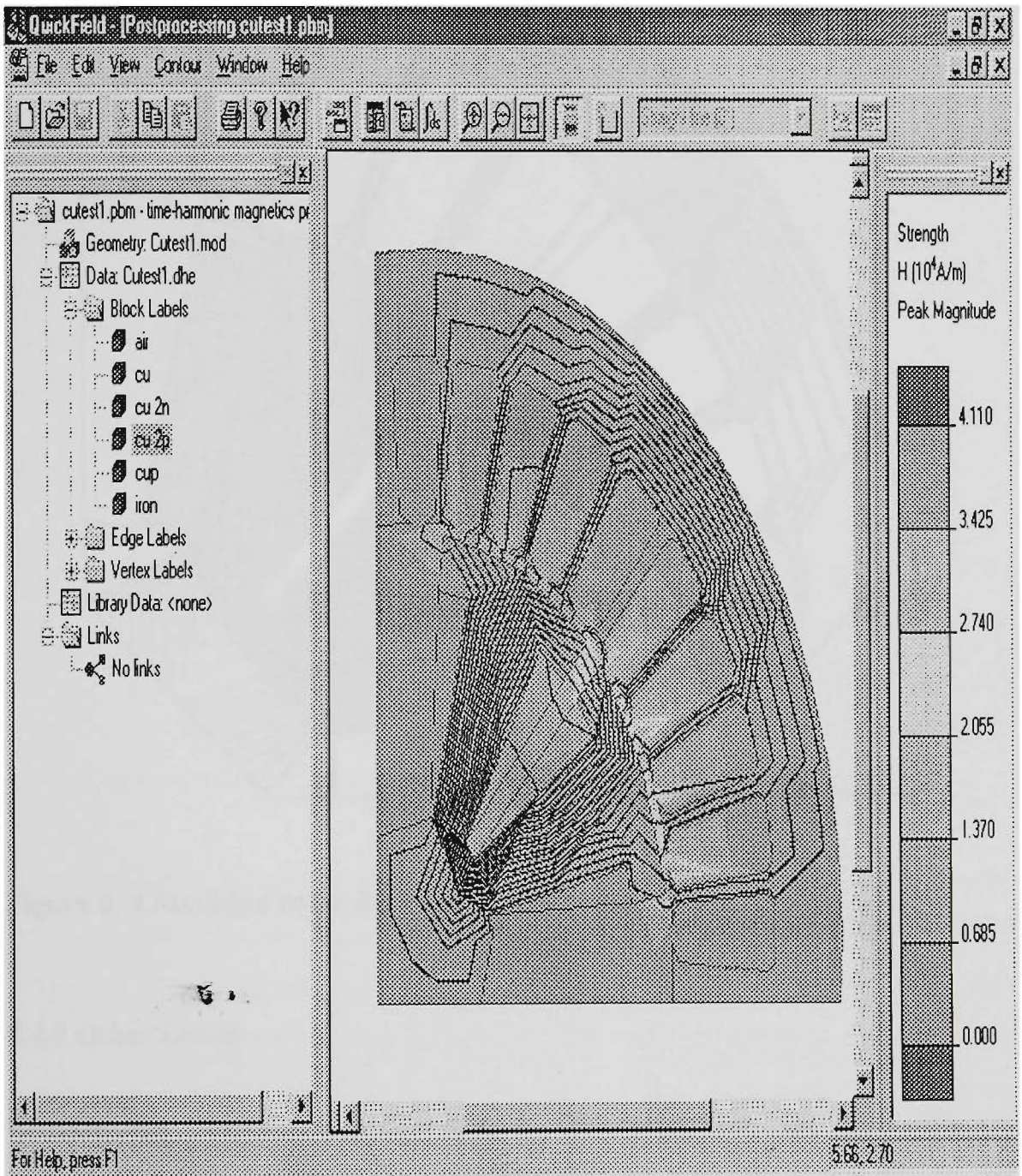


Figure 8. 3 Magnetic field intensity of the WRBM.

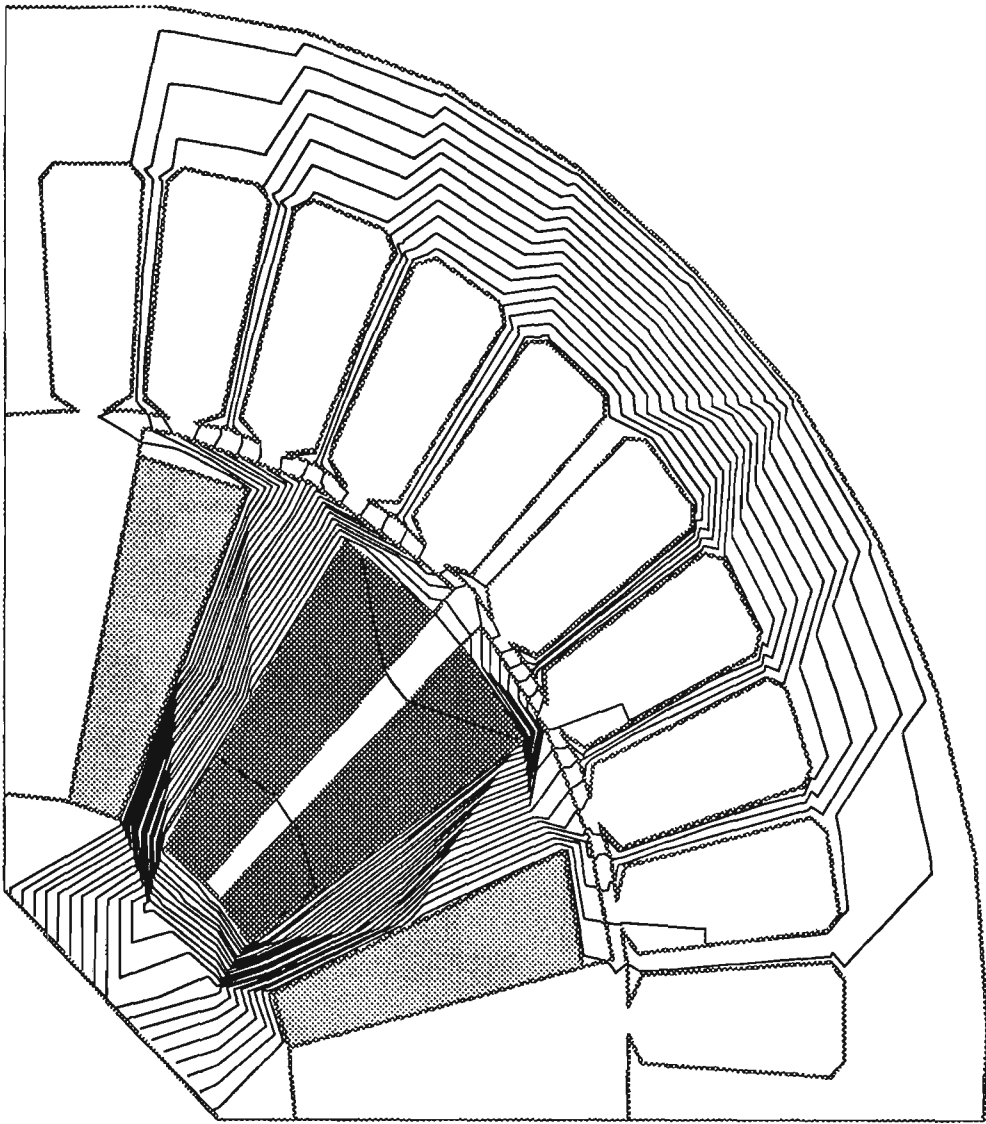


Figure 8. 4 Modified rotor for increased winding area.

8.4.9 Other Losses

Because the purpose of this work is the comparison between different technologies only the losses are considered that are available in one design and not in the other. However, one of the losses that is interesting to note is the rotor core loss due to the variation of the flux density due to the slot openings.

Rotor lamination is in a magnetic field that its frequency is the difference in rotating magnetic field of the stator and the speed of the rotor. Hence, in general, the ac portion of the rotor field has a low frequency (low core loss) and only the static magnetic field or a dc field is generated in rotor that does not cause any core loss. However, there is small variation of flux due to the slot opening as the rotor rotates and this has been quantified in reference [63]. Because the rotor lamination is closer to the stator there could be some increased core loss in the rotor. Because the motor operates in constant power region where the magnetic flux is reduced at high speed hence the increased core losses due to slot opening is not expected to be substantial.

8.5 SUMMARY

In this chapter the design of a permanent magnet motor with high B_r and the design of the WRBM was described. From this design-based comparison it was demonstrated that a WRBM outperforms a permanent magnet motor at high speed in terms of efficiency but at low speed it has lower efficiency than a permanent magnet with high B_r .

A WRBM however has a wide speed range that cannot be obtained efficiently with permanent magnets that use ferrite or rare earth magnets. A permanent magnet with high B_r has good low speed torque but with high core losses at high speed while a permanent motor with low B_r has poor low speed torque and more efficient high speed operation. The reason for this inconsistency is that in permanent magnet motors the airgap flux is fixed and low-speed high-torque operation requires high airgap flux density (higher torque constant) and high-speed low torque requires low airgap flux density.

A WRBM solves this problem by electrically changing the airgap flux. This operation requires some electrical power that reduces the overall efficiency at low speed but improves the efficiency at high speed.

To improve the performance of a WRBM, the following design objectives must be met:

1. The winding area must be increased but not at the expense of reducing pole area especially if the magnetic flux intensity is high because saturation occurs in iron.
2. The airgap must be reduced in order to reduce the amp-turn required for generation of the static magnetic field.
3. The most efficient constant power operation is achieved both by reducing the stator current and rotor winding current to minimise the losses.
4. Design parameter can be changed slightly to obtain the best result. For instance one might reduce the airgap flux density slightly to fit a perfectly matched winding in the rotor winding area. A WRBM provides many design parameters that can be altered for the best design. This design methodology is not basically available in a permanent magnet motor because of the specified remanence flux densities. In a WRBM the flux density set point can be altered to any value electrically as long as the saturation in iron does not occur.
5. Use of FEA analysis is helpful in the design of the WRBM than in design of the permanent magnet motors. The reason is trade off involved in design of the rotor lamination for biggest winding area without iron saturation.
6. A design based on a permanent magnet motor with high B_r is a good start in designing a WRBM. After calculation of the stator windings the rotor winding is designed for minimum copper losses.
7. A WRBM has good performance in terms of peak torque and excellent performance at high speed.

CHAPTER 9

CONCLUSION

9.1 INTRODUCTION

The objective of this research work was to bring about a new drive system that solves the problems in common drive systems. In Chapter 1, it was described that there are three types of motor drive systems that are nowadays used and investigated; Induction Motor (IM) drive systems, Switched Reluctance Motor (SRM) drive systems and Permanent Magnet Brushless Motor (PMBM) drive systems. Our literature survey illustrated that the most efficient of these drive systems is PMBM, that also has the best performance in terms of the low speed torque per unit volume of the motor. PMBM motors are widely used in Electric Vehicles (EV) and areas that require high efficiency and good low speed torque. There are however two major problems with a PMBM. First, the cost of the high remanence flux density motors is high and second the motor operation at high speed becomes inefficient because of high airgap flux density core losses.

9.2 THE QUEST FOR A VERSATILE DRIVE SYSTEM

Constant power operation that is referred to an operation with low-speed high-torque and high-speed low-torque has many industrial and domestic applications, like EV and machine tools. It is the area that a PMBM cannot compete with Vector Control Induction Machine drive systems that can run efficiently in field weakening region, if efficiency is more important than cost.

The best and versatile drive systems were dc brushed motor that could operate at any load no matter what the torque-speed characteristics were. However these

motors had extensive maintenance and RFI problems that has made them almost obsolete at least in modern industrial plants. The advantage of the good old dc motors was that the field and armature currents could be controlled independently and linked if needed to. These characteristics were what the author sought to obtain with the new Wound Rotor Brushless Motor (WRBM) drive system. This motor drive is basically a PMBM but with wound rotor that is powered from a switch mode power supply with primary and secondary cores separated.

To minimise the losses during the design process both the field and stator current were changed to obtain maximum efficiency in constant power. This process is the best quality of the old dc motor with separate field and armature winding excitation than could be used for any load and as described in Chapter 8 this is what can be done with WRBM, separate excitation of the field and stator current.

The limits on the power delivery to the rotary side were increased by adopting resonant modes and sensorless position and speed detection method was proposed. The next stage was to do the sums up and calculate the efficiency of the new WRBM, and to see its comparability to PMBM.

It is demonstrated that a PMBM can be designed to operate either at high speed or at low speed with limited speed range. If a ferrite or a magnet with low remanence flux density is used, a good low speed torque is difficult to obtain but the high speed performance is good in terms of efficiency. If a rare earth magnet with high remanence flux density is used, low speed torque is good but because the flux density is high core losses are high at high speed. This is why a PMBM for wide speed range and operation in constant power region is problematic. By increasing the airgap flux in WRBM electrically, airgap flux could be increased similar to the PMBM with high remanence flux density magnet. By reducing the airgap flux density at high speed it was similar to a ferrite PMBM, so the core losses were

low. If only the efficiency of the power induction to rotor winding was acceptable, there was a motor comparable to the brushed dc motor performance, but with no brushes.

9.2.1 The Question Of Efficiency

At the beginning of this research, it had been anticipated that the WRBM has better efficiency than PMBM at high speed due to the fact that in constant power the required airgap flux is minimised because the torque is reduced. Hence to generate a weak magnetic field did not require a lot of power compared with power consumption of the motor at high speed. It was also indicated in the proposal that the expected efficiency of the WRBM at low speed is lower than a PMBM. The prediction about high and low speed efficiencies were correct but what was surprising was the amount of power saving that could be made at high speed compared with both ferrite PMBM and rare earth magnet PMBM.

Table 8.5 compares the efficiency of different motors at 550 and 12000 rpm. The two designs were based on one stator chassis and although in some cases it cannot be a practical design due to high losses, but the efficiency figures can be referred to as being obtained under similar design conditions. Based on this table, the efficiency of the WRBM is 64.6% for an inefficient design, the efficiency of the ferrite PMBM was 55.94% and the efficiency of the rare earth magnet PMBM was 15.1%. This was an excellent result as the WRBM could exceed the efficiency of the ferrite motor. At low speed however the efficiency of the inefficient WRBM (0.8mm airgap) was 23.2% compared with 47.33% and 15.1% respectively for the PMBM with high and low remanence flux density magnets. The efficiency of WRBM at low speed could be increased to 30% by reducing the airgap to 0.5mm. These efficiency figures include an estimate of the losses of the converter that supplies the rotor winding. These results especially at high speed exceeded expectations of the research proposal.

9.2.2 Further Improvement In Efficiency

In terms of the motor design, because in a WRBM the stator and field currents can be changed independently, the designer has a free hand in changing design parameters to make the design more efficient and robust. A few examples were given in Chapters 7 and 8 in this regard and will not be repeated, hence the design of the WRBM for maximum efficiency is straightforward. But in terms of increasing the efficiency of the power conversion to the rotor and generation of the static magnetic field, many improvements can be made. In terms of the static magnetic field a WRBM best will be designed for high speed and with small airgap. Reducing the airgap will reduce the rotor current for a given airgap flux density and when the current is reduced the losses are reduced by a power of two of the rotor current.

Another important improvement is to fill the rotor winding area with as much as copper that is possible. By increasing the winding area, the resistance of the rotor is reduced and the losses are minimised. The winding area is only limited by the size of the iron poles that carry twice the airgap flux and can saturate if the magnetic flux density is high. For medium-high speed motors, lower airgap flux can be selected and hence there is more winding area for the rotor and the motor will be more efficient.

FEA can be very helpful in the design of the WRBM in maximising the winding area and inspection of the area of the rotor and stator laminations that are subject to saturation.

Further increase in the efficiency of the WRBM drive system can be made by increasing the efficiency of the converter and power induction from the stationary section to the rotary section of the switched mode transformer.

9.2.3 Improvements In Power Conversion Section

The details of power conversion were discussed in Chapter 4 and it was demonstrated that, by implementing a resonant circuit the power levels that could be converted from the stationary core of the transformer to the rotary section can be increased. The main problem with the power conversion from the stationary core to the rotary one of the transformer is the leakage inductance. Using a resonant capacitor in series with the transformer can increase the power levels that can be transferred with a given supply voltage. Also because the transformer has an airgap the magnetisation inductance is low, that makes the power conversion reactive. This results in higher switching current that does not contribute in power conversion. Hence, by increasing the primary inductance of the transformer the reactive current can be reduced and the inverter losses can be minimised.

Reducing the transformer airgap also increases the magnetisation inductance and decreases the leakage inductance and hence the efficiency of the power conversion can increase. Increasing the size of the transformer is required when the transferred power levels are increased. Alternatively the switching frequency can be increased to reduce the size of the transformer.

As the conversion topology is resonant, conduction losses of the transistors are higher but switching losses are lower than a conventional PWM topology. A current control topology is more suitable because a current transformer that is used in series with the primary of the transformer can be used to control the power that is transferred. This power is used to generate the static magnetic field of the rotor and is consumed in the rotor winding resistance.

With the resonant method, the only limit in power conversion level is the temperature rise of the transformer. Due to the rotor rotation, it is best to

incorporate the loss of the transformer in the secondary side so that better cooling is provided due to higher airflow.

Figure 9.1 illustrates the high frequency transformer that was used in the prototype. Despite the basic attachment of the transformer the operation of power conversion was satisfactory.

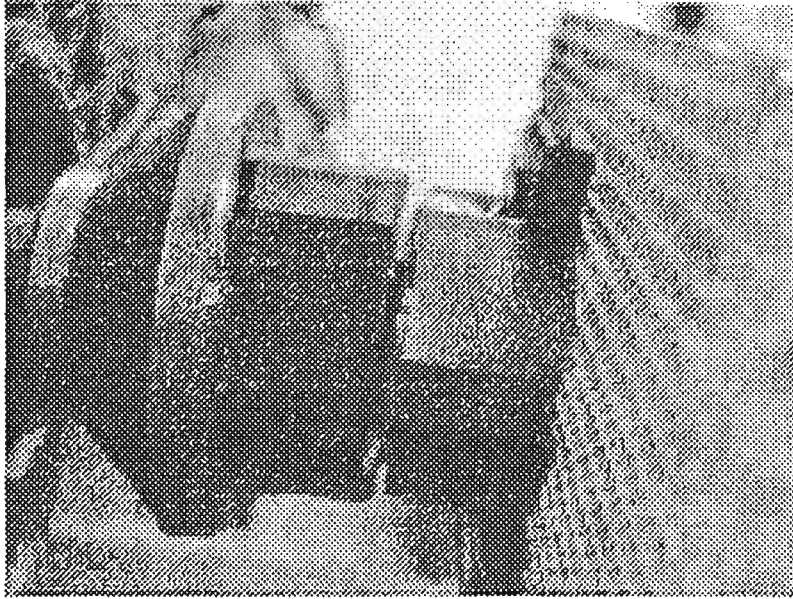


Figure 9. 1 High frequency transformer.

Figure 9.2 illustrates the HF frequency transformer with a bulb that was used in the experiments to verify the operation of the converter. This bulb was lit when the inverter was on and had no contacts to any supply and was only powered by the induction of power from the stationary core to the rotary core. The relative size of the transformer with respect to the motor illustrates the practical arrangement that is incorporated in the design of the WRBM.

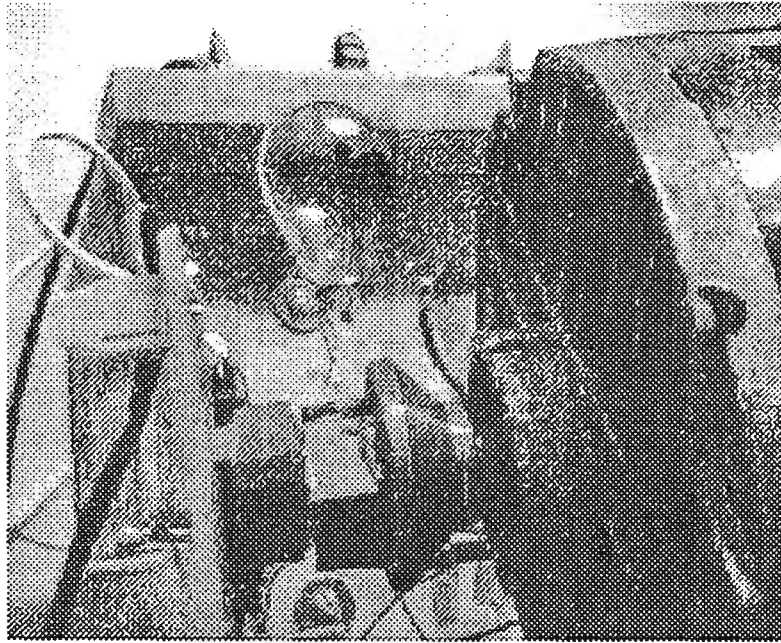


Figure 9. 2 High frequency transformer with the test bulb.

Usually a control circuit power supply is required for the stator drive, DSP and other electronics circuits. High frequency transformer can provide this power and because of the small size of the transformer it can be fitted inside the chassis of the motor. If the motor is only used for high-speed low-torque operation the size of the transformer can further be reduced because the power level that needs to be converted is low.

9.3 *SENSORLESS DETECTION OF POSITION AND SPEED*

A sensorless speed and position detection method was described, that used the construction of the motor to detect small variations of magnetisation inductance. This variation was amplified and based on the method that was described in Chapter 5, was used to detect the speed and position of the rotor. Commutation pulses of the stator winding of the motor can also be generated once the position of the rotor is detected.

In the experiments a triangular waveform was used to simulate the triangular waveform generated by the variation of the magnetisation inductance and commutation pulses were generated that corresponded to the absolute position of the rotor.

The main problem with the sensorless detection was its sensitivity to the rotor winding current, because the only transducer used was a current transformer sampling the high frequency transformer current. Current transducer circuit is basically a peak detector circuit but because the rotor winding current appears as a dc voltage, the variation of the magnetisation inductance that is a low frequency signal, cannot be easily detected at low speeds. At high speed an ac coupled can easily separate the current due to the load (rotor winding) from the magnetisation current. However at low speed operation a variable offset amplifier is used to remove the dc offset that results from the rotor winding current.

In resonant mode, when the resonant frequency is close to the resonant frequency of the series capacitor in resonance with the transformer magnetisation inductance and leakage inductance, higher variation of the transformer current can be achieved and hence sensorless detection of speed and position becomes easier.

9.4 MOTOR OPERATION

With the limited resources that were available, a simple unipolar drive circuit was built and a two-phase 4-pole motor was constructed. The purpose of the experiment was to observe any possible problem in construction of the WRBM. This prototype was not by any means a working unit, but valuable lessons were learned in terms of the issues that were involved in construction of the motor. The resonant circuit is illustrated in Figure 9.3 and stator winding drive circuit is illustrated in Figure 9.4. The motor was operating in synchronous mode and it is needed to be set at very low speed and after start up manually, its speed changed

by varying the frequency of the stator winding drive circuit. By increasing the power to the rotor winding, the speed was constant but the torque was increased. When the power to the rotor was interrupted, the motor stopped. Changing the power to the rotor winding was achieved by changing the frequency of the resonant converter from resonant frequency.

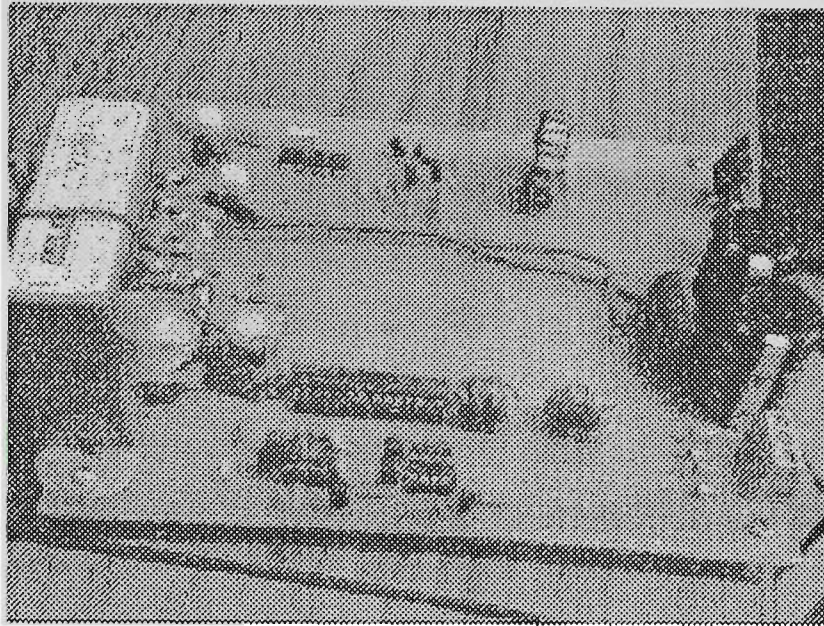


Figure 9. 3 Resonant converter for power induction to the rotor.

The 50 Hz transformer shown in Figure 9.3 is used in prototype circuit for safety reason so that the drive circuits can be worked on with at low supply voltages (i.e. when the input voltage to drive is slowly increased by a variac). The high frequency transformer will supply the control circuit electronics in final prototype.

The motor was a single-phase induction motor. Its rotor was replaced with a 4-pole rotor with 200 turns of 0.63mm winding per pole. The rectifiers that convert the ac voltage of the secondary winding of the transformer to a dc voltage, were mounted on the rotor.

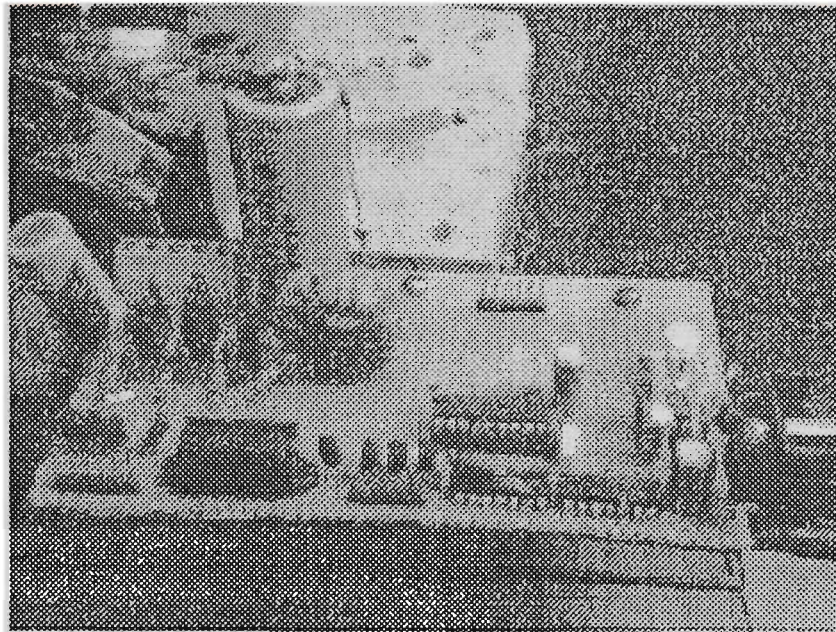


Figure 9. 4 Stator winding driver circuit.

Construction of the motor was made with a very limited budget and a better prototype is required to further test the motor for compliance with the design that was described in Chapters 6-8. It is preferable to change the size of the prototype in any future research to design a direct drive motor. The rotor diameter and the stack length of the prototype used are too small for a direct drive system for the target specification that was set in this work. Particularly at low speed operation 12 N.m. torque is required.

Prototyping a rotor with lamination is very expensive and a proper design needs a cooperation of industry that will be the next suggested phase of this work. However, where possible by means of simple experiments and hardware, a qualitative assessment of the motor performance has been obtained. For instance it was necessary to find out if there was any obstacle in mounting of the high frequency transformer or the levels of the magnetic field generated in rotor. The basic structure of the modified motor that was used in this work was sufficient to investigate these factors, but was not a design that could be evaluated for torque and speed performance. The majority of this work in the motor design section is

based on conventional design methods, simulation and FEA. An attempt was made to build a drive circuit and a motor prototype that with the resonant converter constituted a drive system. This prototype proved the feasibility of the work with the limited resources that was available. This drive system was sufficient to demonstrate the basics of power induction from a stationary core to the rotary one of the transformer and was supported by simulation and experimental results that was described in Chapter 4.

Further experiments, prototyping and testing of the motor require suitable equipment like dynamometer can be performed in a commercialization stage.

Figure 9.5 illustrates the prototype motor rotating with the test bulb connected to the rotary side. The illumination of the bulb while rotating is visible in this figure.

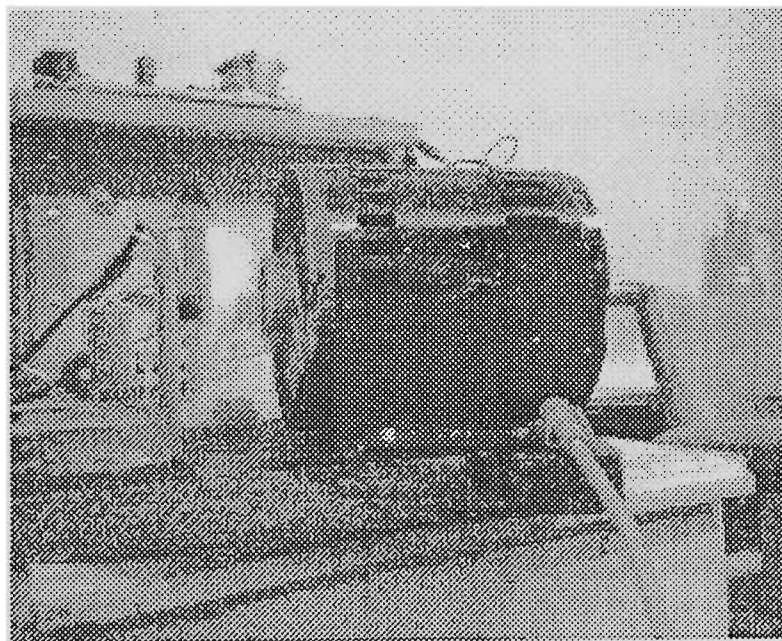


Figure 9. 5 Operation of the prototype motor with the test bulb connected to rotor.

9.5 DESIGN REVIEW

In this section the summary of the important issues that was revealed in literature review or was found to be a good feature in a drive system is discussed and the performance of the WRBM motor drive system is tested for compliance. A motor drive system for industrial and domestic applications must include the following features:

1. Low cost
2. Ability to operate in constant power region
3. Wide speed range
4. Bi-directional operation
5. Good low speed torque performance
6. Good high speed operation
7. Sensorless speed and position detection, as related to reliability and low cost
8. High peak to average torque capacity
9. High efficiency
10. Ease of torque and speed control
11. Low maintenance and high reliability
12. Low Electromagnetic Interference (EMI)
13. Inherent Braking facility
14. Low bearing current
15. Small size
16. Simple in manufacturing

In regard to some of the above items it has already been discussed that a WRBM exceeds the performance of most drive systems but some items needs

to be discussed and tested for WRBM. The most important item is the issue of cost.

9.5.1 Low Cost

In literature review we discussed that the cost of the magnets account for 70% of the cost of the motor. Replacing the permanent magnets with a wound rotor reduces the cost of the motor, and the cost of the inverter does not add too much to the overall cost. The cost comparison is valid even when comparing the motor with an induction motor that requires a cage rotor. The pressed lamination of the stator in the WRBM can be used as the lamination for the rotor that in other cases is usually wasted or reprocessed. Hence the cost of the lamination of the rotor is not an extra cost. These days the cost of power electronic devices and ferrite transformers are cheap and the extra cost of the converter does not exceed \$5-10 that is negligible compared to the cost of motor and permanent magnets. Hence it is expected that the WRBM can be manufactured much cheaper than a PMBM.

9.5.2 Braking

In regard to braking facility, PMBM drives need a clamp device to stop the rotor by shorting the stator winding. When the load speed exceeds the motor speed, the motor is converted to a generator and causes the dc link voltage to increase and the result is catastrophic for the inverter as once observed by the candidate. This fast braking is usually required in many applications like a washing machine for safety reasons and usually performed by clamping the stator windings with a rugged device like IGBT. In WRBM the power to the rotor can be interrupted and hence the energy clamping levels are much less.

9.5.3 Bearing Current

In literature review it was illustrated that a current is induced in the bearing by the stray capacitance between the stator lamination and the rotor. This current can damage the bearing and result in early failure of the motor. A few methods were described to reduce this current, one being to generate a high impedance in the path of the bearing. In WRBM the high frequency flux is induced from the primary core to the secondary core of the transformer, that is in the direction of the rotor shaft and it is possible for the bearing current to increase.

A discussion is that the source of the signal is high frequency and because the reluctance of iron is high due to core losses the stray currents are minimised. On the other hand because the operating frequency of the transformer is high the effect of leakage capacitance is more. Fortunately the stationary part of the high frequency transformer can be mounted on an insulating material so a high impedance to the stray currents are made. Nevertheless the bearing current must be quantified in any future work that requires a close to production prototype.

9.5.4 Small Size

Permanent magnet motors have the best power per volume ratio in all of the motor drive systems in industries (excluding the brushed dc motors). The controller of the PMBM is simple and there are controllers in the market that have speed calculation circuits and only need position detection circuits to run a PMBM. Some controllers use a charge-pump circuit to supply the control circuit that further reduces the control circuit size. Similar technology is also available for the induction motor drive systems for operation in VF (voltage-frequency) mode.

The availability of these controllers are due to the widespread use of motors and although the controllers for the PMBM can be used for the stator winding drive, more dedicated electronics utilise the full potential of the WRBM. Hence comparing with the availability integrated controllers WRBM is lagging behind and although the high frequency transformer can be reduced in size if the operating frequency is increased, a WRBM controller needs more space than a PMBM for the controller. In some cases however, a WRBM can have lower weight (and perhaps size) than a PMBM due to an increase in lamination size in a PMBM for core loss dissipation. This is particularly the case when operation at high speed is required.

9.5.5 Simple In Manufacturing

It is not expected that the manufacturing of the WRBM be more difficult than a PMBM. In fact bonding of the permanent magnets are regarded one of the most difficult processes in manufacturing the PMBM. With primitive tools and limited resources a basic WRBM prototype could be built while the same prototype for the PMBM could not be built with the same tools. This illustrates the ease of manufacturing of the WRBM.

9.5.6 Disadvantages

The only challenge in the design of the PMBM is to increase the low speed efficiency of the motor that with similar design parameters seems difficult. However, it is possible to design a motor with reduced airgap flux that can be more efficient than a PMBM with high remanence flux density for a particular torque. In Table 8.3 it is illustrated that the efficiency of the ferrite motor is higher than the efficiency of the motor with high remanence flux density because of the high speed losses. It means that for a given application and speed range there

could be an optimum airgap flux that results in minimum losses. A WRBM has the advantage of variable flux density and hence a more efficient design than a PBM can be found particularly if a pulley or gearbox is used.

A new type of small and high-speed motor is commonly used for model aircraft that is called ferrite motor with an integral gear box to increase the torque. The reason for this design rather than direct drive could be exactly what was discussed in regard to the efficiency of operation especially for an application that needs excellent efficiency and power per volume. Investigating the high-speed application of a WRBM with use of gearbox or pulley to increase efficiency is a good direction for any future work in design of systems that are powered by a WRBM.

9.6 SCOPE FOR FUTURE WORK

In this work it has been demonstrated that comparison with conventional drive systems, the WRBM not only is feasible but also is advantageous in many aspects. However, like other challenges further effort is necessary to improve performance. Particularly, in the commercialised world one must reduce cost and increase efficiency of any product continuously. The most important step is to design and build a working prototype of a WRBM that can be subjected to performance tests like torque, speed, efficiency and transients. This requires effort in three fronts:

- *To increase the efficiency of the power induction.* Smaller airgap and higher primary winding turns and use of low loss ferrite for transformer are recommended.
- *To improve the performance of the sensorless speed/position detection.* This improvement is the most difficult task and unfortunately is design dependent. It means that unlike a standard position detection sensor that can be mounted on any shaft and be used with any motor, there is no sensorless detection that

can be universally used based on the method described in this work. However, variation to the methods that was described can be used universally. For instance, use of a separate winding on the transformer or use of two primary cores and windings can be used for speed and position detection that is not affected by rotor winding current. This is a valuable research subject that can further enhance the performance of a WRBM motor and can be used for other motor drive systems.

- *To optimise WRBM design to increase efficiency at low speed.* This has already been discussed and two areas for improvement exist. First area is to reduce the airgap and second to increase the winding area of the rotor winding. Trying different shapes of the rotor lamination to minimise saturation of iron can be performed with FEA. Despite the design of a PMBM with little use of FEA, the design of a WRBM can be enhanced and simplified by use of FEA. Particularly, when the airgap is small and the saturation of iron is possible in the design of the motor, a FEA plot of magnetic field intensities and densities can quickly identify the problematic area. Hence a motor can be designed that uses the best of the iron and flux rather than a motor that must be oversized to allow for the safety margins for saturation of iron.

9.7 OTHER APPLICATIONS

Beside the application as a motor, a WRBM can be used as a generator with simple control for voltage and frequency and no maintenance, as there is no ring or brushes in the motor. The application of this device as a motor and/generator is the next stage when this work is expected to continue in a commercialization phase.

Bibliography

- 1 Owen E. L., "Evaluation of Induction Motors- The Ever-Shrinking Motor", Industry Application Magazine, Vol. 3, No. 1, Jan/Feb 1997, pp 16-18.
- 2 Campbell B. H., "Failed Motors: Rewind or Replace", Industry Application Magazine, Vol. 3, No. 1, Jan/Feb 1997, pp 45-50.
- 3 Bennett A. H., " Quality and Reliability of Energy-Efficient Motors", Industry Application Magazine, Vol. 3, No. 1, Jan/Feb 1997, pp 22-31.
- 4 Pillay P., "Applying Energy-Efficient Motors in the Petrochemical Industry", Industry Application Magazine, Vol. 3, No. 1, Jan/Feb 1997, pp 32-40.
- 5 Rama J. C., Giesecke A., "High-Speed Electric Drives: Technology and Opportunity", Industry Application Magazine, Vol. 3, No. 5 Sept/Oct 1997, pp 48-55.
- 6 Finley W. R., Burke R. R., " Proper Specification of Induction Motors", Industry Application Magazine, Vol. 3, No. 1, Jan/Feb 1997, pp 56-69.
- 7 Manz L., "Motor Insulation System Quality For IGBT Drives", Industry Application Magazine, Vol. 3, No. 1, Jan/Feb 1997, pp 51-55.
- 8 Bennett A., "Available Insulation Systems for PWM Inverter-fed Motors", Industry Application Magazine, Vol. 4, No. 1 Jan/Feb 1998, pp 14-26.

- 9 Finlayson P. T., "Output Filters for PWM Drives with Induction Motors", Industry Application Magazine, Vol. 4, No. 1 Jan/Feb 1998, pp 46-52.
- 10 French C., Acarnley P., "Control of Permanent Magnet Motor Drives Using a New Position Estimation Technique", IEEE Transactions on Industry Applications, Vol. 32, No. 5, Sept/Oct. 1996, pp 1089-1097.
- 11 Jouanne V., Enjeti P., Gray W., "Application Issues For PWM Adjustable Speed AC Motor Drives", Industry Application Magazine, Vol. 2., No. 5 Sept/Oct 1996, pp 10-18.
- 12 Perrin M. C., "Large Induction Motor Anti-Friction Bearing Selection", Industry Application Magazine, Vol. 2, No. 2, March/April 1996, pp 16-20.
- 13 Farag S. F., Bartheld R. G., Habetler T. G., "An Integrated On-Line Motor Protection System", Industry Application Magazine, Vol. 2, No. 2, March/April 1996, pp21-26.
- 14 Hodowanec M. M., "Effect of Coupling Installation On Motor Performance", Industry Application Magazine, Vol. 3, No. 1, Jan/Feb 1997, pp 70 77.
- 15 Donner G., Subler W., "API 541 Third Edition: An Improved Purchasing Specification", Industry Application Magazine, Vol. 3, No. 1, 201Jan/Feb 1997, pp 78-80.
- 16 Rajamani H. S., McMahon R. A., "Induction Motor Drives For Domestic Appliances", Industry Application Magazine, Vol. 3, No. 5 Sept/Oct 1997, pp 21- 26.

- 17 Kokalj D. G., "Variable Frequency Drives for Commercial Laundry Machines", *Industry Application Magazine*, Vol. 3, No. 5 Sept/Oct 1997, pp27-30.
- 18 Erickson T., "Turbidity Sensing as a Building Block for Smart Appliances", *Industry Application Magazine*, Vol. 3, No. 5 Sept/Oct 1997, pp 31-36.
- 19 Harmer K., Mellor P. H., Howe D.; " An Energy Efficient Brushless Drive System for a Domestic Washing Machine". *Power Electronics and Variable-Speed Drives*, 16-28 October 1994, Conference Publication No. 399, IEE, pp514-519.
- 20 Maudie T., Wertz J., " Pressure Sensor Performance and Reliability", *Industry Application Magazine*, Vol. 3, No. 5 Sept/Oct 1997, pp 37-49.
- 21 Chan C. C. , Jiang J. Z., Xia W., Chau K. T.; "Novel Wide Range Speed Control of Permanent Magnet Brushless Motor Drives" . *IEEE Transactions on Power Electronics*, V10, NO. 5, Sept 1995, pp539-546
- 22 Morimoto S., Takeda Y., Hatanaka K., Tong Y., Hirasu T., "Design and Control System of Permanent Magnet Synchronous Motor for High Torque Efficiency Operation", IAS 1991
- 23 Chan C. C., Jiang J. Z., Xia W., Chau K. T., "Novel Wide Range Speed Control of Permanent Magnet Brushless Motor Drives", *IEEE Transactions on Power Electronics*, Vol. 10, No. 5, Sept. 1995.
- 24 Radun V.; " High Power Density Switched Reluctance Motor Drive for Aerospace Applications". IAS 1989, pp568-573.

- 25 Moghbelli H. H., Adams G. E., Hoft R. G.; "Comparison of Theoretical and Experimental Performance of 10HP Switched Reluctance Motor". IAS 1989, pp89-98.
- 26 Suriano J. R., Omg C.; " Variable Reluctance Motor Structures for Low Speed Operation". IAS 1993, pp114-121.
- 27 Manz L., Olenkamp J., "Starting High Inertia Loads on Adjustable Speed Drives", Industry Application Magazine, Vol. 4, No. 1 Jan/Feb 1998, pp 27-31.
- 28 Busse D., Erdman J., Kerkman R., Schlegel D., Skibinski G., "Characteristics of Shaft Voltage and Bearing Currents", Industry Application Magazine, Vol. 3, No. 6 Nov/Dec 1997, pp 21-32.
- 29 Chen S., Lipo T. A., "Circulating Type Motor Bearing Current in Inverter Drives", Industry Application Magazine, Vol. 4, No. 1 Jan/Feb 1998, pp 32-38.
- 30 Ogasawara S., Akagi H., " Modeling and Damping of High Frequency Leakage Currents in PWM Inverter-Fed AC Motor Drive Systems", IEEE Transactions on Industry Applications, Vol. 32, No. 5, Sept/Oct. 1996, pp-1105-1114.
- 31 Iida S., Masukawa S., Kubota Y., "Improved Voltage Source Inverter with 18 Step Output Waveform", Industry Application Magazine, Vol. 4, No. 1 Jan/Feb 1998.
- 32 Sinha G., Lipo T. A., "A Four-Level Rectifier System For Drive Applications", Industry Application Magazine, Vol. 4, No. 1 Jan/Feb

1998, pp66-74.

- 33 Chung D., Sul S., "Analysis and Compensation Of Current Measurement Error In Vector-Controlled ac Motor Drives", IEEE Transactions On Industry Applications, Vol. 3, No.2, March/April, pp340-345.
- 34 Xiang Y. Q, Nasar S. A., " A Fully Digital Control Strategy For Synchronous Reluctance Motor Servo Drives, Vol33, No.3, IEEE Transactions On Industry Applications, Vol. 33, No.2, March/April, pp705-713.
- 35 Marchesoni A., Segarich P., Soressi E., " A Simple Approach To Flux and Speed Observation In Induction Motor Drives", IEEE Transaction On Industrial Electronics, Vol 44, No. 4, Aug. 1997.
- 36 Takeshita T., Matsui N.; Sensorless Brushless DC Motor Drive with EMF Constant Identifier". International Conference on Industrial Electronics, Control, and Instrumentation (IECON'94), pp14-19.
- 37 Jovanovic M., Betz R., " Sensorless Vector Controller For a Synchronous Reluctance Motor", IEEE Transaction On Industry Application, Vol. 34, No. 2, March/Aprill 1998.
- 38 Fitzgerald A. E., Kingsley C., Kusko A., "Electric Machinery", McGraw-Hill, 1971.
- 39 Moon S. I., Keyhani A.; "Estimation of Induction Machine Parameters from Standstill Time Domain Data". IAS 1993, pp336-342
- 40 Hurst K. D., Habetler T. G., Griva G., Profumo F.; " Speed Sensorless

- Field-Oriented Control of Induction Machines Using Current Harmonic Spectral Estimation". IAS 1994, pp601-615.
- 41 Fratta A., Vagati A., Villata F; " On the Evolution of AC Machines for Spindle Drive Applications". IAS 1989, pp699-704.
 - 42 Poloujadoff M., Laeuffure J., Obadia J., Rezgui N., "Measuring Speed and Temperature in a Large Air Gap Induction Motor", Industry Application Magazine, Vol. 3, No. 6 Nov/Dec 1997, pp 39-42.
 - 43 Le-Huy H., Viarouge P., Francoeur B.; "Unipolar Converters for Switched Reluctance Motors". IAS 1989, pp551-559.
 - 44 Radum A. V.; "Design Considerations for the Switched Reluctance Motor". IAS V31, NO. 5, Sept/Oct 1995, pp1079-1087.
 - 45 Stephens C. M.; "Fault Detection and Management System for Fault Tolerant Switched Reluctance Motor Drives". IAS 1989, pp574-578.
 - 46 Ehsani M., Ramani K. R.; "Direct Control Strategies Based on Sensing Inductance in Switched Reluctance Motors". IEEE Transactions on Power Electronics, V11, NO. 1, Jan 1996, pp74-82.
 - 47 Nozari F., Mezs P.A., Julian A. L., Sun C., Lipo T. A.; " Sensorless Synchronous Motor Drive for Use on Commercial Transport Airplanes". IAS, V31, NO.4, July/Aug1995, pp850-859.
 - 48 Matsuo T., Lipo T. A.; "Rotor Position Detection Scheme for Synchronous Reluctance Motor Based on Current Measurements". IAS, V31, NO.4, July/Aug1995, pp860-868.

- 49 Wu C., Pollock C.; "Analysis and Reduction of Vibration and Acoustic Noise in the Switched Reluctance Drive". IAS V31, NO. 1, Jan/Feb 1995, pp 91-98.
- 50 Colby R. S., Mottier F. M., Miller T. J. E.; "Vibration Modes and Acoustic Noise in a Four-Phase Switched Reluctance Motor". IAS, V32, NO. 6, Nov/Dec 1996, pp1357-1364.
- 51 Pillay P., Samudio R. M., Ahmed M., Patel R. T. , "A Chopper-Controlled SRM Drive for Reduced Acoustic Noise and Improved Ride-Through Capability Using Supercapacitors", IEEE Transaction On Industry Applications, Vol.31, No. 5, 1995.
- 52 Ferreira C. A., Jones S. R., Heglund W. S., Jones W. D.; "Detailed Design of a 30kW Switched Reluctance Starter/Generator System for a Gas Turbine Engine Application". IAS V31, NO. 3, May/June 1995, pp553-561.
- 53 Ferreira C. , Jones S. R., Drager B. T., Heglund W. S.; "Design and Implementation of a Five-hp Switched Reluctance, Fuel-Lube, Pump Motor Drive for a Gas Turbine Engine". IEEE Transactions on Power Electronics, V10, NO. 1, Jan 1995, pp55-61.
- 54 Toliyat H. A., Walker S. P., Lipo T. A., " Analysis And Simulation Of Five Phase Synchronous Reluctance Machines Including Third Harmonic Of Airgap MMF". IEEE Transactions On Industry Applications, Vol. 3, No.2, March/April, 1998, pp332-339.
- 55 Kreindler L., Testa A., Lipo T.; " Position Sensorless Synchronous Reluctance Motor Drive using the Stator Voltage Third Harmonic". IAS

- 1993, pp679-686.
- 56 Laurent P., Gabsi M., Multon B.; "Sensorless Rotor Position Analysis Using Resonant Method for Switched Reluctance Motor". Proc. of IEEE IAS Society Annual Meeting, 1993, pp687-694.
 - 57 Betz D. E., Jovanovic G., Platt D., "Sensorless Vector Controller For A Synchronous Reluctance Motor", IEEE Transactions On Industry Applications, Vol. 3, No.2, March/April, 1998, pp 346-354.
 - 58 Jones S. R., Dragger B. T., "Sensorless Switched Reluctance Starter/Generator Performance", Industry Application Magazine, Vol. 3, No. 6 Nov/Dec 1997, pp 33-38.
 - 59 Low T. S., Jabbar M. A., Tan T. S., "Design Aspect of a Slottless PM Motor For Hard Disk Drives", Industry Applications Magazine", Vol.3, No. 6. Nov./Dec. 1997.
 - 60 French C., Acarnley P., " Direct Torque Control of Permanent Magnet Drives", IEEE Transactions on Industry Applications, Vol. 32, No. 5, Sept/Oct. 1996, pp 1211-1219.
 - 61 Takeshita T., Matsui N.; "Sensorless Control and Initial Position Estimation of Salient-Pole Brushless DC Motor". Proc. of 4th International Workshop on Advanced Motion Control MIE (AMC-MIE'96), pp18-23.
 - 62 Moreira J. C.; "Indirect Sensing for Rotor Flux Position of Permanent Magnet AC Motors Operating Over a Wide Speed Range". IAS,V32, NO. 6, Nov/Dec 1996, pp1394-1401.

- 63 Hendershot J. R., Miller T. J. E; " Design of Brushless Permanent-Magnet Motors". Magna Physics-Oxford Science Publications,1994.
- 64 Gieras J. F., Wing M. ;"Permanent Magnet Motor Technology, Design and Applications". Marcel Dekker, Inc, 1997.
- 65 Leonardi F., Venturini M., Vismara A.; " PM Motors for Direct Driving Optical Telescope". IAS Magazine, July/Aug 1996, pp11-16.
- 66 Patterson D., Spee R.; " The Design and Development of an Axial Flux Permanent Magnet Brushless DC Motor for Wheel Drive in a Solar Powered Vehicle". IAS V31, NO. 5, Sept/Oct 1995, pp1054-1061.
- 67 Matsui N., Takeshita T., Iwasaki M.; "DSP-Based High Performance Motor/Motion Control". Proc. of 13th World Congress, International Federation of Automatic Control, San Francisco, 1996, pp393-398.
- 68 Chan C. C., Jiang J. Z., Xia W., Chau K. T., Zhu M. L.; "Optimal-Efficiency Control for Constant-Power operation of Phase-Decoupling Permanent-Magnet Brushless Motor Drives". Proc. of 11th International APEC Conference, 1996, pp751-757.
- 69 Jungereis A., Kelly A.; "Adjustable Speed Drive for Residential Applications". IAS V31, NO. 6, Nov/Dec 1995, pp1315-1322.
- 70 Morimoto S., Sanada M., Takeda Y.; "Optimum Machine Parameters and Design of Inverter-Driven Synchronous Motors for Wide Constant Power Operation". IAS 1994, pp177-182.
- 71 Morimoto S., Sanada M., Takeda Y., "Inverter-Driven Synchronous

Motors for Constant Power”, pp18-24.

- 72 French C., Acarnley P., “ Direct Torque Control of Permanent Magnet Drives”, IEEE Transactions on Industry Applications, Vol. 32, No. 5, Sept/Oct. 1996, pp 1080-1088.
- 73 French C., Acarnley P., “ Control of Permanent Magnet Motor Drives Using a New Position Estimation Technique”, IEEE Transactions on Industry Applications, Vol. 32, No. 5, Sept/Oct. 1996, pp 1089-1097.
- 74 Radun A. V., “Design Considerations For the Switched Reluctance Motor”; IEEE Transactions On Industry Applications, Vol. 31, No.5, Sept/Oct. 1995, pp 1079-1087.
- 75 Caricchi F., Crescimbinì F., Santini E.; “ Basic Principle and Design Criteria of Axial-Flux PM Machines Having Counterrotating Rotors”, IEEE Transactions On Industry Applications, Vol. 31, No.5, Sept/Oct. 1995, pp 1062-1068.
- 76 Jack A. G., Mecrow B. C., Haylock J. A.; “ A Comparative Study of Permanent Magnet and Switched Reluctance Motors for High-Performance Fault-Tolerant Applications”; IEEE Transaction On Industry Applications, V32, NO. 4, July/Aug 1996, pp896-903.
- 77 Steimel A., “ Electric Railway Traction in Europe”, Industry Application Magazine, Vol. 2, No. 6 Nov/Dec 1996, pp 6-17.
- 78 Caricchi F., Crescimbinì F., Honorati O., Napoli A. D., Santini E., “Compact Wheel Direct Drive for Evs”, Industry Application Magazine, Vol. 2, No. 6 Nov/Dec 1996, pp25-32.

- 79 Chalmers B., Musaba L., Gosden D.; "Variable-Frequency Synchronous Motor Drives for Electric Vehicles". IEEE Transaction On Industry Applications, V32, NO. 4, July/Aug 1996, pp896-903.
- 80 Liao Y., Liang F., Lipo T. A.; "A Novel Permanent Magnet Motor with Doubly Salient Structure", IEEE Transactions On Industry Applications, Vol. 31, No.5, Sept/Oct. 1995, pp 1069-1078.
- 81 Caricchi F., Crescimbin F., Mezzetti F., Santini E.; "Multistage Axial-Flux PM Machine for Wheel Direct Drive". IEEE Transaction On Industry Applications, V32, NO. 4, July/Aug 1996, pp882-888.
- 82 Vagati A., Fratta A., Franceschini G., Rosso P., "AC Motors for High-Performance Drives: A Design-Based Comparison", Industry Application Magazine, Vol. 32, No. 5 Sept/Oct 1996, pp 1211-1219.
- 83 Xu X., Novotny D. W.; "Selecting the Flux Reference for Induction Machine Drives in the Field-Weakening Region". IAS 1991, pp361-396.
- 84 Suriano J. R., Ong C. M., "Variable Reluctance Motor Structures For Low-Speed Operation", IEEE Transaction on Industry Applications, Vol. 32. No. 2, March/April 1996.
- 85 Statun D. A., Gild M. I. Mc, Miller T. J. E., " Interactive Computer Aided Design Of Permanent Magnet Dc Motors", Transaction on Industry Application, V31, NO.4, July/Aug1995, pp933-940.
- 86 Millman J., Taub H., " Pulse, Digital and Switching Waveforms", McGraw-Hill, 1965.

- 87 Ostlund S., Brokemper M., "Sensorless Rotor-Position Detection From Zero to Rated Speed For an Integrated PM Synchronous Motor Drive, IEEE Transactions on Industry Applications, Vol. 32, No. 5, Sept/Oct. 1996, pp 1158-1165.
- 88 Brassfield W. R., Spee R., Habetler T. G.; "Direct Torque Control for Brushless Doubly-Fed Machines". IAS, V32, NO. 5, Sept/Oct 1996, pp1098-1104.

Reading Bibliography

- 1 Bennett A. H., "Regulatory Impact on the Application of AC Induction Motors", Industry Application Magazine, Vol. 2, No. 2, March/April 1996, pp 4-15
- 2 Sarmiento H., Estrada E., "A Voltage Sag Study in an Industry with Adjustable Speed Drives", Industry Application Magazine, Vol. 2, No. 1, Jan/Feb 1996, pp 16-19.
- 3 Klontz K. W., Divan D. M., Novotny D. W., Lorenz R. D.; "Contactless Power Delivery System for Mining Applications". IAS V31, NO. 1, Jan/Feb 1995, pp 27-35.
- 4 Raad R. O., Henriksen T., Raphael H. B., Hadler-Jacobsen A.; "Converter-Fed Subsea Motor Drives", IEEE Transactions on Industry Applications, Vol. 32, No. 5, Sept/Oct. 1996, pp 1069, 1079.
- 5 Mohamed M.A., Nagrial M. H..., "Dynamic Simulation of Variable Reluctance (VR) Motors", Proc. 3rd international Conf. Modeling and

Simulation, Melbourne, Australia, Oct. 1997.

- 6 Lequesne B., Pawlak A. M., Schroeder T., "Magnetic Velocity Sensors", IEEE Transactions on Industry Applications, Vol. 32, No. 5, Sept/Oct. 1996, pp 1166-1175.
- 7 Azizur M. R., Qin R.; "Starting and Synchronization of Permanent Magnet Hysteresis Motors", IEEE Transactions on Industry Applications, Vol. 32, No. 5, Sept/Oct. 1996, pp 1080-1088.
- 8 Boglietti A., Ferraris P., Lazzari M., Pastorelli M., "Influence of The Inverter Characteristics On the Iron Losses in PWM Inverter-Fed Induction Motors", IEEE Transaction on Industry Applications, Vol. 32, No. 5, Sept/Oct. 1996, pp 1190-1194.
- 9 Melfi M. J., "Optimum Pole Configuration of Variable Speed AC Induction Motors", Industry Application Magazine, Vol. 3, No. 6 Nov/Dec 1997, pp 15-20.
- 10 Strangas E. G., Wagner V. E., Unrich T. D., "Variable Speed Drives Evaluation Test", Industry Application Magazine, Vol. 4, No. 1 Jan/Feb 1998, pp 53-57.
- 11 Deodhar R. P., Staton D. A., Miller T. J. E.; "Modeling of Skew Using the Flux-MMF Diagram". IAS, V32, NO. 6, Nov/Dec 1996, pp1339-1347.
- 12 Mecrow B. C.; "NEW Winding Configuration for Doubly Salient Reluctance Machines". IAS, V32, NO. 6, Nov/Dec 1996, pp1348-1356.
- 13 Acarnley P. P., Mecrow B. C., Burdess J. S., Fawcett J. N., Kelly J. G.,

- Dickinson P. G.; "Design Principles For a Flywheel Energy Store for Road Vehicles". IAS, V32, NO. 6, Nov/Dec 1996, pp1402-1408.
- 14 Swamy M, Rossiter S., Spencer M., Richardson M.; "Case Study On Mitigating Harmonics In ASD Systems To Meet IEEE19-1992 Standards", IEEE Annual Meeting Conference Record, 1994, pp685-690.
 - 15 Kim H., Sul S.; "A New Motor Speed Estimator Using Kalman Filter in Low-Speed Range". IEEE Transactions on Industrial Electronics, V43, NO. 4, Aug 1996, pp498-504.
 - 16 Oshima M., Miyazawa S., Deido T., Chiba A., Nakamura F., Fukao T.; "Characteristics of a Permanent Magnet Type Bearingless Motor". IAS, V32, NO. 2, March/April 1996, pp363-370.
 - 17 Rizk J., Nagrial M., "Finite Element Modeling of Permanent Magnet Machines", Proc. 3rd international Conf. Modeling and Simulation, Melbourne, Australia, Oct. 1997.
 - 18 Degner M., Maaren R. V., Fahim A., Novotny D. W., Lorenz R. D., Syverson C. D.; "A Rotor Lamination Design for Surface Permanent Magnet Retention at High Speeds". IAS, V32, NO. 2, March/April 1996, pp380-385.
 - 19 Husain I., Ehsani M.; "Torque Ripple Minimization in Switched Reluctance Motor Drive by PWM Current Control". IEEE Transactions on Power Electronics, V11, NO. 1, Jan 1996, pp83-88.
 - 20 Kang S., Sul S.; "Direct Torque Control of Brushless DC Motor with Nonideal Trapezoidal Back EMF". IEEE Transactions on Power

Electronics, V10, NO. 6, Nov/1995, pp796-802.

- 21 Okada Y., Dejima K., Ohishi T.; "Analysis and Comparison of PM Synchronous Motor and Induction Motor Type Magnetic Bearings". IAS V31, NO. 5, Sept/Oct 1995, pp1047-1053.
- 22 Kjaer P. C., Nielsen P., Andersen L., Blaabjerg F.; "A New Energy Optimizing Control Strategy for Switched Reluctance Motors". IAS V31, NO. 5, Sept/Oct 1995, pp1088-1095.
- 23 Piper J. W.; Discussion of " A Super High Speed PM Motor Drive Systems by a Quasi-Current Source Inverter"; IAS, V31, NO.4, July/Aug1995, pp848-849.
- 24 Nakamura Y., Kudo T., Ishibashi F., Hibino S.; "High Efficiency Drive Due to Power Factor Control of a Permanent Magnet Synchronous Motors". IEEE Transactions on Power Electronics, V10, NO. 2, March 1995, pp247-253.
- 25 Li S. H., Liang F., Zhao Y., Lipo T. A.; " A Doubly Salient Doubly Excited Variable Reluctance Motor". IAS V31, NO. 1, Jan/Feb 1995, pp99-106.
- 26 Cerruto E., Consoli A., Raciti A., Testa A.; " A Robust Adaptive Controller for PM Motor Drives in Robotic Applications". IEEE Transactions on Power Electronics, V10, NO. 1, Jan 1995, pp62-71.
- 27 Consoli A., Musumeci S., Raciti A., Testa A.; "Sensorless Vector and Speed Control of Brushless Motor Drives". IEEE Transactions on Industrial Electronics, V41, NO. 1, Feb 1994, pp91-96.

- 28 Li P. "Integrated Position Control with a Brushless Motor". IEEE 4th workshop on computers in Power Electronics, 1994, pp198-204.
- 29 Matsui N., Takeshita T.; "A Novel Starting Method of Sensorless Salient-Pole Brushless Motor". Proc. of 29th IAS Annual Meeting, 1994, pp386-392.
- 30 Kim B., Sul S., Park M.; "Maximum Torque Control of an Induction Machine in the Field-Weakening Region". IAS 1993, pp401-407.
- 31 Morimoto M., Aiba K.; "Simple Reluctance Motor Drive System". 5th European Conference on Power Electronics and Applications, 1993, pp88-91.
- 32 Iwabuchi N., Kawahara A., Kume T., Kabashima T.; "A Novel Inductor Type High-Torque Motor with Rare-Earth Magnet". IAS 1991, pp115-120.
- 33 Consoli A., Raciti A., Doria V. A.; "Analysis of Permanent Magnet Synchronous Motors". IAS 1989, pp63-68.
- 34 Chang L., Eastham A. R., Dawson G. E.; "Permanent Magnet Synchronous Motor: Finite Element Torque Calculations". IAS 1989, pp69-73.
- 35 Pillay P., Freere P.; "Literature Survey of Permanent Magnet AC Motors and Drives". IAS 1989, pp74-81.

- 36 Nonaka S., Kawaguchi T.; "Variable Speed Control of Brushless Half-Speed Synchronous Motor by Voltage Source Inverter" IAS 1989, pp253-258.
- 37 Krishnan R., Materu P.; "Analysis and Design of a Low Cost Converter for Switched Reluctance Motor Drives". IAS 1989, pp561-567.
- 38 Nishikata S., Novotny D. W.; "Efficiency Considerations for Low Frequency Operation of Induction Motors". IAS 1988, pp91-96.
- 39 Moallem M., Ong C.M.; " Predicting the Steady-State Performance of a Switched Reluctance Machine". IAS 1989, pp529-537.

INTERNET WEB SITES

<http://www.prisum.iastate.edu/>

<http://www.aurorasolarcar.com/>

<http://www.clarkson.edu/~solarcar/>

<http://www.engin.umich.edu/org/solarcar/index.html>

<http://www.seas.upenn.edu:8080/~solarwww/>

<http://www.eas.asu.edu/~solar/>

<http://www.mit.edu:8001/activities/solar-cars/>

<http://solar.eng.yale.edu/>

<http://engsoc.queensu.ca/solar/>

<http://www.uq.net.au/~zzsgoodw/frame.htm>

<http://www-rohan.sdsu.edu/staff/drjackm/solar/solrcars.html>

<http://www.ecn.purdue.edu/Solarcar/main.html>

<http://www.geocities.com/MotorCity/Factory/1723/Motors.htm>

APPENDIX A

High Frequency Transformer Data Sheet

DATA SHEET

RM12/ILP

RM cores and accessories

Product specification
Supersedes data of January 1999
File under Ferrite Ceramics, MA01

1999 Dec 23

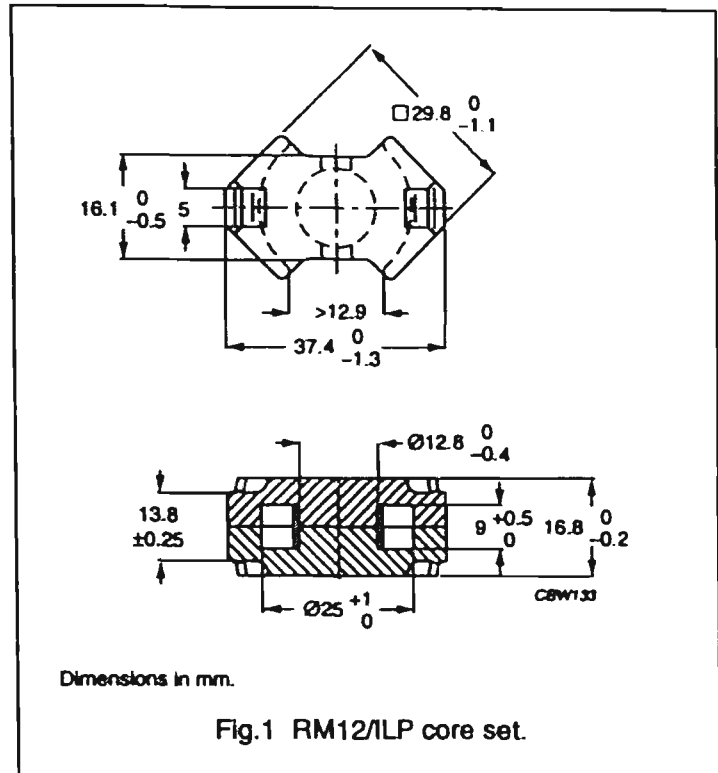
RM cores and accessories

RM12/ILP

CORE SETS

Effective core parameters

SYMBOL	PARAMETER	VALUE	UNIT
$\Sigma(VA)$	core factor (C1)	0.280	mm ⁻¹
V_e	effective volume	6200	mm ³
l_e	effective length	42	mm
A_e	effective area	148	mm ²
A_{min}	minimum area	125	mm ²
m	mass of set	≈34	g



Core sets for general purpose transformers and power applications

Clamping force for A_L measurements, 70 ± 20 N.

GRADE	A_L (nH)	H_e	AIR GAP (μ m)	TYPE NUMBER
3C90	8100 \pm 25%	≈1810	≈0	RM12/ILP-3C90
3C94 	8100 \pm 25%	≈1810	≈0	RM12/ILP-3C94
3C96 	7200 \pm 25%	≈1450	≈0	RM12/ILP-3C96
3F3	6700 \pm 25%	≈1490	≈0	RM12/ILP-3F3
3F4 	3600 \pm 25%	≈800	≈0	RM12/ILP-3F4

RM cores and accessories

RM12/ILP

Properties of core sets under power conditions

GRADE	B (mT) at	CORE LOSS (W) at			
	H = 250 A/m; f = 25 kHz; T = 100 °C	f = 25 kHz; Ḃ = 200 mT; T = 100 °C	f = 100 kHz; Ḃ = 100 mT; T = 100 °C	f = 100 kHz; Ḃ = 200 mT; T = 100 °C	f = 400 kHz; Ḃ = 50 mT; T = 100 °C
3C90	≥315	≤0.75	≤0.79	-	-
3C94	≥315	-	≤0.65	≈2.7	≈1.3
3C96	≥315	-	≈0.45	≈1.9	≈0.9
3F3	≥300	-	≤0.68	-	≤1.2
3F4	≥250	-	-	-	-

Properties of core sets under power conditions (continued)

GRADE	B (mT) at	CORE LOSS (W) at			
	H = 250 A/m; f = 25 kHz; T = 100 °C	f = 500 kHz; Ḃ = 50 mT; T = 100 °C	f = 500 kHz; Ḃ = 100 mT; T = 100 °C	f = 1 MHz; Ḃ = 30 mT; T = 100 °C	f = 3 MHz; Ḃ = 10 mT; T = 100 °C
3C90	≥315	-	-	-	-
3C94	≥315	-	-	-	-
3C96	≥315	-	-	-	-
3F3	≥300	-	-	-	-
3F4	≥250	-	-	≤1.2	≤2.0

APPENDIX B

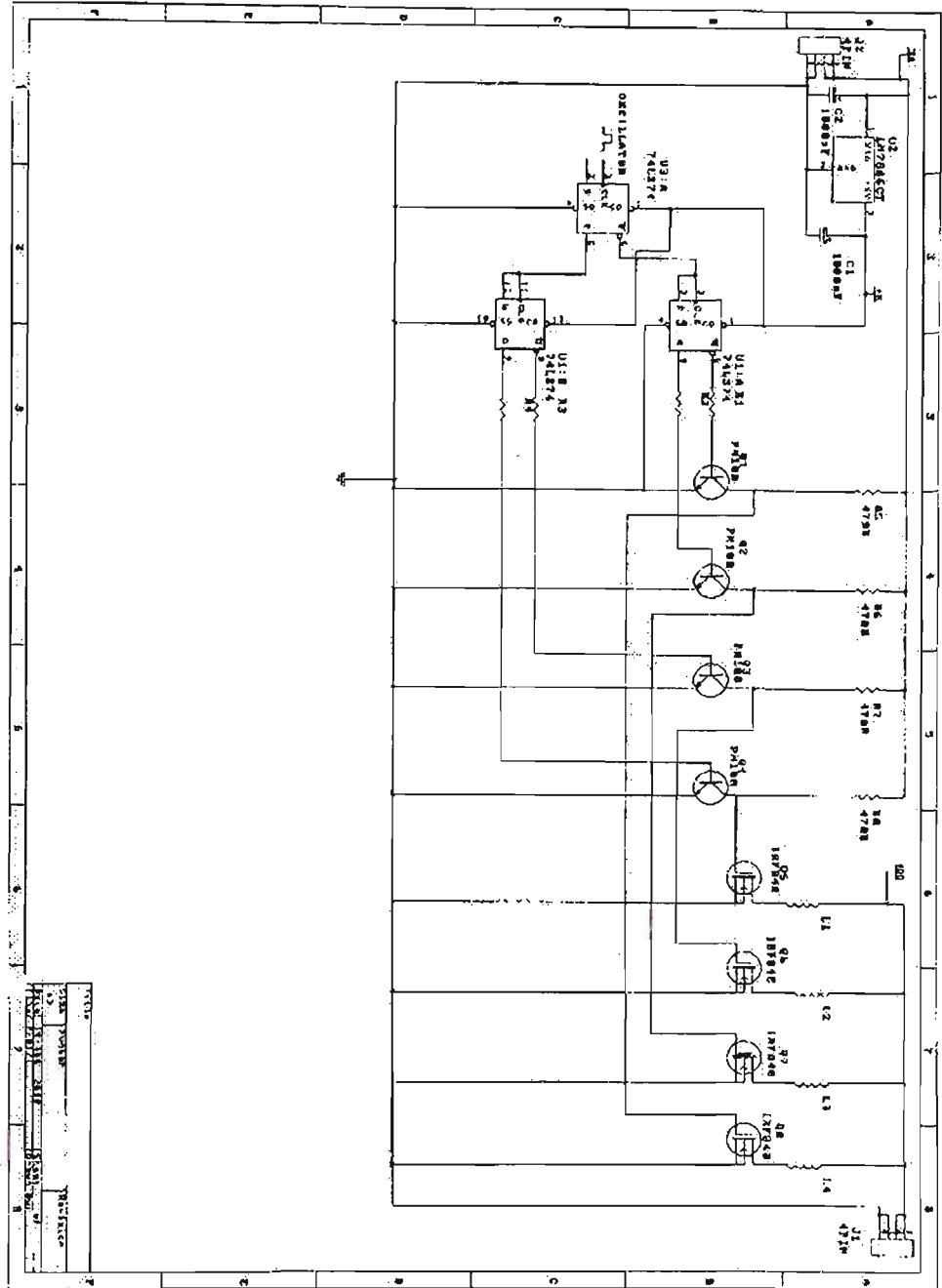


Figure B. 1 Schematic diagram of the stator winding drive circuit.

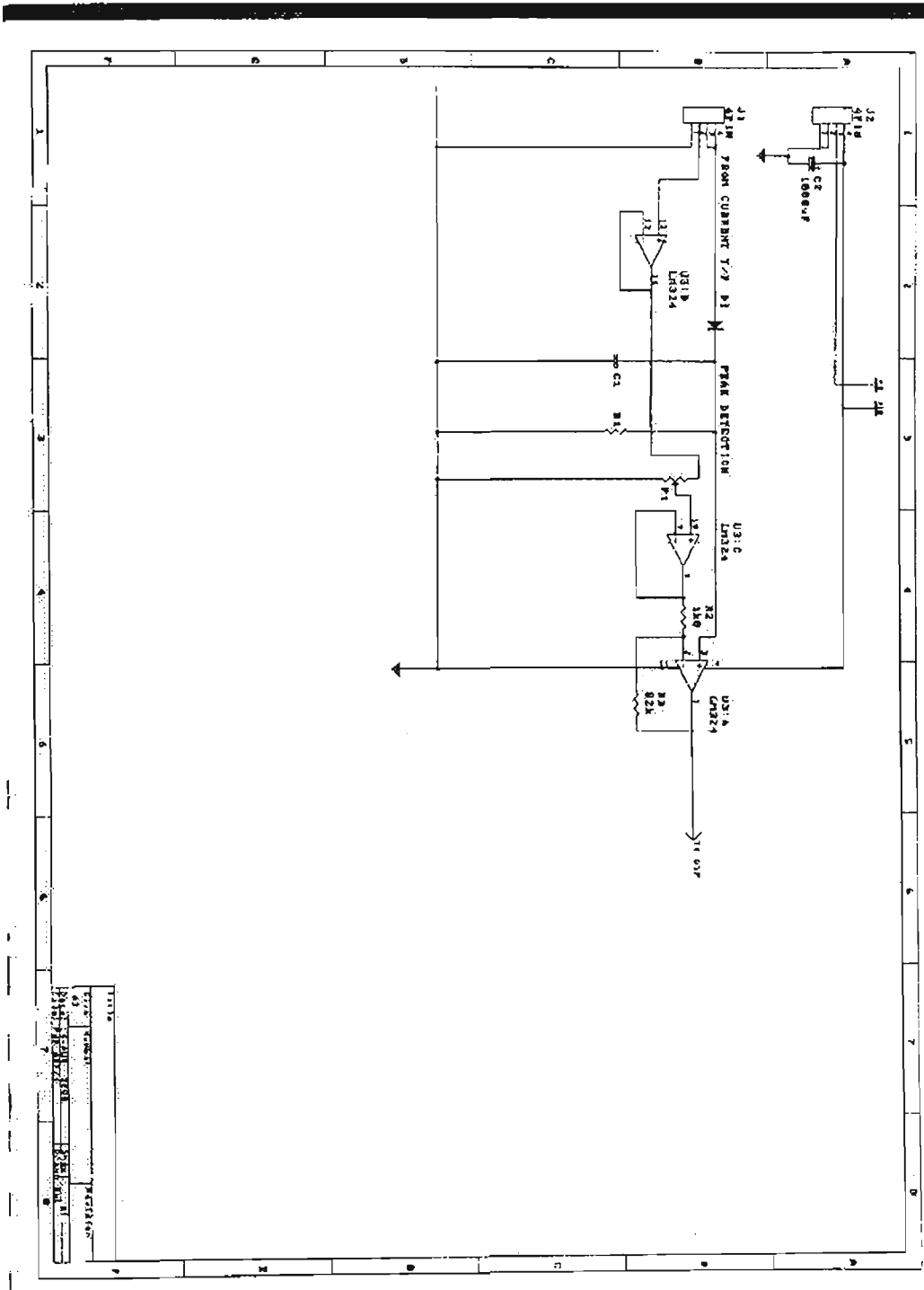


Figure B. 2 Schematic of amplifier for amplification of the magnetisation current.

APPENDIX C

C.1 Sensorless speed/position detection C program

Following program is the C program that was written for the DSP TMS320C25 to find the maximum and minimum of a triangular waveform. The triangle signal was a simulated waveform of the filtered and amplified high frequency transformer primary winding current.

This program is a test program for generation of the commutation pulses for the stator winding from the variation of the transformer current that results from the variation of the magnetisation inductance of the transformer.

This program is a cross compiler program that generates an assembly program which is converted to machine code by the assembler supplied by Texas Instrument Co.. Although the development system is outdated and TMS320C25 is regarded as an old DSP but the C code is portable to other DSP systems with minor modifications.

```
#include "c:\dsp\ioports.h"
#include "c:\dsp\math.h"
#include "c:\dsp\stdlib.h"

main()

{
int i=0;
int i2=0;
int datain;
int p1=20000;
int n1=-20000;
int tog=20000;
int mul=128;
int sta,min,MIN,temp,MAX;
int BASE = 11141;
int STEP = 1229;
int base1, base2,base3,base4,base5,base6,base7,base8;

/* Read current from input port */
/* and find maximum and minimum */
```

```

for(sta=0;sta<30000;sta++)
{
min=_inport1();
temp=_inport1();
if (min<temp)
MAX=min;
else
MAX=temp;
}

/* Test if the value reaches the
corresponding */
/* level to switch ON-OFF output ports */

for(;;)
{
i=_inport1();
if(i>(base1-mul) && i< (base1+mul))
{

_outport0(p1);
_outport1(n1);
_outport2(n1);
_outport3(p1);

}
else

if(i>(base2-mul) && i < (base2+mul))
{
_outport0(p1);
_outport1(n1);
_outport2(p1);
_outport3(n1);
}
else

if(i>(base3-mul) && i<(base3+mul) )

{
_outport0(n1);
_outport1(p1);
_outport2(p1);
_outport3(n1);
}
}

```

```

else

if(i>(base4-mul) && i<(base4+mul))
    {
        _output0(n1);
        _output1(p1);
        _output2(n1);
        _output3(p1);
    }
else

if(i>(base5-mul) && i<(base5+mul))
    {
        _output0(p1);
        _output1(n1);
        _output2(n1);
        _output3(p1);
    }
else

if(i>(base6-mul) && i<(base6+mul))
    {
        _output0(p1);
        _output1(n1);
        _output2(p1);
        _output3(n1);
    }
else

if(i>(base7-mul) && i<(base7+mul))
    {
        _output0(n1);
        _output1(p1);
        _output2(p1);
        _output3(n1);
    }
else

if(i>(base8-mul) && i<(base8+mul))
    {
        _output0(n1);
        _output1(p1);
        _output2(n1);
        _output3(p1);
    }

```

```

    }

/* Delay routine for use in */
/* cases where a delay was */
/* required after outport */

delay(j)
{
int k=0;

for (k=0;k<j;k++)
    {
        k++;
        k--;
    }
}

```

C.2 Command File

/* Following file is called command file and is required by the assembler to converts the assembly code to machine code. */

```

-c
"
-u RESET
"
-o myt.out
"
-m myt.map
"
"
myt.obj
"
-l ..\rts.lib
"
-l ..\flib.lib

MEMORY
{
PAGE 0 :VECS (IRX): origin =0h, length=030h
CODE (IRX): origin = 030h, length =0f90h
PAGE 1 :POD (WIRX) : origin=00300h, length=10000h

```

```
}
```

SECTIONS

```
{
```

```
vectors 00000h      : {} > VECS PAGE 0  
.text              : {} > CODE PAGE 0  
.data              : {} > CODE PAGE 0  
.bss               : {} > POD PAGE 1  
}
```

C3. Batch file

For performing compiling, assembling and code format conversion following batch file is used. The commands in the first argument of each line are related to the Software Development System (SWDS) for TMS320C25 Digital Signal Processor that has been described in Texas Instrument Co. Data book related to SWDS of TMS320C25 DSP.

```
dspcc myt.c  
dspcg myt.if  
dspa -l myt.asm  
dsplnk myt.cmd  
dsprom -t myt.out
```

APPENDIX D

PROGRAM 1.

%In this program, output power of the transformer vs different Q
%is plotted. The fundamental value for the half-bridge is vi,
%leakage inductance Ll, magnetisation inductance Lm, resonant
%capacitor C and different resonant frequencies are wm, wl and wt
%(refer to Chapter 4, Figure 4.5). This program also calculates
%short-circuit current of the transformer Isc. The output of the
%program is the plot of power for various Q.

```
Ll=300e-6;
Lm=450e-6;
c=47e-9;
vi=153;
wm=1/sqrt(Lm*c);
wl=1/sqrt(Ll*c);
wt=1/sqrt((Lm+Ll)*c);
w=(125000:100:400000);
Isc=240*1.4*(c.*w)./(1-w.^2/wl^2);

    for r=10:50:500;
        q=r*c*wl;
        term1=((w.^2/wt^2)-1)./(w.^2/wm^2).^2;
        term2=((w.^2/wl^2)-1)./((q/wl).*w).^2;
        gain=1./sqrt(term1+term2);
        vo=gain.*vi;
        po=vo.^2/r;
        plot(w/(2*pi),po,'r');
        xlabel('Hz');
        ylabel('VA');
        grid on;
        hold on;
    end;
```

PROGRAM 2:

%In this program, the ratio of output voltage to input voltage of
%the transformer vs different Q is plotted. The fundamental value
%for the half-bridge is vi, leakage inductance L1, magnetisation
%inductance Lm, resonant capacitor c and different resonant
%frequencies are wm, wl and wt (refer to Chapter 4, Figure 4.5).
%This program also calculates the short-circuit current of the
%transformer Isc. The output of the program is the plot of power
%for various Q.

```
L1=300e-6;
Lm=450e-6;
c=47e-9;
wm=1/sqrt(Lm*c);
wl=1/sqrt(L1*c);
wt=1/sqrt((Lm+L1)*c);
w=(125000:1000:400000);
Isc=240*1.4*(c.*w)./(1-w.^2/wl^2);

    for q=1:1:5

        term1=( (w.^2/wt^2)-1) ./ (w.^2/wm^2).^2;
        term2=( (w.^2/wl^2)-1) ./ ((q/wl).*w).^2;
        gain=1./sqrt(term1+term2);
        plot(w/(2*pi),gain,'r');
        xlabel('Hz');
        ylabel('Vo/Vi');
        grid on;
        hold on;

    end;
```

PROGRAM 3:

%This program calculates the variation of the transformer current
%due to the variation of the angular position of the primary vs
%secondary of the transformer.

%Definition of angular position teta and magnetisation minimum
%and maximum inductances, Leakage inductance LL, ohmic resistance
%of rotor winding R transferred to primary side, half-bridge
%voltage v, angular frequency w with frequency of 42kHz. The
%output of the program is "i" that is the primary current of the
%transformer.

```
teta=pi/2;
Lmin=330e-6*j;
Lmax=450e-6*j;
LL=330e-6*j;
R=1000;
v=175;
w=2*pi*42000;
teta=0:0.01:pi/2;
Lm=(Lmax-Lmin)*((pi-2.*teta)/pi) + Lmin;

%Place this loop for a range of resistances

    %for R=40:10:100;
        nom=(LL*w.*(R+Lm*w) + R.*Lm*w);
        denom=(R+Lm*w);
        z=nom./denom;
        i=v./abs(z);
        plot(abs(Lm),i,'R');
        xlabel('Henry');
        ylabel('I (Amp)');
        grid on;
        hold on;
    %end;

end;
```

PROGRAM 4:

%This program calculates the variation of the transformer current
%due to the variation of the angular position of the primary vs
%secondary of the transformer for the resonant circuit.
%Definition of angular position θ and magnetisation minimum
%and maximum inductances, Leakage inductance L_L , ohmic resistance
%of rotor winding R transferred to primary side, c is the resonant
%capacitor, half-bridge voltage v , angular frequency ω with
%frequency of 42kHz. The output of the program is "i" that is
%the primary current of the transformer.

```
teta=pi/2;
Lmin=330e-6*j;
Lmax=450e-6*j;
LL=330e-6*j;
c=47e-9*j;
R=100;
v=175;
w=2*pi*26000;
teta=0:0.01:pi/2;
Lm=(Lmax-Lmin)*((pi-2.*teta)/pi) + Lmin;
zc=(LL*c*w^2+1)/(c*w);
%Place this loop for a range of resistances

    %for R=40:10:80;
        nom=(zc.*(R+Lm*w) + R.*Lm*w);
        denom=(R+Lm*w);
        z=nom./denom;
        %z=w*R.*Lm./(R+w.*Lm)+zc;
        i=v./abs(z);
        plot(abs(Lm), i, 'R');
        xlabel('Henry');
        ylabel('I (Amp)');
        grid on;
        hold on;
    %end;

end;
```

PROGRAM 5:

%This program is used in a permanent magnet motor design to
%calculate the number of conductors, torque and efficiency. Some
%of the motor parameters must be specified as constant in the
%program.

```
pm_k=0.9;          %pm_k, 0.9 for rare earth, 0.8 for ferrite****
                    %remanance flux***
br=0.9;           %phases
ph=3;            %slots
slots=36;        %slot area, mm
slot_area=85;    %slot-pitch;
s_p=6;          %slot depth, meter
s_d=0.017;      %winding format
double=2;       %Supply voltage ***
e=240*sqrt(2);  %maximum rpm
rpm=12000;      %stator ID and OD
sid=82e-3;      %airgap
od=140e-3;     %magnet thickness
g=0.8e-3;      %rotor outward diameter
lm=10*g;       %rotor yoke diameter
dr=sid-2*g;    %stack length
dy=dr-2*lm;    %poles
lstk=30e-3;    %magnet pole area
pole=8;        ap=(pi*dy*lstk)/pole;
                    %recoil permeability
u=1;           %airgap flux
                    %commutation frequency
                    %airgap flux
                    flux=bm*ap;
```

```

                                %noload speed
wnl=(2*pi/60)*rpm/pm_k;
                                %Torque and EMF constant
ke=e/wnl;
                                %winding constant
c=0.9;
                                %parallel winding path
a=1;
                                %total conductor fullarc***
z=(3/2)*(a*pi*ke/(flux*(pole/2)*c));
                                %total conductor for 30 degree
z30=z*3/2;
                                %coil numbers***
coil=slots/ph;
                                %number of turns per coil, full and 30 arc
n=round(z/(2*coil));
n30=round(z30/(2*coil));

                                %fill factor 0.3-0.8
alfa=0.4;
                                %wire diameter, select the next lowest
wire_d=sqrt(slot_area*alfa/(n*double));
wire_act=wire_d;
wire_d=(wire_d*10);
wire_d=fix(wire_d)/10;

wire_d30=sqrt(slot_area*alfa/(n30*double));
wire30_act=wire_d30;
wire_d30=(wire_d30*10);
wire_d30=fix(wire_d30)/10;
                                %winding pitch
w_p=pi*s_p*(sid+s_d/2)/slots;

                                %winding end turn curveture factor
cf=0.3*lstk;
                                %average length of coil
lwm=2*(lstk+w_p+cf);
                                %total coil length
wire_c=n*lwm;
wire_c30=n30*lwm;
                                %total phase wire length
wire_tl=wire_c*coil;
wire_tl30=wire_c30*coil;

                                %total phase winding ohmic resistance

if wire_d==0.4
    spec_r=0.13;
end;

    if wire_d==0.5
        spec_r=0.088;
    end;

```

```

if wire_d==0.6
    wire_d=0.55;
    spec_r=0.069;
end;

    if wire_d==0.7
        spec_r=0.043;
        end;

if wire_d==0.8
    spec_r=0.034;
end;

    if wire_d==0.9
        spec_r=0.026;
        end;

if wire_d==1
    spec_r=0.021;
end;

        if wire_d==1.1
            spec_r=0.019;
            end;

        %total phase winding ohmic resistance, 30 degree

if wire_d30==0.4
    spec_r30=0.13;
end;

    if wire_d30==0.5
        spec_r30=0.088;
        end;

if wire_d30==0.6
    spec_r30=0.069;
end;

    if wire_d30==0.7
        spec_r30=0.043;
        end;

if wire_d30==0.8
    spec_r30=0.034;
end;

    if wire_d30==0.9
        spec_r30=0.026;
        end;

```

```

if wire_d30==1
    spec_r30=0.021;
end;

    if wire_d30==1.1
        spec_r30=0.019;
    end;

        %wire resistance

rp=wire_tl*spec_r;
rp30=wire_tl30*spec_r30;

        %EMF calculation
emf=rpm*2*pi*ke/60;
        %stator current
vinv=2;
rs=1;
is=(e-emf-vinv)/(rs+2*rp);
is30=(e-emf-vinv)/(rs+2*rp30);

        %torque
torque=is*ke;
torque30=is30*ke;

        %current density
js=is*4/(pi*wire_d^2);
js30=is30*4/(pi*wire_d30^2);

        %copper losses
pcu=2*rp*is^2;
pcu30=2*rp30*is30^2;

        %core losses
f=(pole/2)*rpm/60;
volume=lstk*((pi/4)*(od^2-sid^2)-slot_area*slots/1e6); %cubic
meter
w_kg=4.6;          %core loss per kg
spec_vol=7750;
weight=volume*spec_vol;
fref=60;          %value that losses are specified, f & B, tesla
                %twice the airgap flux is in iron
bref=1.5;
                %0.55 for equivalent dc flux loss curves
pco_spec=w_kg*(0.55*(f/fref)*(2*bm/bref)^1.6+0.55*(f/fref)^2*(2*bm
/bref)^2);
pco=pco_spec*weight;

        %efficiency
mech_power=2*pi*rpm*torque/60;
mech_power30=2*pi*rpm*torque30/60;
total_loss=pcu+pco;
total_loss30=pcu30+pco;

```

```
eff=100*mech_power/(mech_power+total_loss);  
eff30=100*mech_power30/(mech_power30+total_loss30);
```

```
    %efficiency at nominal torque
```

```
torque_n=1.2;  
mech_powern=2*pi*rpm*torque_n/60;  
in=is*torque_n/torque;  
in30=is30*torque_n/torque30;  
pcun=(in^2/is^2)*pcu;  
pcun30=(in30^2/is30^2)*pcu30;  
effn=100*mech_powern/(mech_powern+pcun+pco);  
effn30=100*mech_powern/(mech_powern+pcun30+pco);  
jsn=in*4/(pi*wire_d^2);  
jsn30=in30*4/(pi*wire_d30^2);
```

```
    %maximum current
```

```
imax=(e-vinv)/(rs+2*rp);  
imax30=(e-vinv)/(rs+2*rp30);
```

PROGRAM 6:

%This program prints the result of motor design program in the
%file Fa_pm_1.doc. This file contains the full magnet arc design
%only.

```

                                %record results is a file

f_wt=fopen('Fa_pm_1.doc','w');
                                %General Parameters
fprintf(f_wt,'EMF Magnet Constant = %4.4f\n',pm_k);
fprintf(f_wt,'Magnet Remanance Flux Density = %4.4f Tesla\n',br);
fprintf(f_wt,'Pole Numbers = %4.4f\n',pole);
fprintf(f_wt,'RPM = %4.2f RPM\n',rpm);
fprintf(f_wt,'Required Torque = %4.4f N.m.\n',torque_n);
fprintf(f_wt,'Supply Voltage = %4.4f Volts\n',e);

                                %Motor Dimensions
fprintf(f_wt,'Stator Slots = %d \n',slots);
fprintf(f_wt,'Slot Area = %4.4f mm2\n',slot_area);
fprintf(f_wt,'Stator OD = %4.4f meter\n',od);
fprintf(f_wt,'Stator ID = %4.4f meter\n',sid);
fprintf(f_wt,'Stack Length = %4.4f meter\n',lstk);
fprintf(f_wt,'Stator Volume = %4.4e meter3\n',volume);
fprintf(f_wt,'Stator Weight = %4.4f Kg\n',weight);
fprintf(f_wt,'Rotor OD = %4.4f meter\n',dr);
fprintf(f_wt,'Rotor ID = %4.4f meter\n',dy);

                                %Magnet Properties
fprintf(f_wt,'Airgap = %4.4f meter\n',g);
fprintf(f_wt,'Magnet Thickness = %4.4f meter\n',lm);
fprintf(f_wt,'Magnet Pole Area = %4.4f m2\n',ap);
fprintf(f_wt,'Maximum Airgap Flux Density= %4.4f Tesla\n',bm);
fprintf(f_wt,'Approximate Flux = %4.4e Webber\n',flux);

                                %Speed
fprintf(f_wt,'Commutation Frequency = %4.4f Hz\n',fc);
fprintf(f_wt,'No Load Speed = %4.2f Rad/sec\n',wnl);
fprintf(f_wt,'EMF Constant = %4.4f V.S/Rad\n',ke);

                                %windings
fprintf(f_wt,'Total Number Of Conductors = %4.2f\n',z);
fprintf(f_wt,'Coil Numbers = %d\n',coil);
fprintf(f_wt,'Actual Wire Diameter = %4.4f mm\n',wire_act);
fprintf(f_wt,'Wire Diameter = %4.4f mm\n',wire_d);
fprintf(f_wt,'Wire Pitch Size = %4.4f meter\n',w_p);
fprintf(f_wt,'Mean Coil Length = %4.4f meter\n',lwm);
fprintf(f_wt,'Coil Wire Length = %4.4f meter\n',wire_c);
fprintf(f_wt,'Total Coil Length = %4.4f meter\n',wire_tl);
fprintf(f_wt,'Total Coil Resistance = %4.4f Ohm\n',rp);

                                %Results
fprintf(f_wt,'EMF = %4.4f Volts\n',emf);
fprintf(f_wt,'Stator Phase Current = %4.4f Amper\n',is);
fprintf(f_wt,'Torque = %4.4f N.m.\n',torque);
fprintf(f_wt,'Current Density = %4.4f A/mm2\n',js);

                                %Losses
fprintf(f_wt,'Maximum Operating Frequency = %4.2f Hz\n',f);
```

```

fprintf(f_wt, 'Copper Loss = %4.4f W\n', pcu);
fprintf(f_wt, 'Core Loss = %4.4f W\n', pco);
        %Mechanical Power
fprintf(f_wt, 'Mechanical Power = %4.4f W\n', mech_power);
fprintf(f_wt, 'Total Loss = %4.4f W\n', total_loss);
fprintf(f_wt, 'Efficiency = %4.4f %%\n', eff);
fprintf(f_wt, 'Stalled Stator Current = %4.4f Amper\n', imax);
        %Checking operation for required torque
fprintf(f_wt, 'Stator Current At Required Torque = %4.4f
Amper\n', in);
fprintf(f_wt, 'Copper Loss at Required Torque = %4.4f W\n', pcun);
fprintf(f_wt, 'Current Density At Required Torque = %4.4f
A/mm2\n', jsn);
fprintf(f_wt, 'Mechanical Power At Required Torque = %4.4f
W\n', mech_powern);
fprintf(f_wt, 'Efficiency At Required Torque = %4.4f %%\n', effn);

fclose(f_wt);

```

PROGRAM 7:

%This program prints the result of motor design program in the
%file Fa_pm_30.doc. This file contains the 30 degree magnet arc
%design only.

```
        %record results is a file

f_wt=fopen('Fa_pm_30.doc','w');
        %General Parameters
fprintf(f_wt,'EMF Magnet Constant = %4.4f\n',pm_k);
fprintf(f_wt,'Magnet Remanance Flux Density = %4.4f Tesla\n',br);
fprintf(f_wt,'Pole Numbers = %4.4f\n',pole);
fprintf(f_wt,'RPM = %4.2f RPM\n',rpm);
fprintf(f_wt,'Required Torque = %4.4f N.m.\n',torque_n);
fprintf(f_wt,'Supply Voltage = %4.4f Volts\n',e);

        %Motor Dimensions
fprintf(f_wt,'Stator Slots = %d \n',slots);
fprintf(f_wt,'Slot Area = %4.4f mm2\n',slot_area);
fprintf(f_wt,'Stator OD = %4.4f meter\n',od);
fprintf(f_wt,'Stator ID = %4.4f meter\n',sid);
fprintf(f_wt,'Stack Length = %4.4f meter\n',lstk);
fprintf(f_wt,'Stator Volume = %4.4e meter3\n',volume);
fprintf(f_wt,'Stator Weight = %4.4f Kg\n',weight);
fprintf(f_wt,'Rotor OD = %4.4f meter\n',dr);
fprintf(f_wt,'Rotor ID = %4.4f meter\n',dy);

        %Magnet Properties
fprintf(f_wt,'Airgap = %4.4f meter\n',g);
fprintf(f_wt,'Magnet Thickness = %4.4f meter\n',lm);
fprintf(f_wt,'Magnet Pole Area = %4.4f m2\n',ap*0.667);
fprintf(f_wt,'Maximum Airgap Flux Density= %4.4f Tesla\n',bm);
fprintf(f_wt,'Approximate Flux = %4.4e Webber\n',flux*0.667);

        %Speed
fprintf(f_wt,'Commutation Frequency = %4.4f Hz\n',fc);
fprintf(f_wt,'No Load Speed = %4.2f Rad/sec\n',wnl);
fprintf(f_wt,'EMF Constant = %4.4f V.S/Rad\n',ke);

        %windings
fprintf(f_wt,'Total Number Of Conductors = %4.2f\n',z30);
fprintf(f_wt,'Coil Numbers = %d\n',coil);
fprintf(f_wt,'Actual Wire Diameter = %4.4f mm\n',wire30_act);
fprintf(f_wt,'Wire Diameter = %4.4f mm\n',wire_d30);
fprintf(f_wt,'Wire Pitch Size = %4.4f meter\n',w_p);
fprintf(f_wt,'Mean Coil Length = %4.4f meter\n',lwm);
fprintf(f_wt,'Coil Wire Length = %4.4f meter\n',wire_c30);
fprintf(f_wt,'Total Coil Length = %4.4f meter\n',wire_tl30);
fprintf(f_wt,'Total Coil Resistance = %4.4f Ohm\n',rp30);

        %Results
fprintf(f_wt,'EMF = %4.4f Volts\n',emf);
fprintf(f_wt,'Stator Phase Current = %4.4f Amper\n',is30);
fprintf(f_wt,'Torque = %4.4f N.m.\n',torque30);
fprintf(f_wt,'Current Density = %4.4f A/mm2\n',js30);

        %Losses
fprintf(f_wt,'Maximum Operating Frequency = %4.2f Hz\n',f);
```

```
fprintf(f_wt, 'Copper Loss = %4.4f W\n', pcu30);
fprintf(f_wt, 'Core Loss = %4.4f W\n', pco);
    %Mechanical Power
fprintf(f_wt, 'Mechanical Power = %4.4f W\n', mech_power30);
fprintf(f_wt, 'Total Loss = %4.4f W\n', total_loss30);
fprintf(f_wt, 'Efficiency = %4.4f %%\n', eff30);
fprintf(f_wt, 'Stalled Stator Current = %4.4f Amper\n', imax30);
    %Checking operation for required torque
fprintf(f_wt, 'Stator Current At Required Torque = %4.4f
Amper\n', in30);
fprintf(f_wt, 'Copper Loss at Required Torque = %4.4f W\n', pcun30);
fprintf(f_wt, 'Current Density At Required Torque = %4.4f
A/mm2\n', jsn30);
fprintf(f_wt, 'Mechanical Power At Required Torque = %4.4f
W\n', mech_povern);
fprintf(f_wt, 'Efficiency At Required Torque = %4.4f %%\n', effn30);

fclose(f_wt);
```

